Electronic Theses and Dissertations

Theses, Dissertations, and Major Papers

1-1-2006

Diagenesis and dolomitisation of the Devonian Upper Stettler and Crossfield, south-central Alberta: Petrologic and isotopic evidence.

Samantha R. Raymus
University of Windsor

Follow this and additional works at: https://scholar.uwindsor.ca/etd

Diagenesis and Dolomitisation of the Devonian Upper Stettler and Crossfield, south-central Alberta: Petrologic and Isotopic Evidence

by

Samantha R. Raymus

A Thesis
Submitted to the Faculty of Graduate Studies and Research
through Earth Sciences
in Partial Fulfilment of the Requirements for
the Degree of Master of Science at the
University of Windsor.

Windsor, Ontario, Canada

2006

© 2006 Samantha Raymus

Canada

ABSTRACT

The Devonian Upper Stettler Formation and the underlying Crossfield Member are mixed evaporite/carbonate assemblages that were cyclically deposited on carbonate ramps during the Famennian. Lithofacies include mudstones, peloidal grainstones, stromatoporoid floatstones, bioclastic packstones/rudstones, and dolostones.

The following events are identified as the most important in the diagenetic alteration of facies in the Upper Stettler and Crossfield: (1) early pervasive dolomitisation from Mg^{2+} - rich refluxing brines; (2) chemical compaction; (3) recrystallisation of early matrix dolomites with changing pore-fluid chemistry; (4) secondary anhydrite, blocky calcite II, and saddle dolomite cements; (5) Deep-burial TSR reactions.

Isotopic values ($\delta^{18}O$ and $\delta^{13}C$) and $^{87}Sr/^{86}Sr$ ratios suggest progressive diagenetic alteration for both calcite and dolomite phases with increasing burial. These values reflect increasing temperatures, interaction with organic carbons, mixing pore-fluids with depth, and TSR processes that have occurred within the Upper Stettler Formation and more particularly, the Crossfield Member.

For my father,
In his lifelong quest for the elusive truth.
You are always with me.

D.W. (Ray) Raymus
(1942-1999)

ACKNOWLEDGEMENTS

First of all, I would like to thank Dr. Ihsan S. Al-Aasm for the opportunity to work on this project. Without the financial support and constructive advice and encouragement he provided, this thesis would not have been completed. Thank you also to my committee members, Dr. Maria Cioppa and Dr. N. Biswas.

I would also like to thank Dr. Jeff Packard and Dr. Bill Martindale for their help at the Core Research Centre in Calgary, and more specifically, for their support and advice during the research process.

On a more personal note, thank you to Melissa Price for all her help in the isotope lab and for all the great conversations. Thank you also to the very efficient Sharon Horne for her advice, encouragement, and help during my time in Windsor.

I am also indebted to JoAnn Adam for always being there for me, encouraging me and making me laugh, even when I didn't feel like laughing. You have been an invaluable friend. I would also like to thank my family for listening to me when I needed to talk and for all their encouragement and support, my mother Florence, and my favourite sister, Lauri-Ann.

Finally, I would like to thank the most important person in my life, my future husband, Bill Gulenchin. When I felt discouraged, he reminded me of the most valuable things in life: our mutual faith in God, our love for each other, our friends and family, and breathing in the beauty of life because you never know when one day will be your last. Ultimately, nothing else is that important.

v

TABLE OF CONTENTS

ix

LIST OF TABLES

LIST OF FIGURES

xii

LIST OF PLATES

CHAPTER I

INTRODUCTION

1.1   Purpose of Study

The dolomitisation of Devonian sequences in the Western Canada Sedimentary Basin (WCSB) has been examined in numerous studies in recent years (Machel and Mountjoy, 1987; Mountjoy et al., 1991; Mountjoy et al., 1992; Shields and Brady, 1995; Lonnee and Al-Aasm, 2000; Al-Aasm and Clarke, 2004; among others). Dolomitisation is important for the development of hydrocarbon reservoirs because it can enhance or destroy porosity and permeability characteristics (Machel, 2004). In spite of the importance of dolomitisation on reservoir development, petrographic and geochemical evidence for many of these dolostone reservoirs in the WCSB remains scarce. The Upper Stettler Formation and Crossfield Member are extensively dolomitised in south-central Alberta, and with the aid of petrographic and isotopic techniques, the mechanisms of dolomitisation and the impact on reservoir development will be examined.

The Crossfield Member is a porous, biostromal unit within the Stettler Formation of the Upper Devonian Wabamun Group in southern Alberta. This oil and gas-producing Crossfield unit extends in a north-south trending belt from the Olds/Garrington area in the north to the Okotoks region in the south in close proximity to the Fifth Principal Meridian (Fig 1.1). The entire Crossfield trend has been significantly affected by diagenetic alteration. The precursor fabrics are further altered within each individual facies through the extensive dolomitisation of the unit.

The main purpose of this study is to characterise dolomitisation processes and determine dolomite genesis in the Crossfield Member and overlying Upper Stettler Formation. Core samples were examined from a total of 11 wells. Seven of these wells were selected to encompass the entire Crossfield trend from the north to the south (townships ranging from 21 through 32) and four wells were chosen to examine Crossfield-equivalent strata west of the main Crossfield trend. The four Crossfield-equivalent wells are in the Moose Mountain, Benjamin (Ghost), Burnt Timber, and Panther River areas. These core samples were examined to determine any lateral alteration away from the Crossfield trend and to compare the extent and types of dolomitisation farther west towards the Jura Creek outcrop (Palliser Formation) in the southern Rocky Mountain Foothills. In order to study original precursor fabrics prior to fabric-destructive dolomitisation within the Crossfield

1

Figure 1.1: Map of Alberta showing study areas as red boxes. Different dominant lithologies are shown as shades of grey (Map modified from Stoakes, 1992)

2
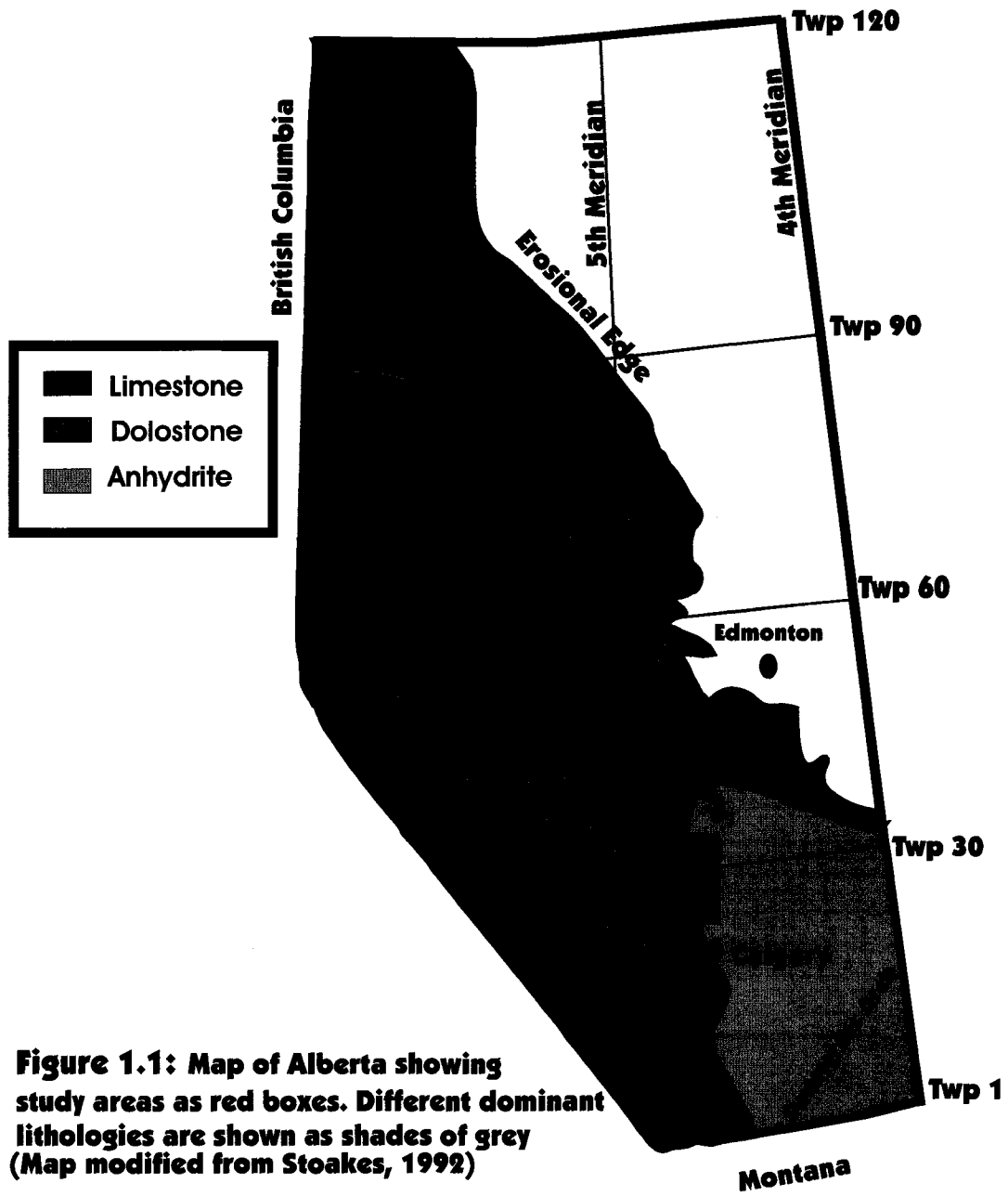
Member, core samples were also examined from Crossfield-equivalent strata in one well NW of the main study area in the Giroux Lake region (township 66) that is not pervasively dolomitised.

In the context of accomplishing the overall purpose of understanding dolomite genesis within the Crossfield Member and Upper Stettler Formation, the primary objectives of this study are:

(1) To test the current proposed dolomitisation models in the Crossfield Member through an examination of dolomites within the Crossfield trend and in the Crossfield-equivalent wells. This will be accomplished by an examination of the distribution and occurrence of secondary dolomites using petrologic methods and stable and radiogenic isotope geochemistry to determine the origin and isotopic signature of dolomitising fluids, and to explain other diagenetic events within the study areas;

(2) To examine the different porosity types within the study area and determine the effects of dolomitisation and other diagenetic events on the creation, preservation and/or destruction of porosity within the Crossfield Member;

(3) To determine the timing of diagenetic events and cementation and develop a paragenetic sequence for the Crossfield Member;

(4) To identify the different lithofacies within the Crossfield trend and examine the timing and relationship of the evaporite phases within the Crossfield Member and the overlying Upper Stettler Formation.

1.2 Previous Studies

Focus on the Stettler Formation and Crossfield Member was most significant in the 1960's in response to the discovery of gas-producing pools along the Crossfield trend. Gas production in the Crossfield area began in the late 1950's, and by the late 1990's, the Crossfield was regarded as mature. After 1995, the discovery of gas along the eastern margin of the Crossfield trend resulted in increased interest in the area (Martindale et al., 2004).

There are few published papers directly related to the Crossfield Member and much of the early focus in the 1950's and 1960's is on the lithofacies and overall geologic history of the Stettler area in Alberta with some research also on faunal succession (Raasch, 1956). Most early work on the Stettler area was by Andrichuk and Wonfor (1954, 1956) and Andrichuk (1958), and this research was the basis for more detailed work by Andrichuk in 1960. Andrichuk (1960) published a paper that presented a thorough description of the different facies in the Wabamun Group in Alberta and the different dolomite types within the

3

Wabamun Group. Furthermore, this was the first paper to suggest a reflux dolomitisation mechanism for the formation of dolomite within the Wabamun Group of Alberta.

By the late 1960's, more detailed work was conducted on sedimentary features within facies from the Stettler area. Descriptions of evaporite deposits within the Crossfield Member and Stettler Formation were published by Workman and Metherell (1969), Metherell and Workman (1969) and Fuller and Porter (1969). Workman and Metherell (1969) also described the lithology of the Upper and Lower Stettler Formation surrounding the Crossfield Member and attributed the main source of gas in the Crossfield East to the *Labechiid* stromatoporoid and gastropod mud bank associated with the Crossfield Member.

In the 1980's, the Crossfield Member was examined by Eliuk (1984) who focussed on thermochemical sulphate reduction (TSR) and other diagenetic features observed in facies from core of the Limestone/Burnt Timber area (Twp 32,west of the Crossfield trend). Eliuk and Hunter (1987) also studied facies from the Limestone/Burnt Timber wells and based on their observations, they described the Crossfield Member as a relatively porous dolomite interval surrounded by anhydrites and other evaporites of the Stettler Formation (or equivalent). The study by Eliuk and Hunter (1987) further discussed the Crossfield Member as a reservoir for hydrogen sulphide-rich gas. Halbertsma and Meijer-Drees (1987) briefly discussed the Crossfield gas field trend in the Southern Alberta plains where the Crossfield Member forms a stratigraphic trap as it wedges into the Stettler Formation.

In a project for Pan Canadian Petroleum Ltd., Packard and Mcnab (1994) examined the facies, porosity, depositional and diagenetic fabrics of the Crossfield and Stettler evaporites and dolomites in order to evaluate reservoir quality and relationships between dolomite and anhydrite. This study was part of a project to examine the reservoir potential of the eastern margin of the Garrington-Okotoks Wabamun gas trend. In a similar study, Erickson et al. (1994) examined the regional Wabamun Group in the Alberta Foothills subsurface and this project included studies of the stratigraphy, facies, reservoir potential, porosity and fractures, structural style, and other features of the Crossfield trend. Limited geochemistry of the Foothills region was also used in this project.

More recent work on the Crossfield Member and Crossfield-equivalent strata was conducted by Yang et al. (2001) who examined thermochemical sulphate reduction (TSR) features using fluid inclusion and stable isotope techniques on Burnt Timber and Crossfield East gas fields. The most recent published work is by Martindale et al. (2004) that described the different depositional facies and divided these lithofacies into 18 facies types within the Crossfield Member and Upper Stettler Formation. Dolomites and other diagenetic features

4

were also examined in this study and a few geochemical analyses were conducted on finely crystalline dolomites for trace elements, oxygen and carbon isotopes, and radiogenic strontium isotopes. Based on petrographic evidence and this limited geochemistry, the authors suggested that a reflux mechanism was responsible for pervasive dolomitisation within the Crossfield Member.

Overall, with limited published work on the Crossfield Member, there have been no extensive studies using isotope geochemistry on a more regional scale along the Crossfield trend and farther west on Crossfield-equivalent strata. There has also been limited focus on the geochemistry and significance of the evaporites in the Crossfield Member, and more significantly, within the Upper Stettler Formation.

There is only one B.Sc. thesis available that examined the Crossfield Member in detail (Ostrom, 1985). Ostrom (1985) described the lithofacies and porosity of the Crossfield Member in the Olds area of the Crossfield trend in southern Alberta. In an MSc thesis by Halim-Dihardja (1986), six samples of sabkha dolomite were examined for oxygen and carbon isotopes from a well in the Okotoks field at the southern end of the Crossfield trend. The focus of this thesis however was not specifically on the Crossfield but examined the lithofacies within the Wabamun Group on a broader scale. Two other theses are important to this study but do not directly pertain to the Crossfield Member: an MSc. thesis by Kaylor (1988) that described the lithofacies and other diagenetic features of the Crossfield-equivalent Palliser Formation in the southern Foothills west of the Crossfield trend and secondly, a Ph.D by Wenbin (1998). Wenbin (1998) examined the diagenesis and sedimentology of several Upper Devonian formations, including the Wabamun Stettler Formation. The study area of the Wenbin (1998) thesis is southeast of the Crossfield trend and gave a detailed description of evaporites and the geochemistry of pervasive dolomites from this particular area of the Stettler Formation. Wenbin (1998) interpreted the pervasive dolomites as forming from downward refluxing brines.

1.3   Sampling Methods and Procedures

A total of 11 wells were selected for this research (Figs 1.2 & 1.3). The chosen cores were from wells north and west of the Crossfield trend and wells along the entire extent of the Crossfield trend. In January and May 2005, 11 wells were described and photographed at the Energy and Utilities Board (EUB) core research facility in Calgary, Alberta. In conjunction with descriptions and photographs, 173 core samples were collected, with 120 samples from the Crossfield Member and Upper Stettler Formation within the

5
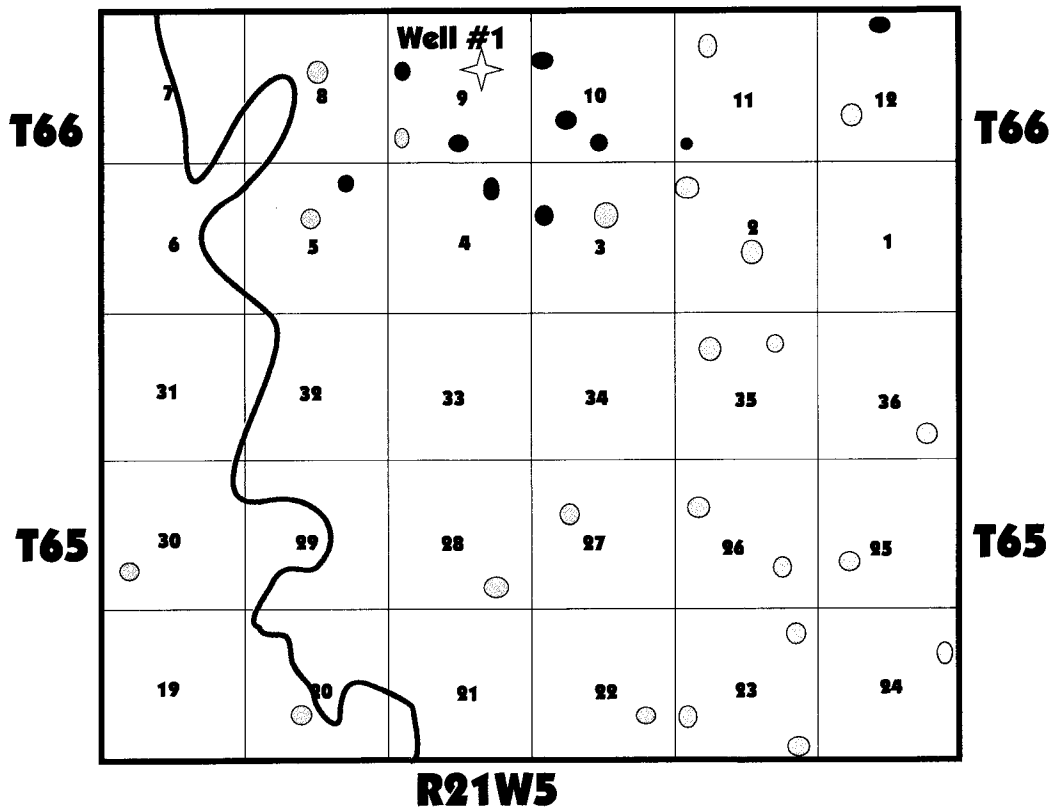
Figure 1.2: Map of Giroux Lake. Study area of well 1 that is not pervasively dolomitised. (Modified from Martin, 2004)

6
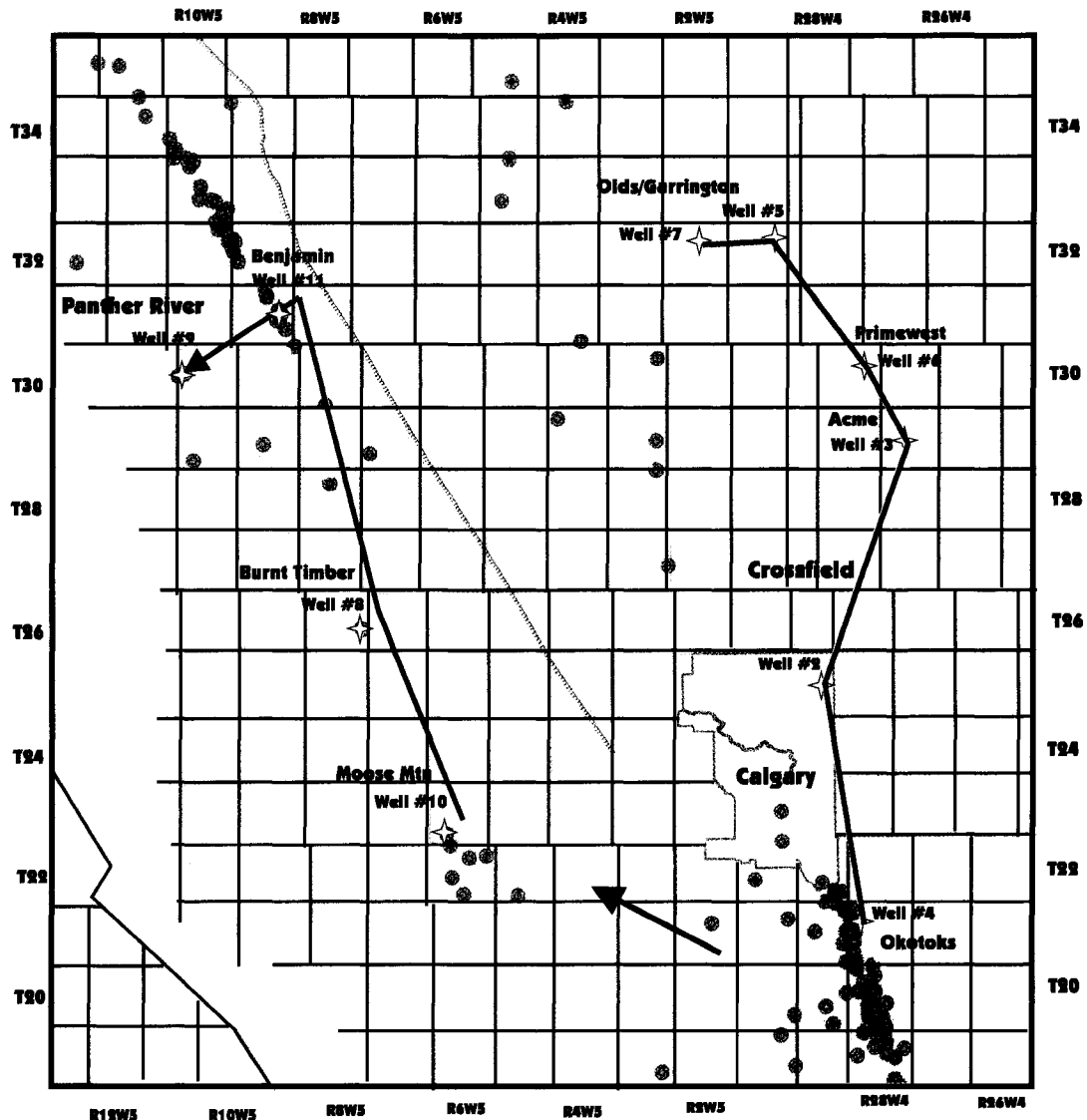
Wells Along Crossfield Trend:
#2 : Jeff Lake/Crossfield : 11-23-25-29W4
#3: Inverness Acme: 13-12-29-27W4
#4: Canoxy Okotoks: 10-18-21-28W4
#5: Amerada Olds: 5-22-32-1W5
#6: Primewest: 10-23-30-28W4
#7: Northstar Garrington: 10-21-32-2W5

Wells Away from Crossfield Trend:
#8: Burnt Timber: 7-23-31-9W5
#9: Panther River: 5-19-30-10W5
#10: Moose Mountain: 10-5-23-6W5
#11: Benjamin: 10-13-26-8W5

(Map modified from Packard, 2005)

Figure 1.3: Map of wells 2-11. Green line represents wells 2-7 along the Crossfield Trend and red line shows wells 8-11 in the Moose Mountain, Burnt Timber, Benjamin Ghost and Burnt Timber areas.

7

Crossfield trend and 53 samples from Crossfield-equivalent strata. Core was sampled for obvious diagenetic features and for specific lithofacies that contained suitable features for geochemical analysis such as primary and secondary cements, clean muds in fenestral and laminated mudstones, and crinoidal grains from fossiliferous samples. The samples were also taken from the entire cored intervals to evaluate any depositional or diagenetic changes with depth.

Of the 173 samples collected, thin sections were made from 127 core samples. After a preliminary examination of the thin sections under a standard petrographic microscope, cathodoluminescence microscopy (CL) was conducted using a Technosyn™ cold cathodoluminescence stage with a 12-18 kV beam and a current intensity of 400-430 μA. Cathodoluminescence microscopy was used to determine zonation in cements and changes in textures and fabrics not visible with a standard petrographic microscope. The thin sections were then stained with a mixture of Alizarin Red-S and potassium ferricyanide following the procedure outlined by Dickson (1966). Staining with this method distinguishes between carbonates according to their composition, with distinctions between ferroan and non-ferroan calcite and dolomite. With staining, ferroan dolomite stains blue and non-ferroan dolomite remains unstained, whereas ferroan calcite stains purple and non-ferroan calcite stains red to pink. Finally, the thin sections were examined under a standard petrographic microscope with a Nikon EPI Fluorescence™ stage attachment for the description of lithofacies, diagenetic features and cements, porosity types, and overall textural relationships. The Nikon EPI Fluorescence™ attachment was also used for distinguishing textural characteristics and for analysing features in cements such as zonation and possible recrystallisation fabrics.

Powdered samples of dolomite, calcite and anhydrite were selected for stable and radiogenic isotope analysis and extracted from core samples using a microscope mounted drill assembly. A total of 82 samples of dolomite and calcite were chosen for oxygen and carbon isotope extractions using the chemical separation method of Al-Aasm et al. (1990). The powdered samples were reacted *in vacuo* with 100% pure phosphoric acid (H_3PO_4) for a minimum of four hours at 50°C for dolomite extraction and 25°C for calcite. The CO_2 gas that was produced during the reaction was then analysed for isotopic ratios on a Thermo Finnigan DeltaPlus isotope ratio mass spectrometer (IRMS) at the University of Windsor. Carbon and oxygen isotope values are given in per mil (‰) relative to the VPDB (Vienna PeeDee Belemnite) standard. The overall precision for the analysis was 0.03 ‰ for $\delta^{13}C$ and 0.07 ‰ for $\delta^{18}O$.

8

For sulphur isotope ($\delta^{34}S$) extractions, 15 powdered samples of primary and diagenetic anhydrite and two samples of native sulphur were selected for analysis. The extractions were conducted at the University of Ottawa using a VarioEL III elemental analyser and flash combusted at 1800°C using helium as a carrier gas. The SO_2 gas produced was then analysed on a Thermo Finnigan DeltaPlus isotope ratio mass spectrometer (IRMS). The sulphur isotope values are reported in per mil (‰) relative to the CDT (Canyon Diablo Troilite) standard and have an overall precision of ±0.2 ‰ CDT.

A total of 17 powdered samples of dolomite, calcite, and anhydrite were selected for strontium ($^{87}Sr/^{86}Sr$) isotope analysis. Strontium isotopic ratios were analysed in a static multi-collector mode with Re filaments with standard references of NBS and ocean water. The strontium isotope values were normalised to $^{87}Sr/^{86}Sr$ = 8.375209 with the mean standard error for NBS-987 of 0.00003.

9

Chapter II
Regional Framework
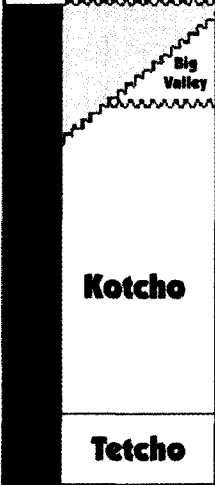
2.1 The Wabamun Group in the Western Canada Sedimentary Basin (WCSB)

Sedimentation in the Famennian Wabamun Group of the Western Canada Sedimentary Basin is considered to represent an overall regressive sequence with several important episodes of transgression (Halbertsma, 1994). The Wabamun cycle was initiated by an increase in the rate of relative sea-level rise that resulted in marine flooding across most of Alberta. As part of the Kaskaskia sequence explaining transgressive/regressive patterns, two major marine transgressions occurred during the Famennian (Richards, 1989; Price, 1994). The first transgression resulted in the development of the stromatoporoid/gastropod carbonates of the Crossfield Member of the Stettler Formation in the southern part of Alberta. In central/northern Alberta, equivalent carbonates to the Crossfield Member were deposited as the Normandville sequence in the Peace River Arch area. The second major transgression resulted in the deposition of open marine, fossiliferous limestones (Big Valley Formation) over much of Alberta (Burrowes and Krause, 1987), which has been eroded north of the Peace River Arch but is observable in the surface and subsurface of central and southern Alberta (Halbertsma, 1994).

This first of the major transgressions occurred after the high sedimentation and infilling associated with the deposition of the underlying Winterburn Group (Fig 2.1). The infilling of the Western Canada Sedimentary Basin (WCSB) during the deposition of the Winterburn Group, resulted in a fairly uniform topography with the exception of the topographic high of the Peace River Arch in the north of Alberta (Stoakes, 1992). Partly as a result of a lack of precursor topography, the Famennian Wabamun Group in the subsurface of the southern Foothills of Alberta comprises a series of both evaporitic (in the south) and open shelf lithofacies that are deposited on a succession of fairly monotonous carbonate ramps that gently dip and deepen westward and northward. The thickness of the Wabamun Group ranges from approximately 150 m in southern Alberta to over 500 m in sections of the Rocky Mountains of Alberta (Andrichuk, 1960).

Strata of the Wabamun Group generally consist of relatively shallow marine bioclastic and peloidal limestones in southeastern sections of Alberta and mud-rich, burrowed pelletal limestones to grainstones in northwestern Alberta (Burrowes and Krause,

10

Period	Belyea and McLaren, 1962	DeWit and Mclaren, 1950	Halbertsma and Meijer-Drees, 1987	Andrichuk, 1960	Alberta Petroleum and Natural Gas Conservation Board, 1956	Wonfor and Andrichuk, 1956
Carbon-iferous	Banff	Banff	Banff	Banff	Banff	Banff
	Exshaw	Exshaw	Exshaw	Exshaw	Exshaw	Exshaw
Upper Devonian		Costigan	Big Valley	"Upper"	Big Valley	Big Valley
		Upper Morro	Upper Cardinal Lake	"Upper Middle"		
	Kotcho		Lower Cardinal Lake			Stettler
		Black Band	Normandville	"Lower Middle"		
		Lower Morro	Whitelaw			
	Tetcho		Dixonville	"Basal"		
	Trout River	Alexo	Winterburn			Crowfoot

Figure 2.1: Stratigraphy of Alberta and B.C. - Study area (Upper Stettler & Crossfield) in red. (Modified from Halbertsma, 1994)

11

1987). The pelletal and peloidal packstones to wackestones of Wabamun reservoirs in central and northern Alberta are pervasively dolomitised (Green and Mountjoy, 2005). Pervasive dolostone intervals are also prevalent in the southern regions of the Wabamun Group. Burrow mottling is another common feature observed in the Wabamun strata of the Alberta Basin and in the Palliser equivalent strata of the Rocky Mountain Foothills (Kaylor, 1988; Kent, 1994).

2.2 Stratigraphy

The subsurface Wabamun Group in southern Alberta has been subdivided into two major units by Wonfor and Andrichuk (1956): the upper (more open marine) Big Valley Formation which consists of argillaceous and fossiliferous limestones and shales (Johnston and Chatterton, 2001) and the lower (more evaporitic) Stettler Formation. The Stettler Formation was further classified by Andrichuk (1960) into four units which divided the formation into the evaporites and marine carbonates below the Crossfield Member from the evaporites above this member, all overlain by the Big Valley Formation, which in turn, is unconformably overlain by the Exshaw shale. This sharp unconformity between the units is indicated by a distinct signature on gamma ray logs that were conducted for a study by Geldsetzer and Meijer Drees in 1984.

2.2.1 Stettler Formation

The Stettler Formation in central/southern Alberta overlies the silty strata of the Graminia Formation. Between the two formations is a gradational contact that resulted from a reworking of the Graminia strata during the Wabamun transgression (Halbertsma, 1994). The shallow water carbonates of the Stettler Formation interfinger with the Besa River shales farther eastward and represent a ramp-style setting (Moore, 1989a). In general, western portions of the Stettler Formation consist of predominantly open-marine limestone (Eliuk and Hunter, 1987) and grade into evaporite-dominated sediments farther southeastward, particularly anhydrites and gypsums, with halite deposits in southwestern Saskatchewan. The Stettler Formation in central/southern Alberta is divided into the Upper Stettler Formation and the Lower Stettler Formation, both of which consist of laminated and nodular anhydrites and anhydritic dolomudstones interpreted to be of subaqueous hypersaline origin (Martindale et al., 2004).

12

2.2.2 Crossfield Member

The Crossfield Member is a porous wedge-shaped unit within the Stettler Formation. In early research by Metherell and Workman (1969) the unit is described as a shallow shelf deposit between open marine sediments of the Stettler Formation to the west and evaporitic, supratidal/intertidal sediments to the east. The unit was further divided into three zones that included an algal base underlying a stromatoporoid/gastropod bank, which is in turn, overlain by another algal bank. The Crossfield Member occurs in roughly a north-south trending belt that varies in thickness from 0 m to over 25 m thick from the Olds/Garrington region in central/north Alberta to the Okotoks in the south (Martindale et al., 2004). Along the eastern edges of the unit, the thickness varies from 15-5 m and in the Acme, Gladys, and Irricana pools (Martindale et al. 2004). The western depositional edges contain the main producing pools (Crossfield East and Okotoks) and the thickness of the unit varies from 15 – 25 m and consists of shallowing-upward cycles of subtidal origin. The Crossfield Member is capped by laminated mudstones (similar to that of the Stettler Formation surrounding the Crossfield Member) (Martindale et al., 2004). It has been determined that the sediments along the eastern edge are of a different age than the sediments along the western margin, and this interval (termed the McDonald Member) is believed to represent a second major transgression of marine waters during the deposition of the Wabamun. The sediments deposited are similar to those of the Crossfield Member, and are of subtidal to peritidal in origin (Martindale et al., 2004).

2.2.3 Palliser Formation

The Palliser Formation that is exposed in the Alberta-British Columbia Front Ranges is the equivalent of the subsurface Wabamun Group in south-central Alberta. Palliser Formation outcrop extends from northwestern Montana to northeastern British Columbia, and similar to the subsurface Wabamun Group, the unit thickens westward (Johnston and Chatterton, 2001). With the exception of the Rocky Mountain Trench area (about 100 m thick), the thickness ranges from about 300 m in the Foothills and Front Ranges to over 600 m in the western Front and Main Ranges of the Rocky Mountains. The Palliser Formation is subdivided into two members: the basal Morro and the overlying Costigan. These units correspond to the Stettler Formation and the Big Valley Formation of southern Alberta respectively (Halbertsma, 1994). Underlying the Morro carbonates is a major unconformity wherein the Morro carbonates overlie Famennian Sassenach sandstones in the southern

13

Rocky Mountains and Frasnian Simla limestones in the more northern areas exposed in outcrop (Halbertsma, 1994).

2.3   Regional Structure of the Western Canada Sedimentary Basin (WCSB)

Along with the eastern Canadian Cordillera, the Western Canada Sedimentary Basin (WCSB) consists of two major sedimentary basins, the Alberta Basin and the cratonic Williston Basin that are separated by the northeast-trending Bow Island Arch (a slight topographic high during the Late Devonian) (Wright et al., 1994).

At the end of the deposition of the Winterburn Group and prior to the deposition of the Famennian Wabamun Group, the WCSB throughout the Alberta Basin was infilled with sediments with relatively low relief (Stoakes, 1992). Significant tectonic features present in the Late Devonian during the deposition of the upper Kaskaskia sequence was the topographic high of the Peace River Arch [although there is no evidence that it was tectonically active during the deposition of the Stettler Formation (Halbertsma, 1994)], as well as the north-south trending Prophet Trough and the cratonic platform (Richards 1989).

The Peace River Arch was a prominent east-northeast trending topographic high through to the Late Devonian and a faulted basin known as the Peace River Embayment from the Mississippian to Permian (Wright et al., 1994). The Prophet Trough was named for the downwarped and downfaulted western margin of North America during the Late Famennian and Early Tournaisian of the Carboniferous (associated with the Antler Foreland Basin) with periods of widespread block faulting and loading and subsidence associated with the Antler Orogeny (Richards, 1989).

Throughout most of the Paleozoic, much of the western margin of the continental margin of North America was a passive continental margin accumulating miogeoclinal sediments and although deformation occurred during orogenic events, the miogeocline fold and thrust belt did not develop until the Cordilleran orogeny beginning in the Jurassic. At the present time, the western boundary of the WCSB consists of exposed and deformed sediments of the ancestral North American margin and the eastern limits of the allochthonous terranes accreted to the North American margin (Wright et al., 1994). The Cordilleran Orogeny during the Jurassic through Early Tertiary resulted in the accretion of oceanic-arc related crust to western Canada with associated imbrication, shortening, and metamorphism of the pre-accretionary miogeoclinal wedge of western Canada (Ross et al., 2005). Regional facies in the foreland basin east of the orogen, including Upper Devonian strata, must

14

therefore be considered in the context of altered spatial distribution of depositional and diagenetic facies. Due to crustal shortening and the structural juxtaposition of once distant sediments or units, each thrust sheet must be palinspastically restored to its depositional position prior to episodes of extension and compressive deformation (Erickson et al., 1994). As a result of the structural complications associated with periods of compression and extension, thickness trends for the Wabamun Group in the Alberta Basin are not projected into the disturbed belt, making it difficult to determine original thicknesses and depths (Halbertsma, 1994).

15

Chapter III

Sedimentology of the Upper Stettler Formation and Crossfield Member

3.1   Introduction

The sedimentology of the Crossfield Member and Upper Stettler Formation will be discussed using the concept of facies analysis. Facies are based on similarities in lithology and depositional structures within a rock unit and how these characteristic features are spatially altered both vertically and laterally within a succession (Walker, 1992). The relationship both between individual facies and within successions of facies will be used in the development of a depositional model for the Upper Stettler Formation and Crossfield Member.

3.2   Facies

The definition of a facies is that of a body or packet of a sedimentary rock with distinctive features from those of other facies (Tucker, 2001). Different features are used to separate units of rocks into specific facies, and these include the basic lithology and colour of the unit, depositional textures and structures, grain sizes and fossil content and abundance (Tucker and Wright, 1990). Facies within the Upper Stettler Formation and Crossfield Member were determined both through the examination of core and detailed petrographic analysis of thin sections. The facies within the study area are for the most part, interpreted to be dolomitised limestones and in rare cases, limestones. As a result of the pervasive dolomitisation of the area, the precursor fabrics of some of the facies have been obliterated, making a determination of the original depositional fabrics difficult to impossible. In these cases, the facies that have been significantly affected by non-mimetic dolomite replacement have been described as dolostones.

The limestone classification scheme used in the description of the limestone facies is that of Dunham (1962) and includes the subsequent modified versions of Embry and Klovan (1971) and Wright (1992). Based on this classification scheme, a number of facies have been identified and described for both the Upper Stettler Formation and the Crossfield Member. These facies include: mudstones, peloidal mudstone-wackestones, peloidal (fenestral) grainstones-packstones, bioclastic floatstone-rudstones, and stromatoporoid

16

floatstones. These major facies are further subdivided into other subfacies that will be discussed in the following sections.

3.2.1 Mudstones/Wackestones

Hand samples of mudstones vary in colour from a light to medium grey and mottled dark brown to tan. The mudstones have variable depositional fabrics including nodular, laminar, massive, burrowed, and peloidal fabrics. Nodular (anhydritic) mudstones are prevalent throughout the Upper Stettler sediments in association with both anhydrite and gypsum but are less significant within the Crossfield sediments. If laminations are present, they are typically thin, wavy and associated with evaporites or algal growth. Bedding is on the scale of tens of centimetres to rare millimetre-scale beds. Fossils are not prevalent in the majority of the laminated mudstone subfacies with the exception of microbial mats and algae. In burrowed and peloidal mudstones, fossils in decreasing order include calcispheres, ostracodes, brachiopods, stromatoporoids, and gastropods.

There are several types of porosity identified in the mudstones facies, including interparticle, intercrystalline, moldic, fracture, pinpoint, and most dominantly, fenestral porosity. Of these types, primary porosities include growth framework in areas of abundant stromatoporoid growth, fenestral (and birdseye structures) in mudstones with microbial growth, intraparticle (intraskeletal) porosity in bioclastic mudstones, interparticle porosity in peloidal fabrics and finally, porosity as a result of burrowing episodes. Both the primary and secondary porosity types (with the exception of intercrystalline porosities associated with pervasive dolomitisation and rare vuggy porosity resulting from leaching events) have been occluded by episodes of cementation, and as a result, the mudstones appear relatively tight and non-porous. In particular, both the laminated and more massive (fissile) mudstones are the most non-porous of the mudstones, with the exception of extensively fractured areas within the massive mudstone subfacies.

3.2.1.1 Mudstone/Wackestone Facies

1) Nodular mudstones consist of two types. The first type (already mentioned) includes the nodular fabric created through the development of distinct nodules (with crenulated edges) of anhydrite in a mudstone matrix (Plate 1-4, 1-5). This type of mudstone is dominant in the Upper Stettler Formation units and occurs in wells 1 through 11.

17

Nodules are generally ivory to grey in colour, relatively translucent, and are mostly composed of anhydrite cement (and in some cases, minor diagenetic gypsum). The mudstone matrix surrounding nodules is pale grey or light brown to tan. The presence of soft sediment deformation (enterolithic folding) of surrounding muds due to the displacive nature of the anhydrite crystallisation indicates that the development of nodules occurred relatively early in the depositional process (pre-lithification). This primary nodular anhydrite is a significant facies in the study area and occurs in association with both massive and laminated sediments. The nodular fabrics in most of the more massive mudstones is however primarily of a secondary nature and tends to occur as a void-filling cement (Plate 1-3), whereas when in association with laminated mudstones, it is of a primary nature. The second type of nodular mudstone is the development of nodules as a result of chemical compaction and the development of stylobrecciated fabrics. This type of mudstone is not as abundant as the nodular (anhydritic) mudstone but is often observed in wells 3 and 5 in the Crossfield trend and is significantly more abundant in wells 9 and 10. Unoccluded porosity in the primary nodular (anhydritic) mudstones is rare and occurs as a result of diagenetic processes in the form of fractures. Minor vuggy porosity occurs in association with vug-filling cements in the more massive nodular mudstones with secondary cement occlusion. Within the second type of nodular mudstone associated with chemical compaction features porosity is minor, with secondary porosity identified in association with diagenesis. The most significant porosity is vuggy porosity that occurs as small vugs along stylolites created by dissolution and leaching episodes and subsequently, partly-occluded with secondary cements. In the sediments surrounding nodules there is also fracture, interparticle, and intercrystalline porosity in pervasive dolomite fabrics.

2)   Laminated (& algal) mudstone occurs mostly in the Upper Stettler Formation and to a lesser degree, in Crossfield Member units (Plate 2-1, 2-2). The laminated mudstones are grey to tan in colour. Laminations are generally thin (millimetre scale) and are relatively planar to slightly undulose in appearance. As previously mentioned, laminated mudstones are often identified in association with nodular (anhydritic) mudstones. With the exception of algal growths and the development of microbial mats, there are no other types of bioclastic material identified in the laminated mudstones. The growth of microbial mats in laminated mudstones is relatively minor, occurring as thin laminations within laminated muds and evaporites. The growth of algae is also apparent in massive

18

and peloidal mudstones and forms a thrombolitic pattern associated with shallow marine waters. In terms of primary porosity, the laminated mudstones are tight and non-porous with rare fenestral porosity in the vicinity of microbial mat growth. In this facies, secondary porosity includes fracture and intercrystalline porosity. Minor fracture porosity occurs in cross-cutting fractures through laminated sediments, and is partly occluded with secondary cements. Intercrystalline porosity is the most abundant secondary porosity and has developed between dolomite crystals in pervasive dolomite fabrics and between secondary diagenetic gypsum crystals in association with primary laminated anhydrites. Since the precursor fabric is tightly-woven, the pervasive dolomite tends to mimic this texture, explaining the minor occurrence of this porosity, such that intercrystalline porosity is low in this facies, and is significantly more apparent in fabrics with coarser precursor grain sizes.

3)   Peloidal bioclastic mudstone/wackestone (Plate 2-3) is most abundant in wells 1, 8, 10 and 11. Since well 1 has not been pervasively dolomitised, the precursor fabric is relatively intact and identification of bioclasts is uncomplicated. This facies is destructively dolomitised however in wells 8, 10, and 11 where pervasive dolomitisation has occurred, and as a result, were identified using a white card technique (Folk, 1987). Pervasive dolomitisation resulted in the destruction of some features within these wells, and with the exception of well 11 where most of the precursor fabric has been diagenetically altered, the dolomitisation mimics some of the original textures and bioclasts (ghost fossils), allowing for identification of the facies. Peloidal bioclastic mudstone/wackestones range in colour from light brown to dark grey. Peloids in this facies are generally rounded, suggestive of a fecal or microbial origin (Flügel, 2004). To a lesser degree there are also mud peloids that have developed from the reworking of sediments that are larger (up to 1mm) irregularly shaped grains that are deposited as poorly sorted sediments. Mud peloids in this facies and in the peloidal grainstone/packstone facies are commonly identified with intraclastic material deposited in an intertidal setting. The presence of bioclasts within this facies is variable, ranging from a common to rare occurrence. Fossils (in order of abundance) include: calcispheres, ostracodes, algae, echinoderms (crinoids), brachiopods, gastropods, rare bivalves, and unidentified skeletal fragments. Also present within this facies are mottled burrowed sections that have been selectively dolomitised. Primary porosity includes interparticle porosity within the peloidal fabric and rare fenestral porosity occluded with calcite

19

PLATE 1: Lithofacies

(1)   Core photograph of burrowed and nodular mudstone: Well location 10-13-26-8W5 (3582.4m). Red arrow indicating up direction. Black arrow pointing to burrow structures.

(2)   Photomicrograph of burrowed fabric with Epi-Fluorescence: Well location 5-22-32-1W5 (2595.6m) Scale = 100μm.

(3)   Core photograph of massive mudstone with secondary anhydrite: Well location 5-22-32-1W5 (2589.1m). Red arrow indicating up direction. (A) for anhydrite in nodules.

(4)   Core photograph of nodular and laminated mudstone: Well location 10-18-21-28W4 (2616.4m). Red arrow indicating up direction. (A) for anhydrite in nodules

(5)   Photomicrograph of anhydrite in nodular mudstone (xpl): Well location 13-12-29-27W4 (2254.5m) Scale = 100μm. (A) for anhydrite in nodules.

(6)   Core photograph of burrowed peloidal mudstone: Well location 10-5-23-6W5 (2583.7m). Red arrow indicating up direction.

20

Plate 1 Lithofacies

21
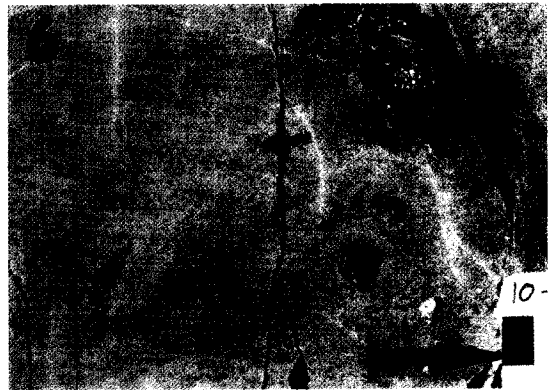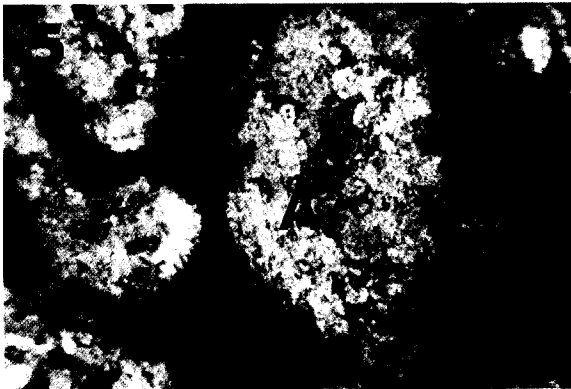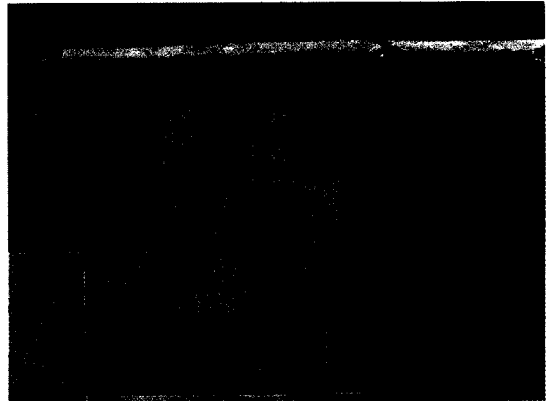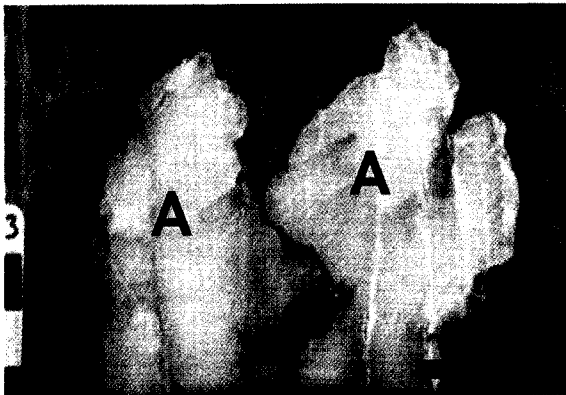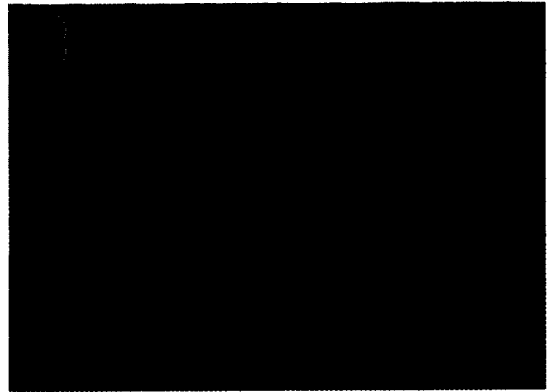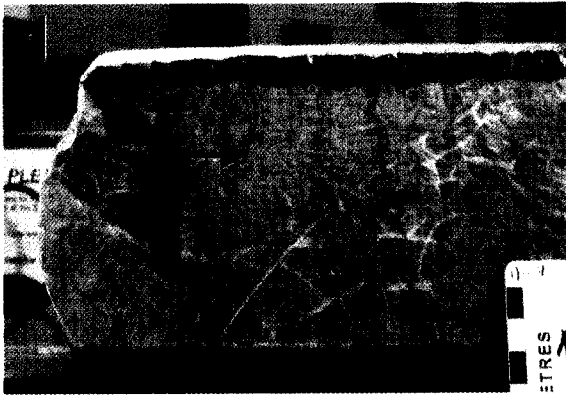
PLATE 2: Lithofacies

(1)   Core photograph of algal mudstone: Well location 5-22-32-1W5 (2574.4m). Red arrow indicates up direction.

(2)   Core photograph of laminated mudstone: Well location 13-12-29-27W (2247.2m) Red arrow indicates up direction. Black arrows indicating laminae of anhydrite.

(3)   Photomicrograph of fenestral bioclastic mudstone (ppl) (scale = 100µm): Well location 10-9-66-21W5 (2400.5m). Yellow arrow indicating calcite-occluded fenestrae.

(4)   Core photograph of fenestral peloidal grainstone: Well location 10-23-30-28W4 (2397.3m). Red arrow indicates up direction. Black arrow showing fenestrae. Small Round fossils are crinoid fragments.

(5)   Photomicrograph of peloidal grainstone fabric (ppl) (scale = 100µm): Well location 10-9-66-21W5 (2408.5m). Sparry calcite between dominantly round peloids. Peloids indicated by yellow arrows.

(6)   Photomicrograph of peloidal fabric with intraclasts in packstone matrix with Fluorescence. Peloids indicated by yellow arrows.
(EpiFl) (scale = 100µm): Well location 10-21-32-2W5 (2750.4m)

22

Plate 2 Lithofacies

23
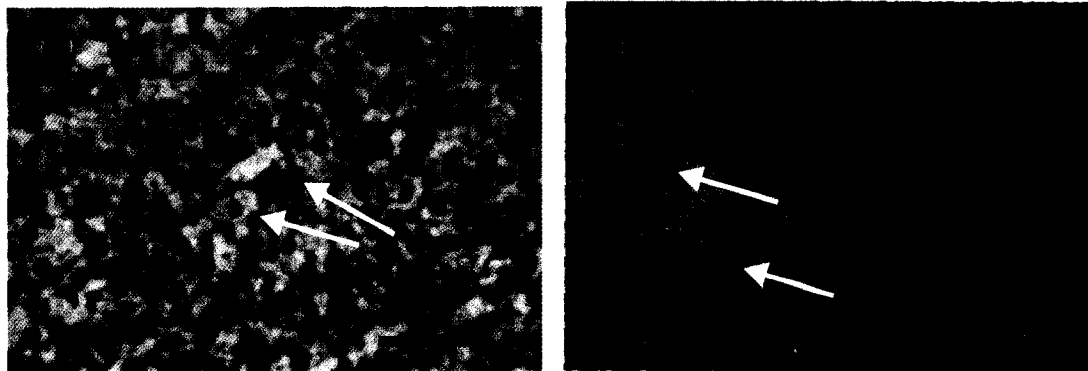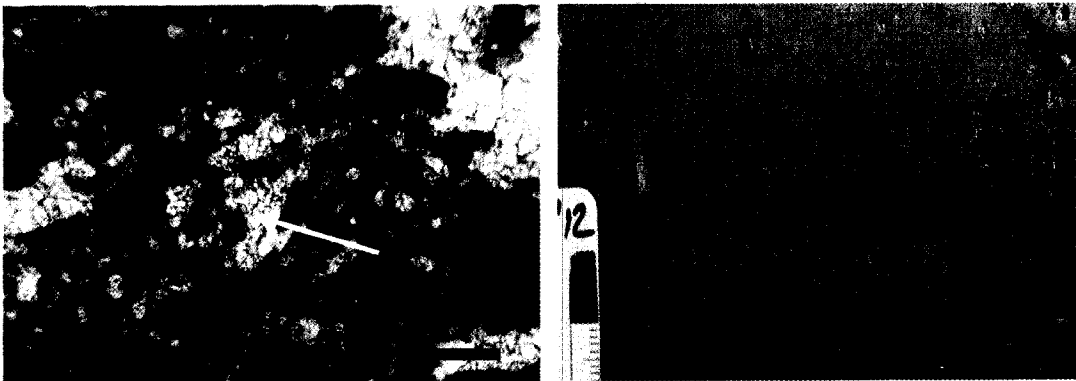
cements. Secondary porosity occurs mostly as intercrystalline porosity between pervasive dolomite crystals and minor amounts of vuggy and moldic porosity associated with dissolution that are for the most part occluded with secondary cements.

4) Fenestral mudstone is massive and non-skeletal. Fenestrae are irregular to laminoid and abundant to minor in occurrence. This facies is pervasively dolomitised, grey and tan through medium brown in colour and occurs in wells 2 through 7. With the exception of well 2, the fenestrae in wells 3 through 7 are 70-80% occlusion-free of secondary cements. In well 2, the larger (>1.25 mm) fenestrae are cemented with secondary anhydrite/gypsum and calcite cements and the fabric in sections appears weakly burrowed. Fenestral porosity in the most abundant porosity type in this facies. Secondary porosity types are mainly interparticle (between dolomite crystals of pervasive fabric), fracture and rare vuggy porosity. Vuggy porosity occurs mainly in well 3, and is associated with dissolution seams.

5) Burrowed mudstone is massive to peloidal (Plate 1-1, 1-2, 1-6) and is commonly mottled medium brown through greenish - tan in colour. As a separate facies, massive burrowed mudstones are a minor occurrence in wells 2-7 and occur to a slightly greater degree in wells 8-11. Mottled (burrowed) fabrics are also apparent to varying degrees in all of the peloidal and bioclastic mudstone facies. Dolomitisation events have contributed to the mottled appearance of the bioturbated fabric through the creation of a lighter colour (greenish-tan) replacement of burrows in comparison to the surrounding mudstone matrix. The mottled colour may be partly related to the finer grain-size fill of the burrowed areas in comparison to the surrounding micrite that resulted in the selective dolomitisation of burrow fills. Discrete burrows in the more massive and peloidal (bioclastic) grainstone/packstones have been interpreted to be from the Thallasinoides (Erickson et al, 1994) and Paleophycus (Packard and McNab, 1994). Besides dolomitised primary burrow porosity, other porosities are secondary and include: vuggy, fracture, and intercrystalline (between dolomite crystals of pervasive fabric).

3.2.2 Packstone/Grainstones

The only units classified as a packstone/grainstone are peloidal (fenestral) packstone/grainstones (Plate 2-4, 2-5, 2-6). This facies is one of the most abundant facies within the Upper Stettler Formation and Crossfield Member and is identified in all the wells 1 through 11. The amount of peloidal material within the facies is variable ranging from

24

<10% to > 50% and some of the units within this classification contain minor bioclastic material. Fenestral porosity is also variable, ranging from weakly fenestral to moderately fenestral.

3.2.2.1 Packstone/Grainstone Facies

Peloidal (fenestral) grainstone/packstone is dominantly pale brown (tan) through light to dark grey in colour. Peloids are mainly fecal pellets (round and rod), mud peloids (in association with intraclasts) and to a rarer extent, of clotted microbial origin. The complete micritisation of fossil fragments has also contributed to the development of the peloidal fabric. Fenestrae are variable in occurrence throughout this facies ranging from <10% to 60-70% of the overall fabric. The fenestrae are irregular shaped and with the exception of wells 5-7, are mostly occluded with secondary calcite and anhydrite cements. In units with bioclasts (wells 1, 2 and 8), the order of abundance for fossils is: echinoderms (crinoids), brachiopods, calcispheres, and rare bivalves. Porosity in this facies includes fenestral and interparticle (within peloidal matrix) primary porosities, and vuggy, fracture, intercrystalline, and moldic secondary porosities. Vuggy porosity is the most abundant and represents 70% of the secondary porosity in this facies. Vugs are typically occluded with calcite cements and to a lesser degree, anhydrite and dolomite. Microfractures cross-cut units and are typically also occluded with calcite cements.

3.2.3 Floatstone/Rudstones

Two types of facies are identified as floatstone/rudstones: stromatoporoid floatstones and bioclastic floatstone/rudstones (Plate 3: photos 1- 6). Floatstone/rudstones vary in colour from dark to medium brown through tan in hand sample. Fossils include (in order of abundance): Stromatoporoids (tabular and *Labechiid*), echinoderms (crinoids), brachiopods, ostracodes, bivalves, and rare gastropods. Porosities in the two floatstone/rudstone facies include growth framework, pin-point, vuggy, fracture, intercrystalline, intraparticle, and moldic porosity. Identified within both these facies are sections of asphaltene-stained intercrystalline porosity.

25

PLATE 3: Lithofacies

(1)   Core photograph of stromatoporoid (*Labechiid*) floatstone in mudstone matrix: Well location 13-12-29-27W4 (2258.7m). Red arrow indicates up direction. Black arrow indicates stromatoporoid framework. (A) = Anhydrite.

(2)   Core photograph of bioclastic rudstone: Well location 10-18-21-28W4 (2639.5m). Red arrow indicates up direction. Bioclasts indicated by yellow arrows.

(3)   Core photograph of bioclastic floatstone: Well location 10-21-32-2W5 (2756.3m). Red arrow indicates up direction.

(4)   Photomicrograph of stromatoporoid in mudstone/wackestone matrix with fluorescence (EpiFl) (scale = 100μm): Well location 10-9-66-21W5 (2403.2m). Black arrows indicate stromatoporoid framework. (C) = blocky calcite cement.

(5)   Photomicrograph of bioclastic rudstone with crinoid spine in centre (Cr) (xpl) (scale = 100μm): Well location 5-19-30-10W5 (2606.0m)

(6)   Photomicrograph of crinoidal floatstone (ppl) (scale = 200μm): Well location 11-23-25-29W4 (2670.6m). (Cr) = Crinoid.

26

Plate 3 Lithofacies
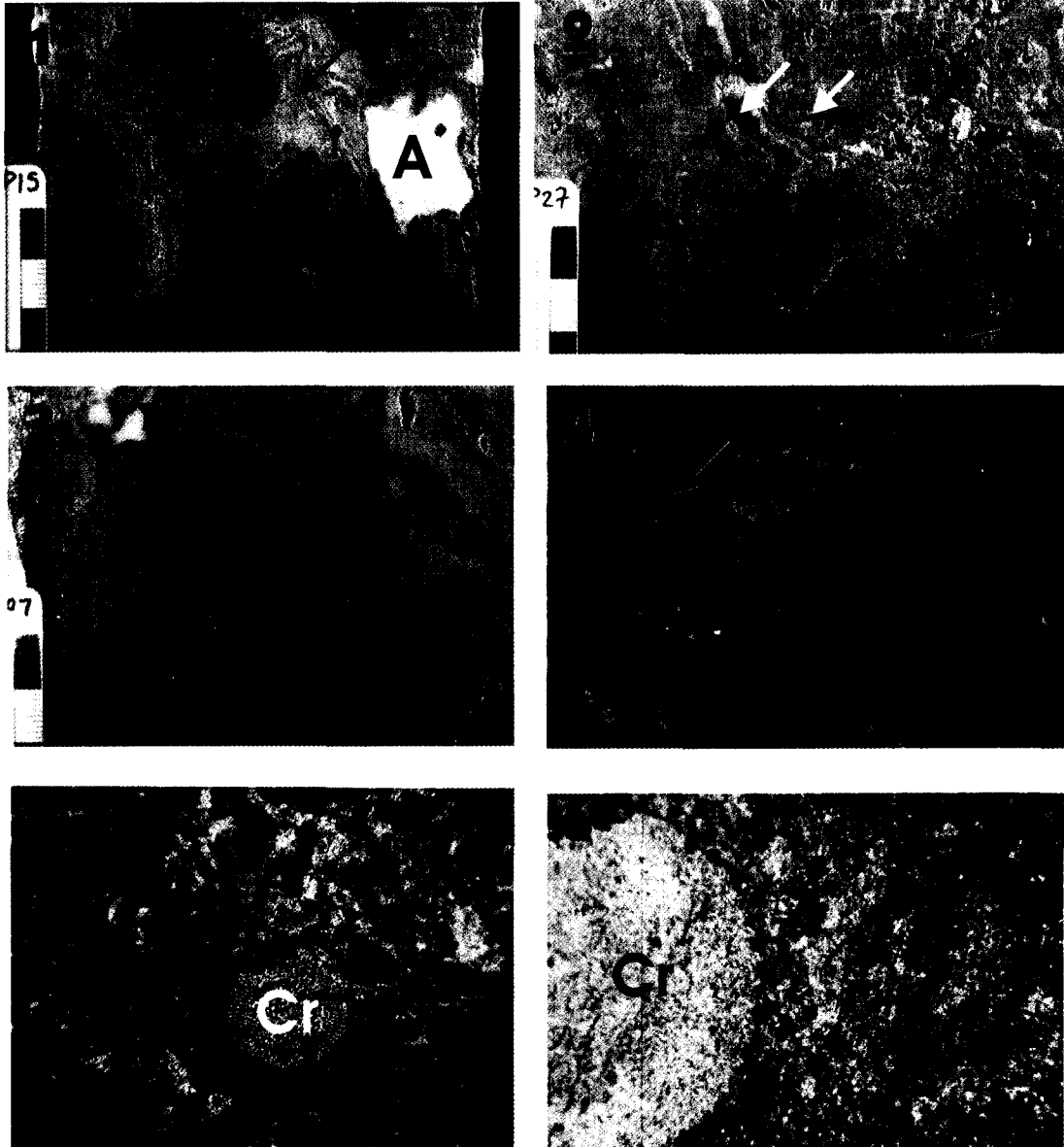
3.2.3.1 Floatstone/Rudstone Facies

1) Stromatoporoid floatstones are most significant in wells 1, 2, 9 and 10.
    Stromatoporoids form a bindstone structure in a mudstone matrix. Colour in hand
    samples range from medium to dark brown and tan. Along with the stromatoporoid
    framework of tabular and irregular (*Labechiid*) stromatoporoids, these floatstones
    typically also contain minor bioclasts of echinoderm (crinoids) and rare bivalves. Other
    identifiable features are intraclasts within the mudstone matrix. Porosity is this facies
    includes growth framework and pin-point (with calcite cement between stromatoporoid
    fabric), intercrystalline in pervasive dolomite fabric, vuggy, and fracture porosity. Large
    (mm-scale) vugs are partly occluded with blocky calcite cements and smaller vugs are up
    to 70% occlusion-free. Microfractures are also occluded with secondary calcite and
    dolomite cements.

2) Bioclastic floatstone/rudstone is identified in wells 1-4 and 8-10. Hand samples are
    grey and dark brown to tan in colour. This facies contains both peloidal (fecal pellets)
    and intraclastic grains surrounded by calcite spar cements. Within larger (>1mm)
    intraclasts are fragments of bioclasts and peloids. There is a diverse range of bioclasts
    identified including (in order of abundance): echinoderms (crinoids), brachiopods,
    bivalves, tabular and irregular stromatoporoids, ostracodes, foraminifera, gastropods, and
    rare coral. Also present in this facies are thrombolitic stromatolites and minor burrow
    structures. Primary porosity types are growth framework, intraparticle, and minor burrow
    porosity. Growth framework and intraparticle porosities are occluded to partly-occluded
    with secondary cements of calcite and minor dolomite. Burrow sediments are replaced
    with matrix pervasive dolomite. Secondary porosities include intercrystalline (in
    pervasive dolomite matrix) and vuggy porosity, and minor fracture and moldic porosity.
    Subvertical microfractures are mostly occlusion-free or occluded with calcite cements.
    Dissolution-seam associated vuggy porosity is partly-occluded with blocky calcite
    cements. Asphaltene-staining is present in interparticle porosity and along small vugs
    throughout the facies (Erickson et al., 1994).

28

3.2.4 Dolostones

As all facies in wells 2-11 have been pervasively dolomitised, certain units have been classified as dolostones. This dolostone facies includes all of the units that have an unidentified precursor fabric due to the destruction of the original fabric during pervasive dolomitisation episodes. Classified within this facies are also units that have some visible components (such as ghost fossils) that are identifiable but the entire fabric cannot be classified into a specific facies. Dolostones are most abundant in wells 8-11. Units within these wells appear to be more affected by diagenetic alteration and the effects of burial than wells 2-7 in the Crossfield trend. This facies is predominantly light to dark grey and light brown to tan in colour. In terms of porosity, the most abundant porosity types are secondary porosities of fracture and vuggy porosity with minor amounts of breccia porosity. The most abundant fracture porosity is identified in dolostone facies from wells 8-11. Cross-cutting, subvertical fractures (calcite veins) are partly filled with calcite and to a minor degree, dolomite cements. Vugs are occluded with secondary cements of calcite, saddle dolomite, and anhydrite.

3.3 Depositional Model

Shallow marine carbonates deposited in the Alberta Basin are generally of two major geologic settings (Machel and Hunter, 1994); first, a shallow shelf with a shelf margin reef and second, a gently sloping ramp with peritidal to supratidal facies and evaporitic intervals. Different attributes of facies are indicators of depositional processes and their associated environments. Facies can be further grouped into specific zones based on factors such as water energy, fossil assemblages and indicator fossils, textures of sediments and abundance of micrite, and porosity (Machel and Hunter, 1994). The identified facies in the Upper Stettler Formation and Crossfield Member are characteristic of a sloping ramp from peritidal to shallow subtidal carbonates with restricted supratidal sediments and stromatoporoid mounds.

Five main mudstone facies were identified: nodular (anhydritic) mudstones, laminated (dolo) mudstones, peloidal bioclastic mudstone/wackestones, fenestral mudstones and burrowed mudstones. One packstone/grainstone facies was identified as fenestral peloidal grainstone and two facies were identified as floatstone/rudstones. The two floatstone/rudstone facies are stromatoporoid floatstones and bioclastic floatstone/rudstones.

29
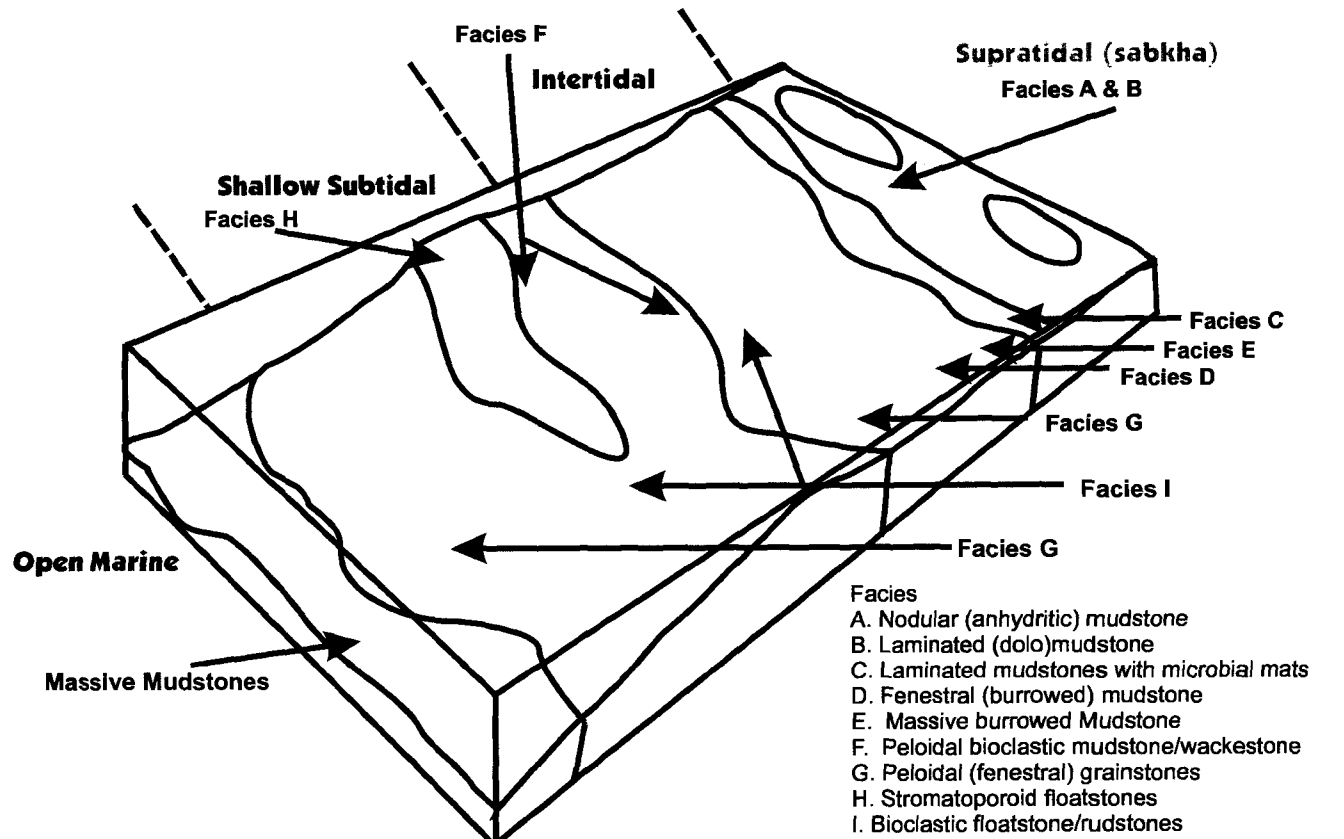
Figure 3.1: Depositional Model For
Upper Stettler Formation and Crossfield Member
with division of facies into supratidal/intertidal/shallow subtidal/open marine realms.

Facies F

Intertidal

Supratidal (sabkha)
Facies A & B

Shallow Subtidal
Facies H

Facies C
Facies E
Facies D

Facies G

Facies I

Open Marine

Facies G

Facies
A. Nodular (anhydritic) mudstone
B. Laminated (dolo)mudstone
C. Laminated mudstones with microbial mats
D. Fenestral (burrowed) mudstone
E. Massive burrowed Mudstone
F. Peloidal bioclastic mudstone/wackestone
G. Peloidal (fenestral) grainstones
H. Stromatoporoid floatstones
I. Bioclastic floatstone/rudstones

(Diagram modified from Martindale 2005)

Massive Mudstones

30

Nodular (anhydritic) mudstones developed in supratidal subaqueous environments in association with laminated (dolo) mudstones. Laminated mudstones are typical of upper sabkha sediments and were precipitated in ephemeral ponds or salinas (Martindale, 2005). The laminated mudstones with microbial mat development is also indicative of a supratidal depositional setting (Flügel, 2004) and microbial mats developed in massive (algal) mudstones are suggestive of upper intertidal sediments. Facies with significant fenestral porosity are commonly associated with upper intertidal to supratidal environments. Fenestral (weakly burrowed) mudstone is most likely therefore to be deposited in an upper intertidal setting. Burrowed fabrics are significant in both shallow intertidal muds and subtidal facies. Massive burrowed mudstones were deposited in the intertidal zone and also in shallow subtidal lagoons. The bioclast diversity, weak burrowing and peloidal fabric indicate that the peloidal bioclastic mudstone/wackestone facies is characteristic of lower intertidal to shallow subtidal settings (including shallow lagoonal environments). Peloidal (fenestral) grainstones are deposited in the lower intertidal zone with units in this facies with minor to rare fenestrae , more sandy peloidal grainstones were deposited slightly further seaward in the shallow subtidal. The bioclastic diversity of the bioclastic floatstone/rudstones is typical of a shallow subtidal environment, protected to a certain degree from high energy events but periodically exposed (with a reworking of muds and the development of intraclasts). Stromatoporoid floatstones were deposited in mounds on the gently-sloping ramp with peloidal (mud peloid) grainstones surrounding these in a shallow subtidal environment. On the landward side of the stromatoporoid mounds, shallow lagoons developed where the deposition of the majority of the burrowed, peloidal, and bioclastic facies occurred. Seaward of the stromatoporoid mounds are greenish-grey mudstones deposited in deeper subtidal to open marine depositional settings. These greenish-grey mudstones are massive and are rare in occurrence in the Upper Stettler and Crossfield sediments, and therefore have not been discussed in detail as a separate facies.

31

Chapter IV

Diagenesis of the Upper Stettler Formation and Crossfield Member

4.1   Introduction

Diagenesis is defined as all the processes that affect the character and composition of sediments from just after deposition through to the realm of increased temperature and pressure associated with metamorphism (Morrow and McIlreath, 1990). Diagenetic processes affecting carbonates occurs in the meteoric, marine, and subsurface realms. All of these realms have characteristic pore fluids that affect diagenetic processes such as marine and meteoric fluids near the surface and mixtures of marine-meteoric waters and basinal-derived brines with increasing depth (Moore, 2001). These fluids (along with changes in pressure and temperature with burial) essentially define the characteristic diagenetic features observed in sediments and the changes in porosity and permeability from surface deposition through deep burial processes. Diagenesis is a ubiquitous process and includes all the changes in sediments due to compaction (both mechanical and chemical), cementation, dolomitisation, dissolution and leaching, and recrystallisation.

The Upper Stettler Formation and Crossfield Member have been significantly affected by diagenetic processes. The most dominant processes affecting the study areas are dolomitisation, cementation, and recrystallisation, although other diagenetic alterations of the original precursor fabrics have also occurred. Besides the most dominant diagenetic processes of dolomitisation, cementation, and recrystallisation, sediments have also been altered by both mechanical and chemical compaction, episodes of fracturing, and changes in original primary porosity and permeability characteristics as a result of variabilities in diagenetic fluids, and burial temperatures and pressures. Original fabrics have been affected by changes in pore water chemistry associated with burial diagenesis that contributed to the destructive (mimetic and non-mimetic) replacement of precursor mineralogy. The diagenetic processes or evolution of the sediments in the Upper Stettler Formation and Crossfield Member have been identified using petrographic methods, including Epi-Fluorescence and Cathodoluminescence (CL) microscopy. The following sections describe the diagenetic features identified in the Upper Stettler Formation and Crossfield Member using these petrographic methods.

32

4.2 Micritisation

Micritisation is the process whereby the original fabrics of carbonate grains are altered to cryptocrystalline textures (Reid and Macintyre, 2000). This is a shallow subsurface or seafloor process that involves the boring of bioclastic material by endolithic algae, fungi, or bacteria resulting in the development of holes around skeletal margins (Tucker and Wright, 1990). During the process of micritisation, the holes are then subsequently filled with fine-grained sediments that results in the development of fabrics ranging from micritic envelopes surrounding bioclasts to the complete micritisation of bioclasts. Early micritisation processes have altered bioclastic material in peloidal bioclastic mudstones/grainstones and bioclastic floatstone/rudstones in the Upper Stettler Formation and Crossfield Member. A study conducted by Peterhänsel and Pratt (2001) on the geologically equivalent Palliser Formation suggests that this region (during the Late Famennian) had a prolific increase in microendoliths that obliterated bioclasts (especially crinoids) through processes such as micritisation and encrustation. This early micritisation process is the first type of diagenetic alteration identified in the facies of the Palliser-equivalent Crossfield and Upper Stettler (Plate 4; 1-3). Lithofacies in wells 1-10 have been affected by micritisation processes by the development of micrite envelopes and the infilling of bioclastic material with micrite. The effect of micritisation is not evident in the lithofacies in well 11. This lack of evidence is possibly a result of the extensive dolomitisation and diagenetic alteration that has affected the sediments in this well. The same facies are present in well 11 as in the other wells (1-10), and consequently, micritisation probably also affected the lithofacies in well 11 prior to extensive dolomitisation episodes.

4.3 Neomorphism

Neomorphism is described as the process of mineral transformations occurring in the presence of water and results in the replacement, inversion, or recrystallisation of a carbonate rock (Folk, 1965; Flügel, 2004). Replacement fabrics result from the dissolution of one mineral and the simultaneous precipitation of another. Machel (1997) uses the term 'significant recrystallisation' as an alternate genetic term to explain the changes occurring during recrystallisation processes specifically affecting dolomites/dolostones. This type of recrystallisation occurs relatively late in the diagenetic process for the Upper Stettler

33

PLATE 4: Micritisation and Neomorphism

(1)   Photomicrograph of the effects of micritisation on a gastropod shell (scale = 100μm). Well 10-9-66-21W5 (2410.8m). Yellow arrows showing micritisation.

(2)   Photomicrograph of micritisation of fabric with large intraclast (scale = 100μm). Well 10-23-30-28W4 (2412.2m). Yellow arrow indicating intraclast.

(3)   Photomicrograph of micritised stromatoporoid framework (scale = 50μm).Well 10-9-66-21W5 (2406.1m). Black arrow show stromatoporoid Framework with calcite (c) in growth framework.

(4)   Photomicrograph of gypsum (G) replacing fine laths of anhydrite (scale = 50μm). Well 11-23-25-29W4 (2647.3m). Red arrow shows replacement of anhydrite with gypsum.

(5)   Photomicrograph of etched and dissolved dolomite crystals suggestive of recrystallisation textures (scale = 200μm). Well 5-22-32-1W5 (2589.8m). Red arrow showing dissolved rims, and black etched cores indicated by yellow arrows.

(6)   Photomicrograph of planar-e dolomite showing evidence of recrystallisation with fluorescence (fl) (scale = 100μm). Well location 10-9-66-21W5 (2406.85m). Red arrows show recrystallised dolomite rhombs

(7)   Photomicrograph of planar-e dolomite rhombs with cloudy cores and clear rims under fluorescence (fl) (scale = 200 μm). Well location 7-23-31-9W5. Red arrow indicates recrystallised dolomite rhomb.

34

Plate 4 - Micritisation & Neomorphism
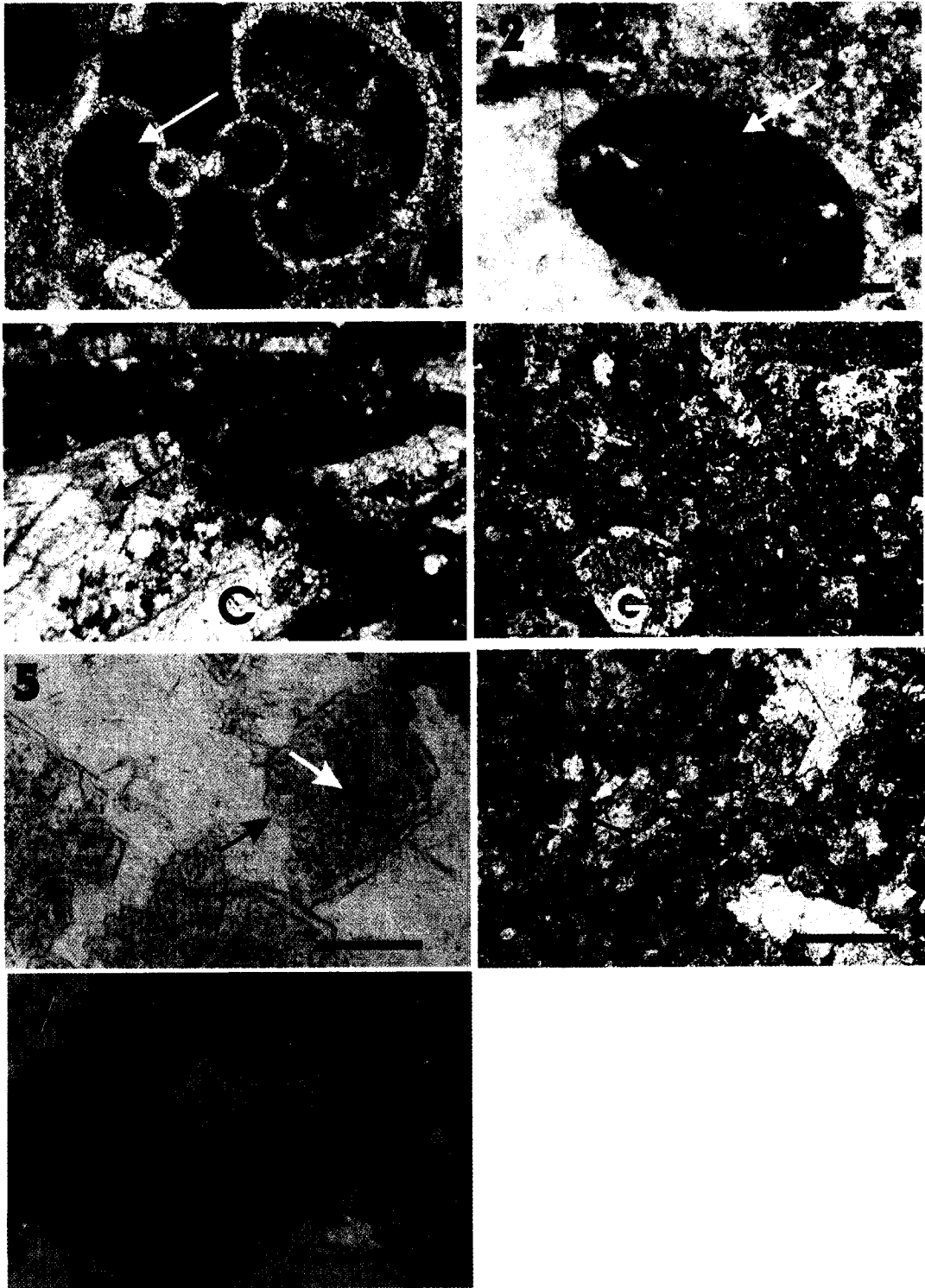
Formation and Crossfield Member and will be discussed in greater detail when dolomitisation processes are examined (plate 4:5-7). There are also other neomorphic processes that have occurred in an earlier context in the diagenetic history of the Upper Stettler Formation and Crossfield Member (plate 4: 4-7). One early neomorphic feature is the formation of neomorphic spar through aggrading recrystallisation. Aggrading recrystallisation (neomorphism) results in crystal enlargement, wherein carbonate minerals increase in size from micrite to spar (Chillingar et al., 1967). In the study area, the development of neomorphic spar is most apparent in grainstone and floatstone/rudstone facies in wells 1-10 but is relatively minor in occurrence. This spar is most prevalent in the peloidal grainstone and floatstone/rudstone facies where peloids and bioclasts can be seen essentially floating within the spar. The spar itself is relatively cloudy, irregular, and of variable-size, distinguishing it from other calcite cements. The process of stabilisation is also an early diagenetic feature in the Upper Stettler Formation and Crossfield Member and is defined as the process whereby unstable minerals invert to a more stable form with the same chemical composition. This process includes the replacement of a mineral with its more stable polymorph such as the alteration of aragonite to calcite or Mg-calcite to calcite (Tucker and Wright, 1990). A widespread example of neomorphism within the Upper Stettler Formation and Crossfield Member, and present within all of the wells, is the transformation of anhydrite to gypsum and gypsum to anhydrite (Plate 4-4). Often seen within gypsum crystals are fragments of anhydrite laths, and to a lesser degree, blocky anhydrite contains remnants of gypsum. This process began relatively early in the diagenetic history of the study area and continued throughout the burial process and occurred further during subsequent episodes of sediment uplift, suggested by the recrystallisation of anhydrite to gypsum with uplift.

4.4   Compaction

Although it has been suggested that chemical compaction is a significantly more important process than mechanical compaction (Wanless, 1979), compaction processes as a whole can produce extensive diagenetic alteration of carbonate sediments. Compaction initially affects carbonates in the shallow subsurface as a result of the stresses associated with an increasing overburden. As sediments are buried, increasing overburden pressure causes the development of mechanical (physical) compaction features. Later in the burial process, chemical (pressure-solution) compaction also begins to affect the buried carbonates

36

(Tucker, 2001). During progressive burial, both mechanical and chemical compaction has occurred within the Upper Stettler Formation and Crossfield Member, resulting in the development of compactional features and an overall decrease in sediment thickness.

4.4.1 Mechanical compaction

The process of mechanical compaction begins during the shallow burial process of carbonates. Mechanical compaction causes the closer packing of grains and the brittle or ductile transformation of grain boundaries within sediments (particularly in grainier samples), and also compresses features such as burrows, pellets, bioclasts and micritic envelopes (Tucker, 2001). In conjunction with the closer packing of grains and the compression of allochems and sedimentary structures, there is also a significant reduction in porosity and permeability. In experiments by Shinn and Robbin (1983), porosity (as a result of grain reorientation and dewatering) in mud-dominated sediments decreased from approximately 70% to 40% with further losses in porosity during subsequent chemical compaction processes. Uncemented, mud-dominated sediments also tend to be more greatly affected during very early compaction as sediments dewater and grain-supported sediments by contrast, may have a slightly different compactional history (Moore, 2001).

Within the Upper Stettler Formation and Crossfield Member, the most prominent mechanical compaction features occur in facies that are dominantly mud-supported (Plate 5: 1-3). Common features present within mudstone and wackestone facies include: (1) slightly compacted burrow structures in burrowed mudstones; (2) minor compression of fenestrae in fenestral mudstones in all of the wells (1-10) that have not been exposed to completely destructive dolomitisation processes as observed in the facies in well 11 ; (3) the bending and reorientation of allochems (particularly bivalves and brachiopod fragments) (Plate 5: 1-2); (4) minor clumping of bioclastic material, and; (5) the clotting of peloidal material within peloidal mudstones. In peloidal grainstone facies, peloids are dominantly uncompressed. However, in instances of minor compression, slightly compressed fabrics consist of flattened or elongated peloids. The overall lack of compaction seen in the peloidal grainstone facies suggests that this facies was probably exposed to episodes of cementation fairly early in its depositional history.

37

PLATE 5: Mechanical and Chemical Compaction

(1) Photomicrograph of bent/broken bioclasts resulting from mechanical compaction (xpl) (scale = 100μm). Well 10-9-66-21W5 (2408.1m). Red arrow indicating bent bioclast from mechanical compaction.

(2) Photomicrograph of broken bioclast with calcite cement between fragments (scale = 200μm). Well 10-9-66-21W5 (2408.53m). Red arrow shows broken bivalve fragment from mechanical compaction.

(3) Photomicrograph of stylolitisation in dolomicrite between fossil fragments; mechanical compaction (offset fragments) and evidence of pressure solution (xpl) (scale = 50μm). Well 10-21-32-2W5 (2751.7m). Red arrow shows thin dissolution seam developed through pressure solution.

(4) Photomicrograph of stylobrecciated fabric forming a nodular mudstone texture (scale = 100μm). Well 10-9-66-21W5 (2403.2m).

(5) Photomicrograph of high-amplitude stylolites with fitted fabric in stromatoporoid floatstone with coarse blocky calcite cement (C)(scale = 100μm). Well 10-9-66-21W5 (2404.14m). Red arrow shows high amplitude stylolite.

(6) Photomicrograph of stylolites cross-cutting crinoid ossicle (Cr) in fitted fabric texture (fl) (scale = 100μm). Well 11-23-25-29W4 (2670.6m).

(7) Photomicrograph of stylolaminated fabric with horsetail stylolites (fl) (scale = 50μm). Well 10-23-30-28W4 (2397.3m). Red arrow pointing to horsetail stylolite at end of anastomosing stylolite.

(8) Photomicrograph of stylobrecciated fabric in recrystallised dolomitised mudstone under fluorescence (fl) (scale = 100μm). Well 10-13-26-8W5 (3574.9m).

38

Plate 5: Mechanical and Chemical Compaction
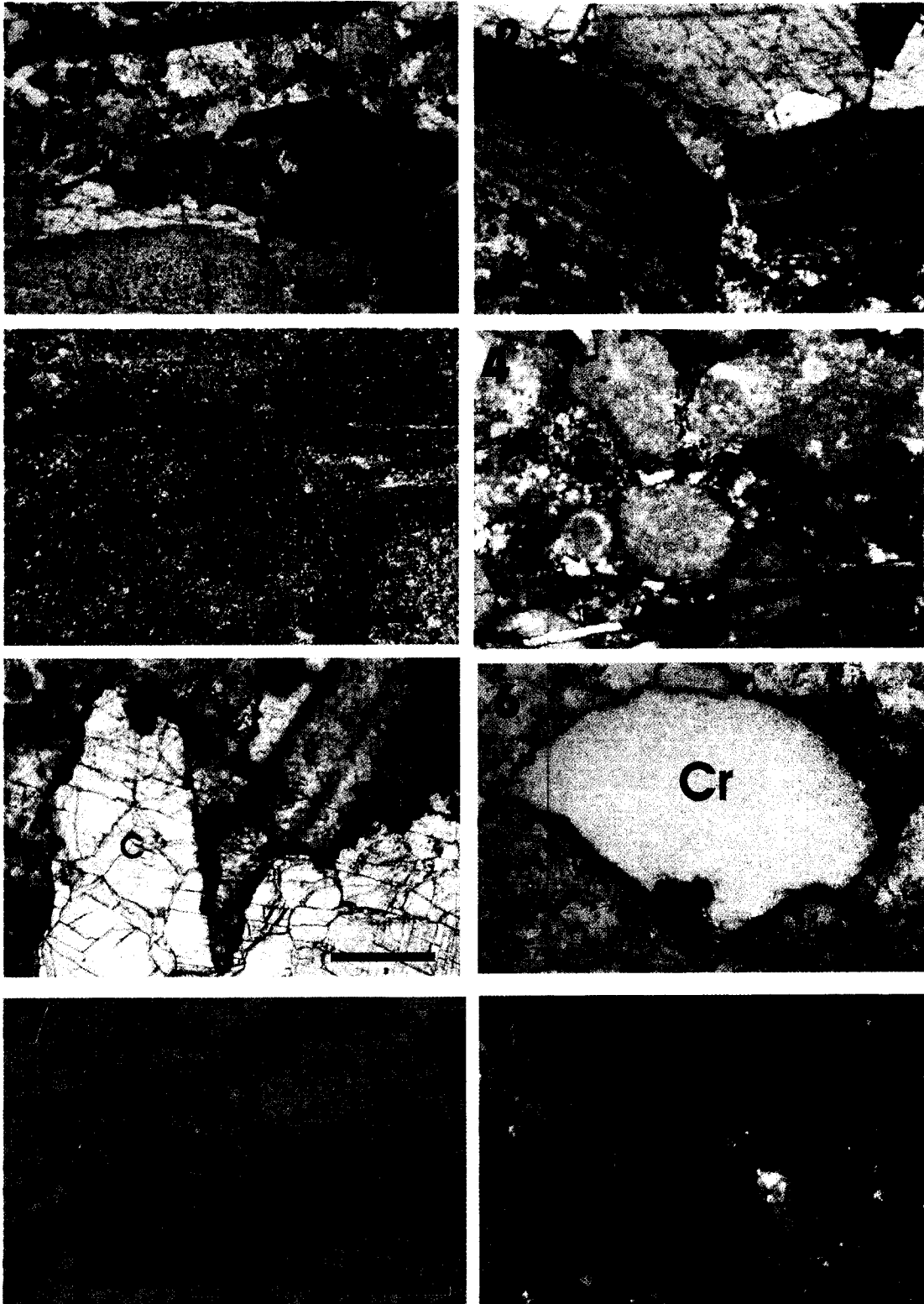
4.4.2 Chemical compaction

Chemical compaction occurs as a result of increased solubility along grain contacts and is commonly initiated at burial depths between 200 to 1500 metres (Boggs, 1995; Buxton and Sibley, 1981). This solubility (pressure-solution) develops in carbonates during these late burial stages as a result of overburden pressure and tectonic stresses (Tucker, 2001). Pressure-solution also causes the liberation of moles of $CaCO_3$ in solution which may be precipitated in close proximity as calcite cements or carried in pore waters to be precipitated at distant sites from the original region of pressure-dissolution (Choquette and James, 1990). The common chemical compaction features present in the Upper Stettler Formation and Crossfield Member are fitted fabrics, stylolites, and the development of pressure-dissolution seams (Plate 5: 4-8).

Fitted-fabrics are defined as a framework of interpenetrant grains with sutured to planar or curved surfaces between grains (Tucker and Wright, 1990). In terms of fitted fabrics, the most common example of this type of diagenetic feature is identified in the bioclastic mudstone facies, where large crinoid fragments are cross-cut and fitted with mud-rich sediments or bioclastic and peloidal fabrics are cross-cut and fitted with dissimilar fabrics (Plate 5-3; 5-6).

The two most significant diagenetic features identified in the facies of the Upper Stettler and Crossfield carbonates, that occurs in all wells (1-11), is stylolitisation and the development of pressure-dissolution seams.

Stylolites are sutured surfaces that cross-cut grains, cement, or matrix and are richly concentrated in insoluble residue (clays, organics, and iron-rich residue) that is produced from carbonate dissolution processes (Tucker, 2001). Types of stylolites and pressure-dissolution structures identified in the study area include: parallel, anastomosing stylolites producing stylolaminated fabrics that generally follow bedding structures; low- and high-amplitude stylolites; columnar stylolites; horsetail stylolites; and the development of stylobrecciated structures of irregular, anastomosing stylolites creating nodular-mud type fabrics (Plate 5-4 to 5-8). Stylolitisation in the Upper Stettler and Crossfield carbonates occurred in more than one stage in the burial process. The first significant period of stylolite development occurred relatively early and resulted in the formation of thin, anastomosing stylolites that were subsequently healed by matrix dolomite. This episode of stylolitisation occurred after early calcite cementation but prior to pervasive dolomitisation of the matrix and along with wells 2-11, is also evident in the non-dolomitised mudstone facies in well 1. The second stage of stylolitisation occurred much later in the burial history of the Upper

40

Stettler and Crossfield carbonates. Stylolites of this stage formed after early calcite cementation and pervasive dolomitisation, but prior to the precipitation of late- stage blocky calcite and saddle dolomite cements. These stylolites are also more variable in terms of types and fabrics and include both high- and low-amplitude stylolites. They are also either bed-parallel (along bedding planes) or irregular (cross-cutting precursor fabrics), and have developed as singular seams or as swarms of multiple stylolites.

Pressure-dissolution seams have been identified in all of the facies in wells (1-11) within the study area. These dissolution seams are typically anastomosing and like stylolites, are composed of insoluble residues of organics, clays, and iron-rich sediments. Mudstone, grainstone, and floatstone/packstone facies in the Upper Stettler and Crossfield carbonates all have dissolution seams that either cross-cut fabrics (destroying precursor fabric) or develop around existing grains and bioclasts forming stylonodular fabrics.

4.5   Evaporite formation

The precipitation of evaporites occurs throughout the diagenetic history of the Upper Stettler Formation and Crossfield Member (Plate 6 & Plate 7). The recrystallisation of evaporites is a continuous process that can occur both at the onset of deposition and during diagenetic alteration as the evaporites are exposed to changes in temperature, pressure, and salinity. Gypsum precipitation is favoured by conditions of lower temperature and pressure, and relatively lower salinities than anhydrite, which in turn, is commonly precipitated in higher temperature and pressure environments with higher salinity (Warren, 1989). Since both anhydrite and gypsum can pseudomorphically replace each other, anhydrite may develop syndepositionally with gypsum as a primary phase and also precipitate as the anhydritisation of gypsum during early to late diagenesis (Kasprzyk, 2003). The anhydrite to gypsum transformation that occurs as buried sediments are exposed to uplift (which involves an increase in volume of more than 50% during hydration processes) can also mask any earlier formed deformational fabrics within the evaporites. Deformational features may in some cases resemble primary depositional features, which may further exacerbate the problem of distinguishing whether the realm of precipitation of anhydrite-gypsum deposits is of primary origin or the product of secondary diagenetic alteration (Shreiber and Helman, 2005).

Fine-crystalline laths of anhydrite and fine-crystalline lenticular or tabular gypsum have been interpreted to be products of primary precipitation within sediments of the Upper

41

PLATE 6: Core photographs of evaporites

(1)   Core photograph of nodular mosaic (primary) anhydrite (A) in Upper Stettler laminated and nodular anhydrite facies. Well 7-23-31-9W5 (3636.9m). Red arrow at bottom – up direction.

(2)   Core photograph of secondary anhydrite (A) in nodules, surrounded by laminated anhydrites and displacement of muds surrounding nodules during anhydrite growth. Well 10-23-30-28W4 (2388.3m). Red arrows indicate up direction.

(3)   Core photograph of mud deformation during precipitation of primary Anhydrite (A). Well 10-18-21-28W4 (2619.5m). Small red arrows show development of small mud lithoclasts. Red arrow at bottom indicates up direction.

(4)   Core photograph of late-stage secondary anhydrite (A)with inclusions and crenulated margins. Well 10-5-23-6W5 (2578.5m). Red arrow – up direction.

(5)   Core photograph of extensive secondary anhydrite (A) precipitation in large dissolution vugs and fractures. Well 7-23-31-9W5 (3650.9m).

(6)   Core photograph of secondary anhydrite (A) in dissolution vugs with porous dolomite and carbonaceous rims (indicated by small red arrow). Well 10-18-21-28W4 (2633.1m). Large red arrow shows up direction.

42

Plate 6: Core photographs of Evaporites

43
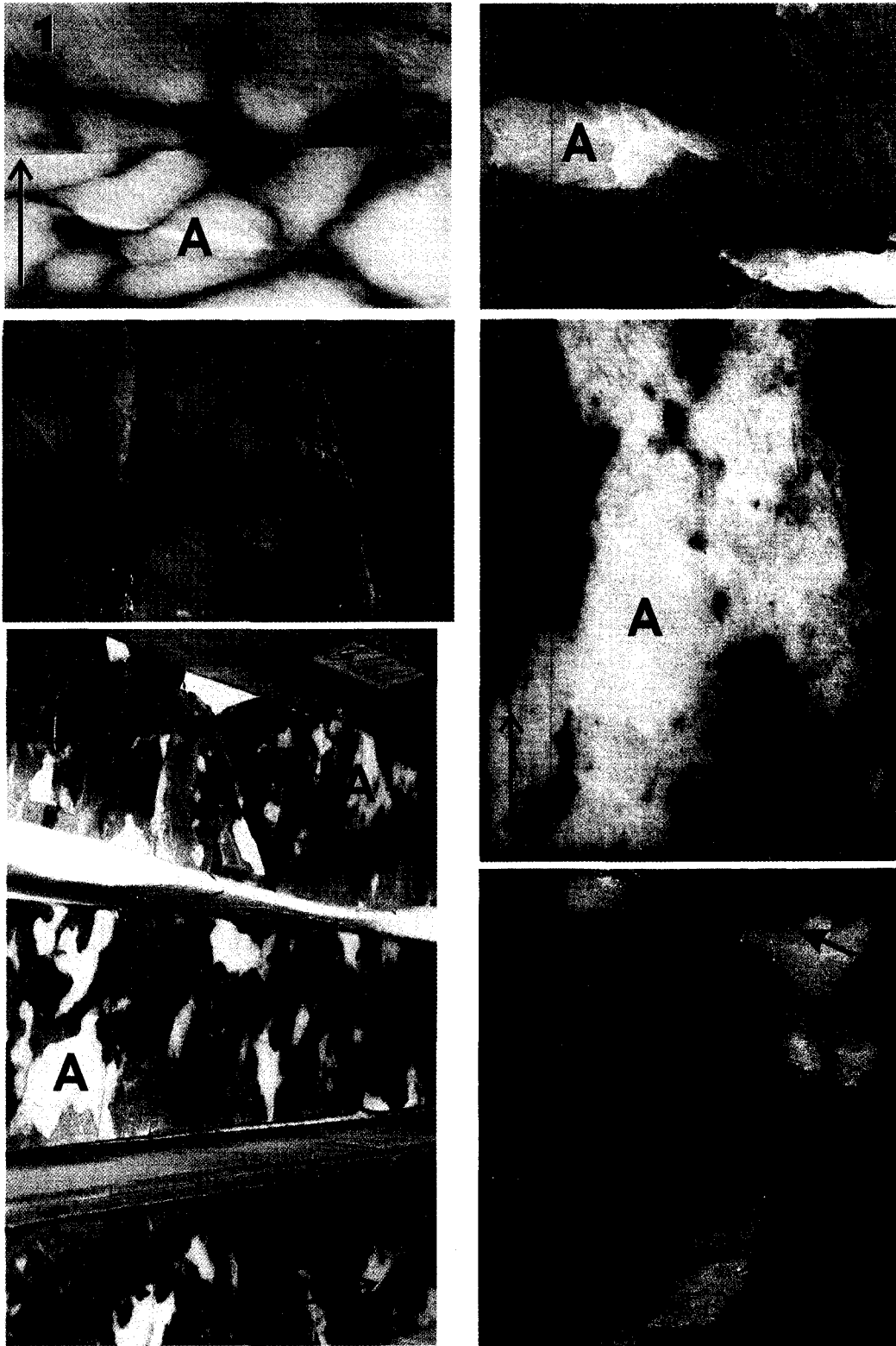
PLATE 7: Photomicrographs of evaporites

(1) Photomicrograph of gypsum overlain by laminated anhydrite (xpl) (scale = 50μm). Anhydrite (A). Well 7-23-31-9W5 (3636.9m). Red arrow indicating gypsum crystals.

(2) Photomicrograph of gypsum precipitating in leached intercrystalline pore spaces of matrix dolomites (xpl) (scale = 100μm). Well 11-23-25-29W4 (2663.3m). Red arrow indicating leached areas with gypsum occlusion.

(3) Photomicrograph of nodular anhydrite (A) laths in dolomudstone matrix (xpl) (scale = 50μm). Well 5-22-32-1W5 (2574.4m).

(4) Photomicrograph of anhydrites (A) precipitated in fractures through dolomitised and deformed laminated mudstones (xpl) (scale = 50μm). Well 10-18-21-28W4 (2616.0m).

(5) Photomicrograph of coarser secondary anhydrite laths (felty anhydrite) (A) replacing earlier evaporites in vugs (xpl) (scale = 100μm). Well 11-23-25-29W4 (2656.3m).

(6) Photomicrograph of secondary felty anhydrite replacing earlier evaporite phases in nodules (xpl) (scale = 50μm). Well 13-12-29-27W4 (2248.2m).

(7) Photomicrograph of coarse replacement gypsum surrounded by blocky calcite (pseudomorphic after anhydrite) and saddle dolomite in vug (xpl) (scale = 100μm). Gypsum (G), Calcite (C), Dolomite (D) Well 11-23-25-29W4 (2650.5m).

(8) Photomicrograph of pile-of-brick anhydrite being replaced by blocky II calcite (xpl) (scale = 100μm) Calcite (C), Dolomite (D). Well 11-23-25-29W4 (2650.5m). Red arrow pointing at anhydrite crystals.

44

Plate 7: Evaporite Cements
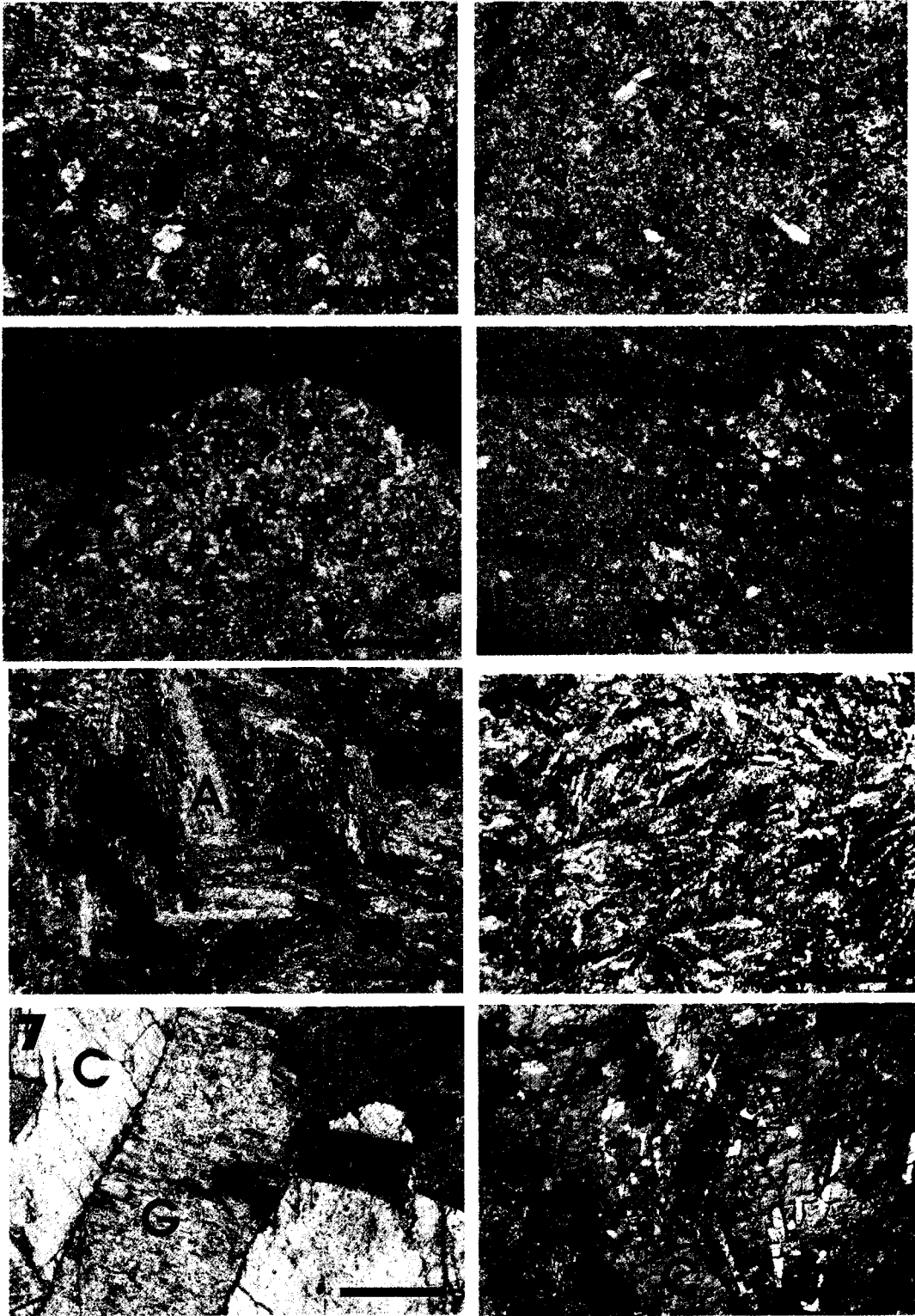
Stettler Formation and Crossfield Member. These evaporites were deposited as either laminated sediments or within nodules in mudstone fabrics in shallow, hypersaline environments. By contrast, secondary evaporites also consist of a mixture of anhydrite and gypsum but were precipitated as coarser, often inclusion-rich cements within vugs or fractures. Secondary phases of primarily anhydrite and to a lesser degree, gypsum have been identified in all of the facies in wells 1-11.

4.5.1 Anhydrite

Anhydrites in the Upper Stettler Formation and Crossfield Member are typically either of primary origin (or as an early replacement of gypsum) prior to the main burial process, or as intermediate and deep burial cements within dissolution vugs and fractures. Primary anhydrite is identified as dominantly fine- to medium – grained (30-400 μm), subhedral to euhedral mosaic laths (within laminations or nodules in laminated and nodular mudstone facies) and is present within all of the examined wells (Plate 6: 1-6). Felted mat textures are also a common primary anhydrite fabric within early nodules (Plate 7-6).

Two main types of secondary anhydrite cement fabrics are identified in the Upper Stettler and Crossfield. The most dominant cement texture is in the form of blocky tabular anhydrite (ranging from 500-1000 μm) that is seen occluding vugs and fractures. The second type of texture is in the form of coarse anhydrite lath mosaics (up to several mm's) that are typical of late, vug-filling cements (Plate 7-5). Both types of secondary cements are identified in association with both saddle dolomite and late-stage blocky calcite cements. In hand sample, there also appears to be two different textures with a more 'intermediate' stage anhydrite that is often slightly opaque and crenulated along the edges (Plate 6-2), and secondly, a milky white anhydrite that is typical of much later-stage cements (Plate 6-5; 6-6). The presence of both types of secondary anhydrite confirms that the precipitation of anhydrite is a continuous process that begins at shallow burial and continues with increasing burial depth.

4.5.2 Gypsum

Gypsum in all of the wells (1-11) is typically replaces anhydrite, and often has inclusions of fine-grained anhydrite laths. This type of gypsum has either developed as: large subhedral to euhedral tabular laths (1-2 mm) (Plate 7-7); as subhedral to euhedral lenticular crystals (up to 1mm) with many inclusions of fine-grained anhydrite; or as small tabular laths (50-100 μm) within leached matrix dolomite fabrics (Plate 7-2). In wells 5 & 6 there also appears to

46

PLATE 8: Calcite Cements

(1) Photomicrograph of bladed/equant calcite cement surrounding bioclast fragments (xpl) (scale = 200μm). Well 10-9-66-21W5 (2408.1m).

(2) Photomicrograph of drusy mosaic calcite cement (DM) within bioclast fragments (xpl) (scale = 200μm). Well 10-9-66-21W5 (2408.1m). Red arrow pointing to drusy mosaic cement.

(3) Photomicrograph of bladed calcite cement (BC) surrounding edges of vug with twinned blocky calcite in centre portion (xpl) (scale = 200μm). Well 10-9-66-21W5 (2406.8m).

(4) Photomicrograph of neomorphic spar (NS) between peloids and bioclast fragments (xpl) (scale = 200μm). Well 10-9-66-21W5 (2408.5m).

(5) Photomicrograph of syntaxial calcite cement (SC) on crinoids and surrounding fabric (xpl) (scale = 100μm). Well 10-9-66-21W5 (2410.8m).

(6) Photomicrograph of drusy mosaic/equant calcite (DM) within brachiopod mold (xpl) (scale = 100μm). Well 10-9-66-21W5 (2410.8m).

(7) Photomicrograph of stromatoporoid framework with equant to blocky calcite (C) within structure and more fibrous calcite lining framework (fl) (scale = 100μm). Well 10-9-66-21W5 (2406.9m).

(8) Photomicrograph of blocky I calcite in dissolution vug with saddle dolomite, calcite (C), dolomite (D) (ppl) (scale = 100μm). Well location 11-23-25-29W4 (2663.3m).

47

Plate 8: Calcite Cements
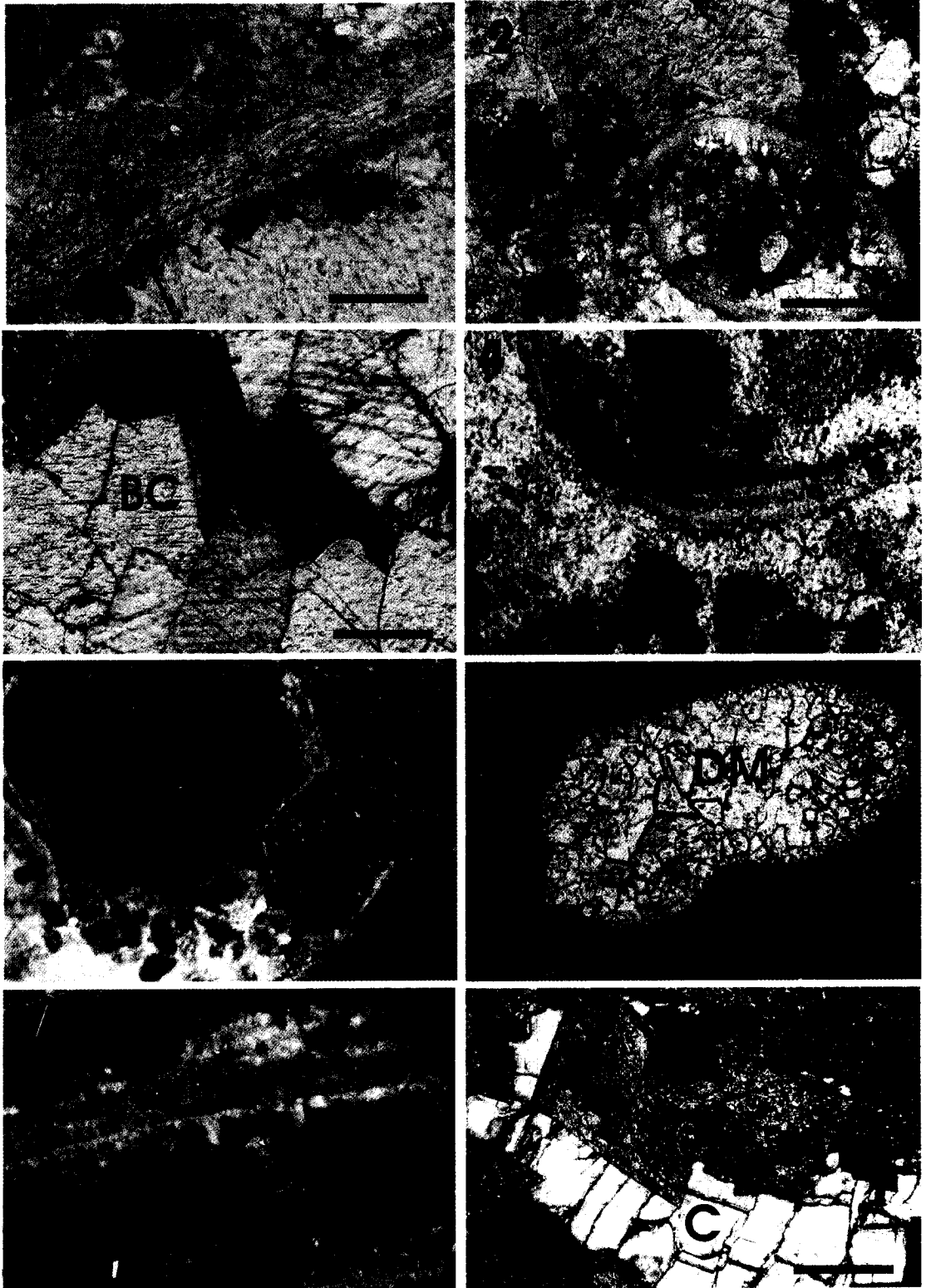
be remnants of gypsum in graded beds that have been subsequently altered to anhydrite lath mosaics.

4.6 Calcite cementation

Calcite cementation has occurred throughout the diagenetic history of the Upper Stettler Formation and Crossfield Member from early shallow-burial to late-stage vug-filling calcites (Plate 8). Since cement develops in pores as a chemical precipitate from solution, it requires supersaturation of the pore fluids with respect to the particular mineral precipitating (Flügel, 2004). The composition and textures of calcite cement is characteristic of the pore fluids from which they precipitated and are as a result, indicative of the diagenetic environment from which they formed. The types of calcite cement identified in the Upper Stettler Formation and Crossfield Member include: dogtooth, drusy mosaic, syntaxial, multiple stages of blocky, and bladed to equant cement.

4.6.1 Dogtooth cement

Dogtooth cements are relatively rare, but occur to a minor degree along the edges of bioclasts and are generally found surrounded by equant cement fabrics (Plate 8-1). This cement consists of roughly scalenohedral crystals (30-60 μm) that are non-ferroan, non-luminescent/fluorescent, relatively clear and with pointed terminations. The precipitation of this cement is indicative of a marine phreatic zone or shallow burial (Flügel, 2004).

4.6.2 Drusy mosaic cement

This cement is relatively common and occludes fabrics within ostracodes, brachiopods, gastropods, and calcispheres in the bioclastic mudstone/wackestone and peloidal grainstone facies in all of the wells (1-11) (Plate 8-2 & 8-6). Drusy mosaic cement is also seen to a rarer degree as pore-occluding cements in intergranular pore spaces. Crystals within bioclasts are typically clear, equant to slightly elongate, non-ferroan, subhedral, and range from 20 – 80 μm, with coarser grains characteristically in the centre of void spaces and bioclasts. Cements of this type are also non-luminescent/fluorescent.

49

4.6.3 Syntaxial cement

Syntaxial cements (Plate 8-5) are common within all the bioclastic facies (most significantly in the packstone/floatstones) and are typically identified as overgrowths on echinoderm fragments. All the syntaxial cements are non-luminescent/fluorescent and non-ferroan. Typical crystals are relatively cloudy and moderately twinned, with surrounding fabrics destroyed by syntaxial cement precipitation, creating large crystals that not only include the echinoderm ossicles but also other adjacent fabrics. In several examples, particularly in well #1, syntaxial precipitation appears to postdate minor mechanical compaction features, wherein the cement fills pore spaces between broken bioclasts. The presence of mechanical compaction features would suggest that cementation occurred at the very least, in the shallow subsurface.

4.6.4 Blocky cement

Blocky calcites are the most abundant type of pore-filling calcite cement and have been identified in all the examined wells in the Upper Stettler and Crossfield (Plate 8-7 & Plate 8-8). This cement was precipitated in two stages: blocky I is a shallow to intermediate-stage cement within fractures and vugs, and blocky II is a late-stage cement that is also found occluding vugs and fractures. Crystals of blocky I are relatively clear, ranging from 400 - 800µm (quite coarse), non-ferroan, non-luminescent/fluorescent, and with only minor inclusions of gypsum and anhydrite. In contrast, blocky II tends to be coarser (up to 1.2 mm), cloudier, often twinned, and with many inclusions of blocky and lath anhydrite. This cement is also non-ferroan, and non-luminescent/fluorescent. Quite typically blocky II is found replacing secondary blocky anhydrite in late-stage fractures and large (mm-scale) dissolution vugs and in close proximity to saddle dolomite cements. Sulphide minerals are also seen in close association with late blocky II calcites.

4.6.5 Bladed to equant cement

Bladed to equant cements are relatively minor pore-occluding cements seen as pore-lining cements in vugs and fractures in the mudstone and grainstone facies (Plate 8-3). In these vugs, central portions are often occluded with blocky calcite. Crystals sizes are quite variable, ranging from relatively small, more equant crystals (100 – 150 µm) to larger (500 -

50

800 μm) bladed crystals with slightly pointed to tabular terminations. This cement is also non-ferroan and non-luminescent/fluorescent.

4.7   Silicification

This is a rare phase in the paragenesis of the Upper Stettler Formation and Crossfield Member (Plate 13-4) and developed relatively early (in the eogenetic realm). As a phase, it is not seen in any of the pervasively dolomitised wells and must have occurred prior to any major dolomitisation episodes. It occurs primarily as microquartz in nodular fabrics in well 1 within stromatoporoid floatstone facies where *Labechiid* frameworks are preferentially silicified. Silicification also occurs in minor amounts in well 9, in undolomitised strata, where it also forms chert nodules with slightly larger crystal sizes (up to 50 μm) in radial structures. Due to the very rare occurrence of this phase, it has not been determined to be a significant process in the diagenetic history of the Upper Stettler and Crossfield.

4.8   Dolomite

In terms of importance, dolomitisation is the most significant and widespread diagenetic process that affected the Upper Stettler Formation and Crossfield Member. Evidence of dolomitisation is present in all the facies in wells (1-11). In facies within the Crossfield and farther west of the main Crossfield study area (wells 2-11), dolomite fabrics range from minor pore-lining cements to the complete pervasive alteration of the precursor matrix. In the facies of well 1, only minor dolomitisation has occurred in the form of dissolution-seam related dolomite and rare pore-lining cements. A close examination of all the dolomitisation processes and fabrics identified in the study area is crucial for the development of an understanding of how dolomitisation phases affect overall reservoir quality, and in particular, porosity and permeability characteristics. Interpreting the timing, overall distribution, and mechanism(s) of dolomitisation based partly on petrographic evidence is therefore an important undertaking in assessing the overall quality of the reservoir rocks for future exploration potential.

There are six types of dolomite identified in the facies of the Upper Stettler Formation and Crossfield Member. They are, in approximate order of occurrence (oldest phase first):
(1) dolomicrite (Plate 9-1; 9-2) ; (2) fine- to medium-crystalline matrix dolomite (Plate 9-3); (3) coarse-crystalline matrix dolomite (Plate 9-4); (4) dissolution-seam associated dolomite (Plate 10-1; 10-2); (5) fracture-lining dolomite (Plate 10-7); (6) saddle dolomite (Plate 10-5;

PLATE 9: Pervasive Matrix Dolomite

(1) Dolomicrite with original peloidal fabric identified with a white card (ppl) (scale = 40μm). Well 11-23-25-29W4 (2671.9m). Small black arrows pointing to precursor fabric.

(2) Dolomicrite to fine-crystalline matrix dolomite of micritic precursor (ppl) (scale = 40μm). Well 13-12-29-27W4 (2248.2m).

(3) Fine- to medium-crystalline matrix dolomite with interparticle porosity (xpl) (scale = 50μm). Well 10-18-21-28W4 (2639.5m).

(4) Coarse-crystalline matrix dolomite (planar-e) (xpl) (scale = 100μm). Well 7-23-31-9W5 (3670.4m).

(5) Stylolite dividing fine-crystalline planar-s matrix dolomite from medium-crystalline matrix dolomite (fl) (scale = 50μm). Well location 10-18-21-28W4 (2633.0m).

(6) Coarse-crystalline replacement dolomite with sutured textures associated with burial, mostly nonplanar fabric (ppl) (scale = 200μm). Well location 11-23-25-29W4 (2665.4m).

(7) Cloudy, coarse-crystalline sucrosic texture of planar-e to nonplanar dolomite, with bitumen-staining (xpl) (scale = 50μm). Well 5-19-30-10W5 (2519.5m).

(8) Cloudy, coarse-crystalline matrix dolomite with sieve texture and blocky calcite cement (C) in intercrystalline pores (xpl) (scale = 50μm). Well 7-23-31-9W5 (3637.5m).

52

Plate 9: Pervasive Matrix Dolomite

53
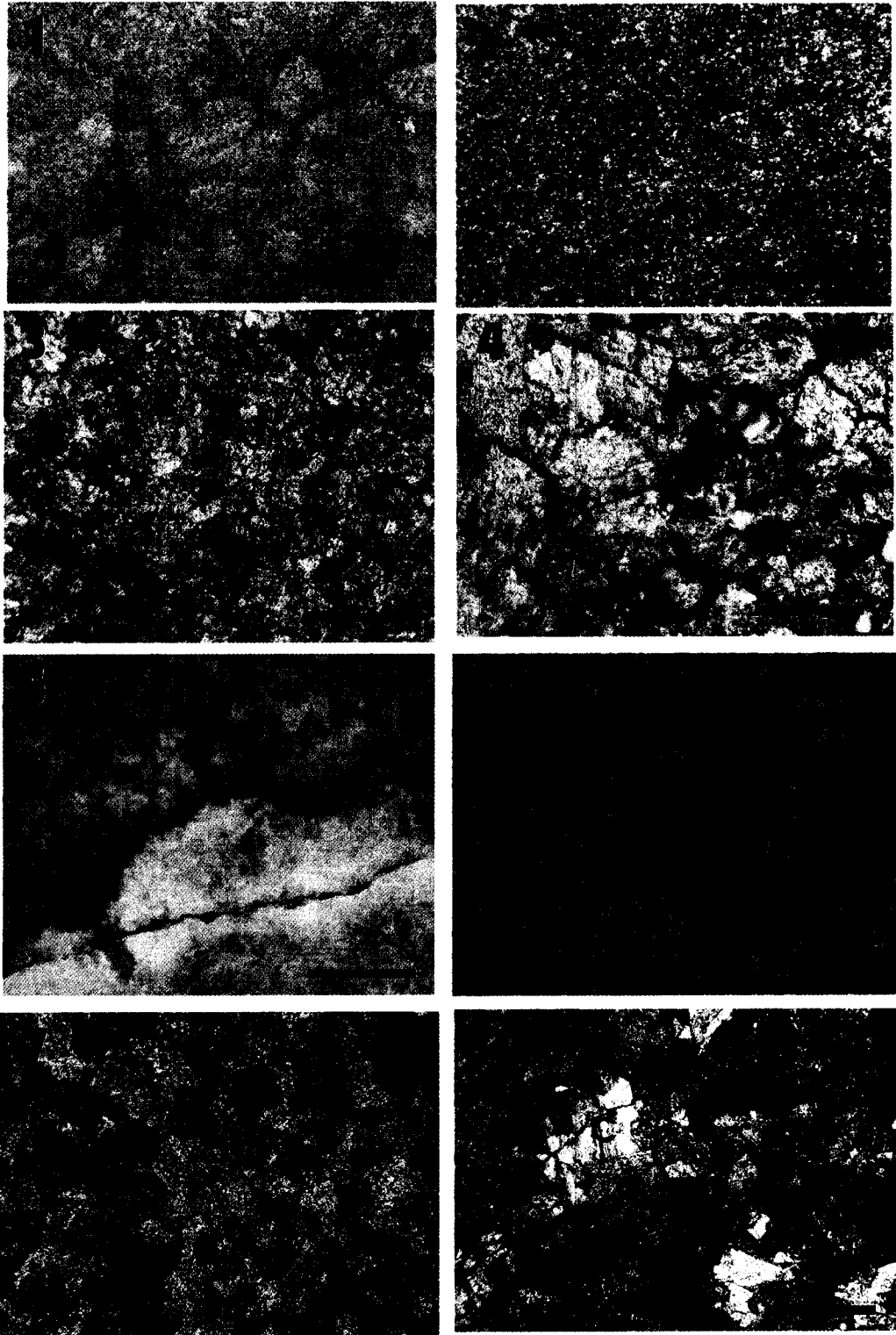
10-6). Dolomites (1) – (3) are essentially a single phase wherein they represent a continuous process of pervasive dolomitisation. These dolomites have been divided into three different types based on crystal-size, although they are genetically related and represent this continuous process of dolomitisation and subsequent recrystallisation. Fine- and medium-crystalline matrix dolomite have been categorised as one type on the basis that they are very similar and only vary slightly in crystal-size. Dolomicrite has been categorised in a separate category as well in that it is significantly finer than either the fine- or medium-crystalline matrix dolomite. Following this rationale, coarser fabrics have also been categorised separately. The coarse-crystalline matrix dolomite textures are slightly different than the finer grained equivalents, which may be related to the effects of recrystallisation processes with depth. All of these pervasive matrix types however may simply vary in crystal-size due to mimic-replacement of the original textures and crystal-sizes of the precursor fabric.

The textural classification of dolomite follows Randazzo and Zachos (1983), and Gregg and Sibley (1984) and Sibley and Gregg (1987). In extensively dolomitised sections where the precursor fabric has been unidentifiable, both a white card technique (Folk, 1987) and fluorescence microscopy (Dravis and Yurewicz, 1985) have been used to identify the precursor fabrics, which in some cases proved unsuccessful. Peloidal and bioclastic facies however, were more successfully identified with these methods, particularly using the white card technique.

4.8.1 Dolomicrite

Dolomicrite is the least abundant phase (approximately 25% of total matrix dolomite) in comparison to the other pervasive matrix dolomites (Plate 9-1) and generally occurs in the mudstone facies, particularly in the Upper Stettler Formation. This dolomite is mostly identified in facies in wells 3-7 and 9, with a minor occurrence in well 11. Predominantly, dolomicrite is identified in peloidal, nodular, and laminated mudstones, from supratidal to upper intertidal depositional settings. The prominence of this cement in these facies suggests that the development of dolomicrite in place of coarser-crystalline textures is related to the overall finer crystal size of the precursor fabric. This dolomite consists of typically cloudy, very fine-crystalline (2- 25 μm), subhedral to anhedral, tightly-woven, interlocked planar-s crystals. Crystals are non-luminescent with cathodoluminescence (CL) and very weakly fluorescent (pale green) using Epi-Fluorescence (Epi-Fl) with pinpoint areas of brighter green/yellow in areas of higher organics.

54

PLATE 10: Dolomite Phases

(1)   Dissolution-seam dolomite precipitated between stromatoporoid framework (ppl) (scale = 100μm). Well 10-9-66-21W5 (2406.9m). Red arrow indicating euhedral dolomite rhombs between stromatoporoid framework.

(2)   Dissolution-seam dolomite within dolomicrite (ppl) (scale = 100μm). Well 11-23-25-29W4 (2645.9m). Red arrow pointing to dolomite surrounded by insoluble residues.

(3)   Zoned planar-e dolomite in association with dissolution seams with cathodoluminesence (cl) (scale = 100μm). Well 13-12-29-27W4 (2249.1m). Red arrow pointing toward zoned euhedral rhomb.

(4)   Coarse, zoned, planar-e dolomite in dissolution area (fl) 10-9-66-21W5 (2412.2m). Red arrow pointing towards planar-e dolomite.

(5)   Saddle dolomite (SD) with undulose extinction and curved crystal boundaries (xpl) (scale = 50μm). Well 10-5-23-6W5 (2582.3m).

(6)   Saddle dolomite (SD) with twinned late-stage blocky II calcite (C) in dissolution vug (xpl) (scale = 100μm). Well 11-23-25-29W4 (2663.3m).

(7)   Pore-lining dolomite with blocky calcite in centre of vug (Calcite (c)) (xpl) (scale = 50μm). Well 10-5-23-6W5 (2571.8m).

(8)   Pore-lining dolomite with zonation, blocky calcite in centre of vug with fluorescence (Calcite (c)) (fl) (scale = 100μm). Well 11-23-25-29W4 (2650.5m).

55

Plate 10: Dolomite phases
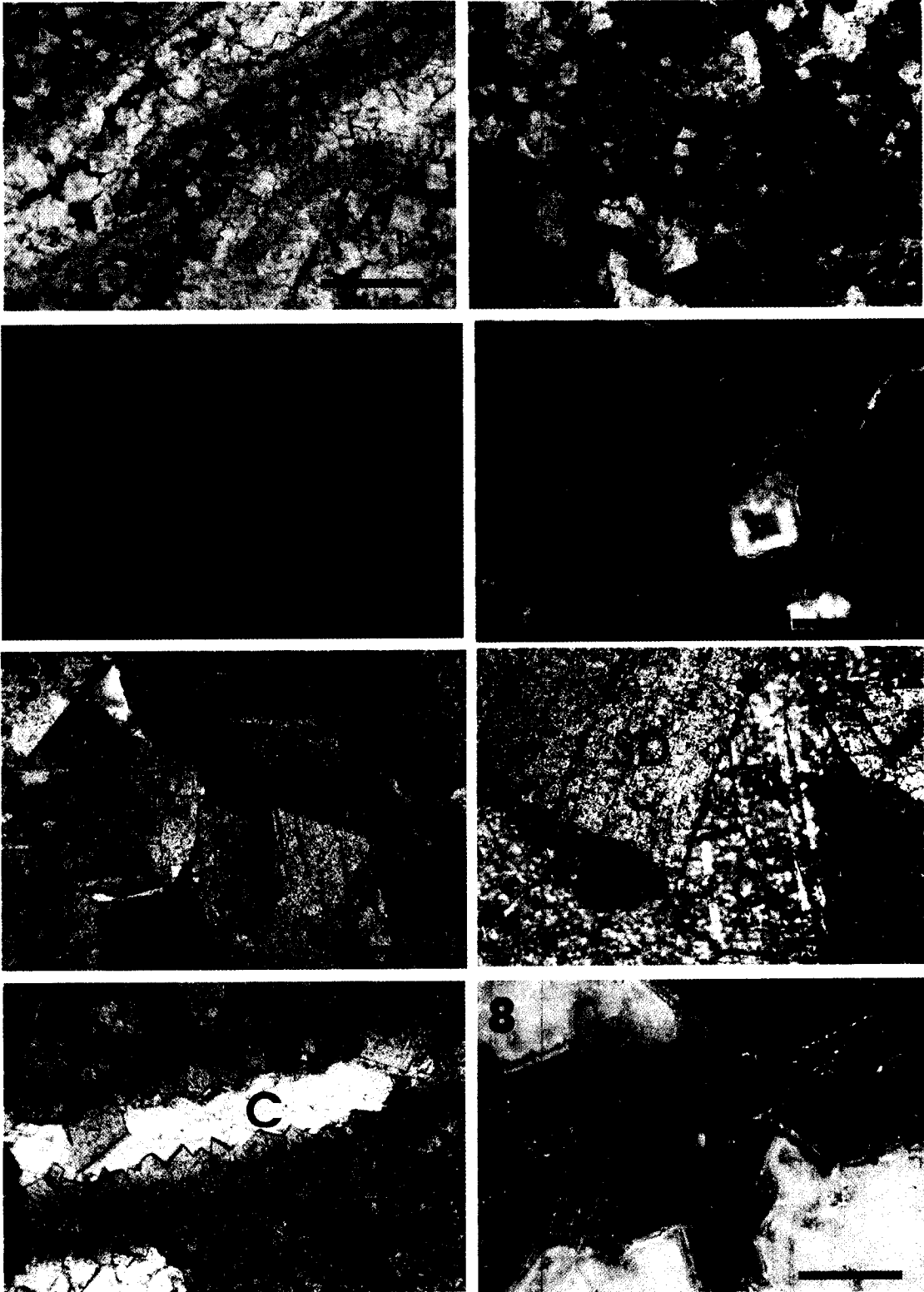
4.8.2 Fine- to Medium - crystalline matrix dolomite

Fine- to Medium- crystalline matrix dolomite is the most abundant type of dolomite in the Upper Stettler Formation and Crossfield Member and forms approximately 45% of the total pervasive dolomite (Plate 9-2 -3 & 9-5). It is commonly seen in facies in wells 2-6 and 10 with very rare occurrences in well 7. It is present in the peloidal and bioclastic mudstones, peloidal grainstones (to a lesser degree), and within the floatstone/packstone facies. Once again, the crystal-size of the dolomite is a reflection of the precursor fabric and all other characteristics and textures are similar. Crystal sizes range from 50-100 μm for the fine crystals to 100-200 μm for medium crystal sizes. This dolomite consists of planar-s to non-planar, tightly-woven, interlocked mosaics of subhedral to anhedral crystals, and is typically non-luminescent with CL and pale yellow/green with Epi-Fluorescence.

4.8.3 Coarse- crystalline matrix dolomite

Coarse- crystalline matrix dolomite comprises approximately 30% of the total pervasive dolomite within the Upper Stettler Formation and Crossfield Member (Plate 9-4; 9-6-8). This is the most prominent dolomite type in well 11, which contains zoned and etched crystals suggestive of recrystallisation textures. Coarse- crystalline matrix dolomite is also identified in facies in wells 8-11 further west of the Crossfield trend and in facies in wells 2, 4 & 7 along the Crossfield trend. Development of most of the coarse- crystalline textures has been fabric destructive with precursor fabrics in some cases unidentifiable. In many cases, the samples have simply been referred to as dolostones. Crystals are unequigranular, cloudy and coarse (200-450 μm) with planar-e and nonplanar sucrosic textures. Under CL, the crystals are for the most part, non-luminescent but fluorescent, with cloudy bright centres and clear, darker etched crystal rims. Most of the coarser crystals, particularly in wells 8-11 are also asphaltene-stained.

4.8.4 Dissolution seam dolomite

This dolomite is the second most abundant dolomite after the pervasive matrix dolomite (Plate 10 -1-4) and is identified in variable amounts cross-cutting units in all of the wells (1-11). It occurs in association with dissolution-seams of insoluble residues of clays, organics, and iron-rich residues and forms planar-e crystals ranging from 50-250 μm. Crystals are often zoned with CL (Plate 10-3) and with Epi- Fluorescence (Plate 10-4). As this dolomite is only found in association with cross-cutting dissolution-seams, it tends to be fabric-destructive. The presence of zoned crystals suggests that it developed in more than

57

one stage in the diagenetic history of the Upper Stettler and Crossfield, but for the most part, it is an intermediate to late diagenetic event that occurred with deeper burial.

4.8.5 Pore-lining dolomite

This cement is a relatively minor occurring phase (in comparison to the previously discussed dolomite types) in wells 2-10. Pore-lining dolomite is identified along the edges of fenestrae and late-stage vugs and fractures (Plate 10-7 & 10-8), and consists of euhedral to subhedral crystals (40 – 250 μm) with cloudy cores and clear rims. Crystals are non-luminescent to very dull-luminescent and have yellow/green cloudy cores and darker-green, clearer rims under Epi-Fluorescence. Blocky calcite often fills the central portions of vugs with pore-lining dolomite developing along the edges.

4.8.6 Saddle dolomite

Saddle dolomite is one of the latest diagenetic events in the diagenetic history of the Upper Stettler Formation and Crossfield Member (Plate 10-5 & Plate 10-6). It occurs in a minor amount in the facies of wells 5-8, and with greater abundance in the facies of wells 10 & 11. Saddle dolomite crystals are typically cloudy with curved crystal faces, anhedral to subhedral, and coarse (up to 2 mm) with undulose extinction. This dolomite is often found lining late-stage fractures and vugs in association with sulphides, secondary anhydrites, and blocky II calcites. In many cases, both the blocky calcites and saddle dolomite are extensively asphaltene-stained. In wells west of the Crossfield (10 & 11), which appear to have been more affected by diagenetic alteration, some of the coarse-grained pervasive matrix dolomite fabrics also have characteristic undulose sweeping extinction indicative of late-stage recrystallisation processes. Saddle dolomite in these wells is non-luminescent to dully luminescent, and surprisingly, does not show zonations under either CL or Epi-Fluorescence.

4.9 Dissolution

Dissolution affects all of the facies in all of the wells (1-11) and has occurred both early and late in the diagenetic history of the study area (Plate 11). Early dissolution resulted in the formation of fossil voids (particularly in ostracodes, brachiopods, and gastropods) that were subsequently filled with calcite cements. Intermediate to late dissolution created secondary porosity fabrics that are greater in abundance than porosity created early in the

58

PLATE 11: Dissolution and Fracturing

(1) Leached pore spaces along stylolite in dolomicrite matrix (ppl) (scale = 50μm). Well 13-12-29-27W4 (2258.7m). Red arrow pointing to leached areas along stylolite.

(2) Leached cements cross-cutting micritic intraclast (xpl) (scale = 100μm). Well 10-9-66-21W5 (2415.9m).

(3) Dissolution of fabrics along thick dissolution seams. Asphaltene-staining between matrix dolomite crystals in interparticle pore spaces (ppl) (scale = \ 50μm). Well 10-5-23-6W5 (2575.8m). Red arrow pointing towards asphaltene-stained intercrystalline pore spaces.

(4) Dissolved edges of bioclast shell with non-fluorescent drusy mosaic calcite (DM) in fossil mold with fluorescence (fl) (scale = 100μm). Well 10-9-66-21W5 (2402.9m). Red arrow indicating dissolved edges of bioclast.

(5) Dissolved and leached matrix dolomite visible under ppl, seams visible with fluorescence (fl) (scale = 50μm). Well 10-5-23-6W5 (2578.5m).

(6) Core photograph of pin-point vugs in stromatoporoid floatstone with late-stage dissolution episode. Well 10-21-32-2W5 (2756.3m). Red arrow at bottom of photograph indicates up direction. Small arrow indicates vugs in fabric.

(7) Core photograph of subvertical and horizontal fractures. Well 10-5-23-6W5 (2575.5m). Red arrow indicates up direction.

(8) Photomicrograph of horizontal and subvertical fracture network. Well 10-18-21-28W4 (2640.2m).

59

Plate 11: Dissolution and Fracturing

60
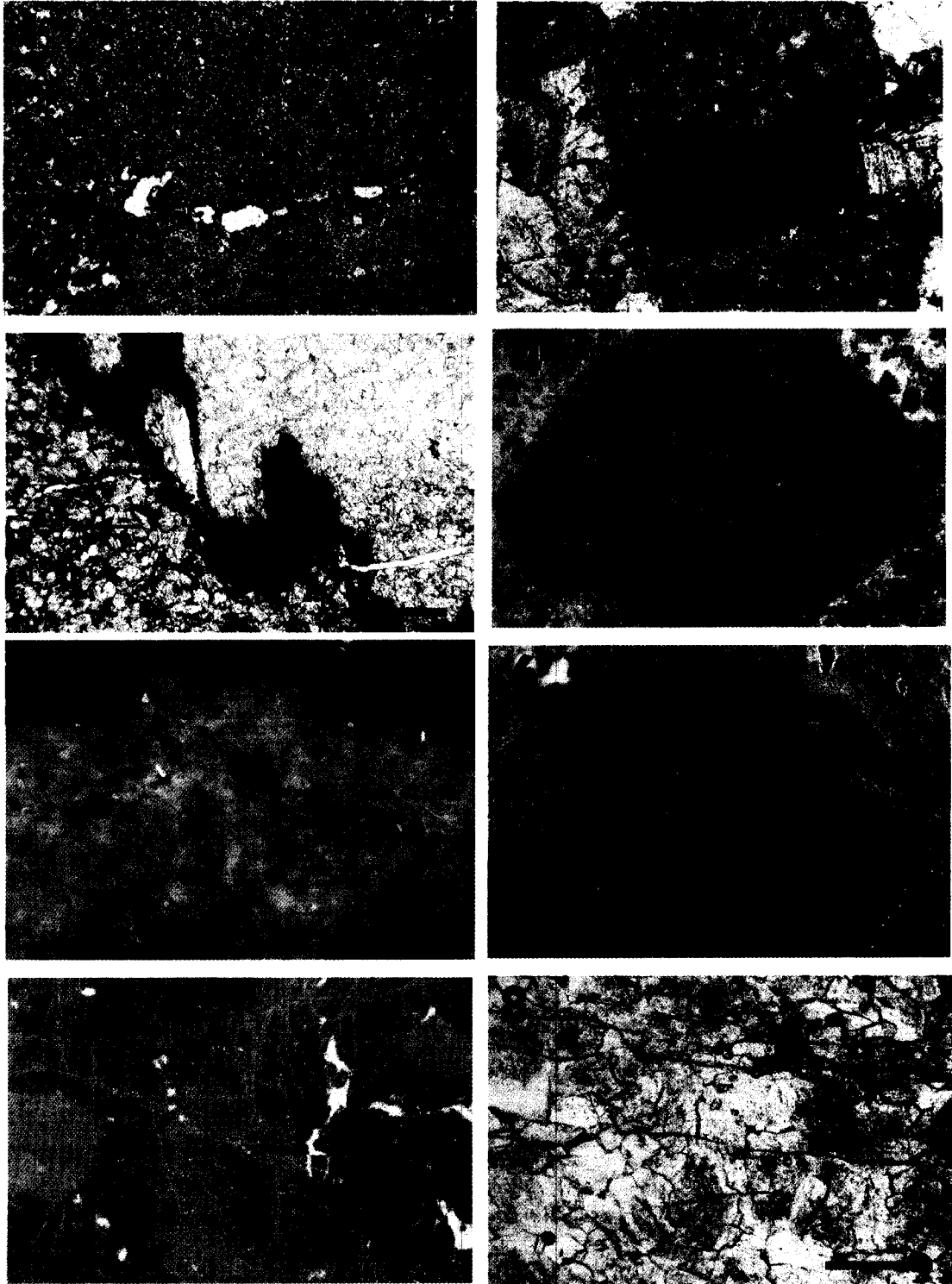
diagenetic history of the study area. Late dissolution formed large vugs (mm- to cm- scale) that were later filled with secondary anhydrites, blocky calcites, pore-lining dolomites, and saddle dolomite. Leached areas within pervasive dolomite fabrics and along dissolution seams and stylolites is further evidence of the intermediate to late timing of dissolution. More than one late dissolution event is seen in the diagenetic history of the Upper Stettler and Crossfield, with evidence of the dissolution of some secondary cements and the precipitation of new cements very late in the diagenetic process. There is also evidence of etching within larger dolomite rhombs particularly in coarse- crystalline matrix dolomite and within dissolution seam dolomites, that are further indicative of the occurrence of intermediate to late dissolution episodes.

4.10 Fracturing

More than one generation of fractures is evident in the Upper Stettler and Crossfield Member (Plate 11). Early fractures (fracture I) are thin, anastomosing, and approximately horizontal that follow along lamination and bedding planes and occur prior to pervasive dolomitisation episodes. Matrix dolomite occluded many of the fractures which are not visible under plane-polarised light but can be seen using Epi-Fluorescence. The second generation of fractures are subvertical microfractures that cross-cut matrix dolomites and early calcite cements. A third generation of subvertical fractures cross-cuts secondary anhydrites as well as late-stage blocky calcite II and pore-lining dolomite in vugs, but these fractures are relatively rare. There is also evidence of late-stage vertical and horizontal fracturing in many of the facies in wells 8-11, that may be evidence of larger-scale compressional and tensional forces.

4.11 Sulphide mineralisation

Sulphide mineralisation is generally a very late process in the diagenetic history of the Upper Stettler and Crossfield Member (Plate 12). With the exception of rare framboidal and more common, cubic pyrite (50-100 μm) identified in wells 1 & 5, most sulphide mineralization although rare volumetrically, occurs as elemental sulphur in small concentrations within vugs in association with blocky II calcite, blocky secondary anhydrite, and saddle dolomite. The highest concentrations of sulphur are seen in dolostone facies in wells 10 & 11, however facies in wells 4-7 also contain scattered crystals of sulphur within small vugs and intercrystalline pore spaces.

61

PLATE 12: Sulphide Mineralisation and Asphaltene

(1) Core photograph of elemental sulphur in association with secondary anhydrite. Well 10-13-26-8W5 (3575.9m). Red arrow at bottom indicates up direction. Small red arrow pointing to elemental sulphur.

(2) Core photograph of secondary anhydrite in association with elemental sulphur in dissolution vug. Well 5-19-30-10W5 (2519.5m). Red arrow at bottom indicating up direction.

(3) Pyrite (P) in microbial mat sediments (ppl) (scale = 100μm). Well 5-22-32-1W5 (2589.8m).

(4) Sulphides (S) in association with blocky I calcite cement in stromatoporoid floatstone (ppl) (scale = 100μm). Well 10-9-66-21W5 (2406.9m).

(5) Elemental sulphur and iron sulphides developed during TSR reactions, fracturing is the result of minor heat produced during TSR (exothermic) in association with secondary anhydrites (ppl) (scale = 50μm). Well 10-13-26-8W5 (3581.5m).

(6) Pile-of-brick, dissolved anhydrite (A) in late-stage vugs, surrounded by asphaltene-stained blocky II calcite (not in FOV) (ppl) (scale = 50μm). Well 10-13-26-8W5 (3581.5m).

(7) Medium- to coarse-crystalline planar-e matrix dolomite with asphaltene within intercrystalline pore spaces (xpl) (scale = 50μm). Well 10-5-23-6W5 (2575.8m). Red arrow pointing to asphaltene-stained intercrystalline pore spaces.

(8) Late-stage dissolution vugs with occluding cements of blocky II calcite (C) surrounded by saddle dolomite (SD), cements are asphaltene-stained related to TSR reactions (xpl) (scale = 200μm). Well 10-5-23-6W5 (2582.3m).

62

Plate 12: Sulphide Mineralisation & Asphaltene

63
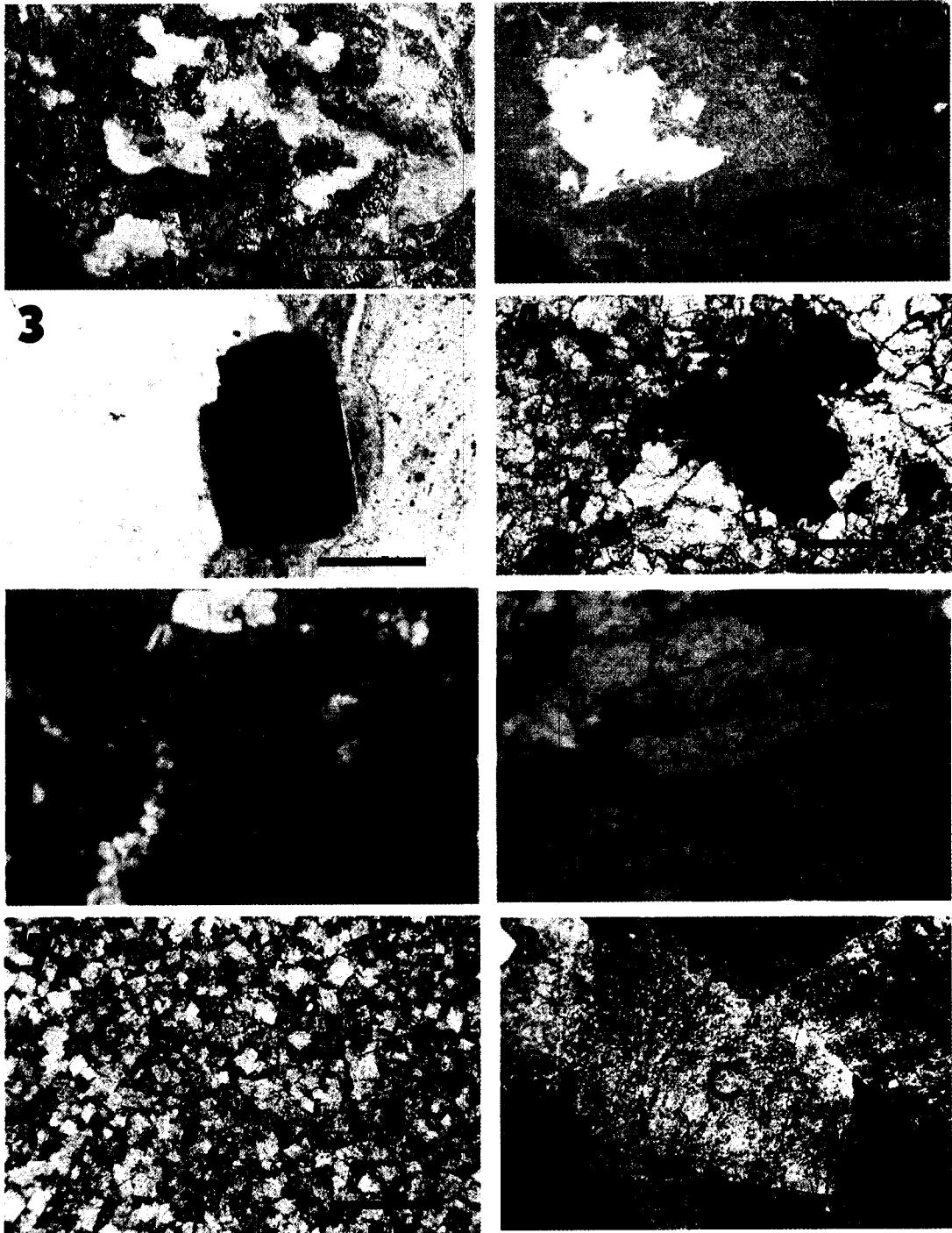
PLATE 13: Other Fabrics and Minerals

(1)   Photomicrograph of unusual fabric identified in the Upper Stettler and Crossfield, replaced by fine-crystalline matrix dolomite with fluorescence (fl). Matrix dolomite replacing primary anhydrites (scale = 100μm). Well 10-23-30-28W4 (2397.9m).

(2)   Photomicrograph of another unusual fabric identified in well 2 (fl) (scale = 100μm). Well 11-23-25-29W4 (2665.4m).

(3)   Photomicrograph of fluorite precipitated as an early diagenetic feature from seawater, seen only in well 1 (fl) (scale = 50μm). Well 10-9-66-21W5 (2406.1m). Red arrow pointing to fluorite crystal.

(4)   Photomicrograph of rare chert precipitated in nodules (xpl) (scale = 100μm). Well 5-19-30-10W5 (2519.5m).

(5)   Photomicrograph of bitumen-staining of matrix dolomites with fluorescence (fl) (scale = 100μm). Well 11-23-25-29W4 (2663.3m). Red arrow pointing to bitumen developing in intercrystalline pore spaces between matrix dolomite fabric.

64

Plate 13: Other Fabrics & Minerals

65
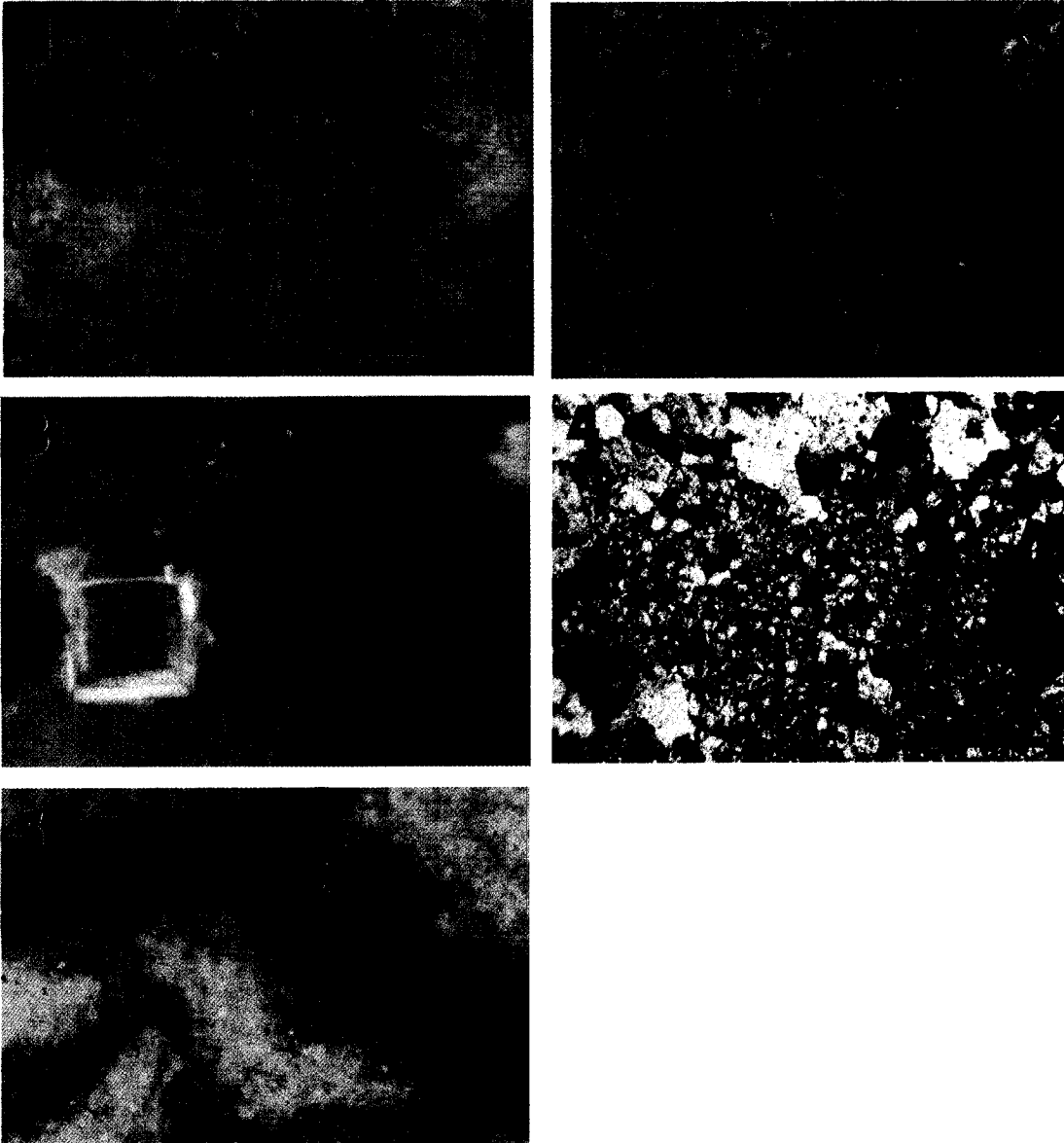
4.12 Pyrobitumen/Asphaltene

Pyrobitumen is a common feature in all of the facies, it is found within intercrystalline pore spaces between pervasive matrix dolomite and within blocky I calcite filled vugs, indicating that it occurred both after the precipitation of blocky I calcite and the dolomitisation of the matrix (Plate 13-5). Asphaltene primarily occurs in wells 8-11, and is most abundant in wells 10 & 11 (Plate 12-7 & 12-8). It is a very late diagenetic event, as it is found staining late-stage blocky II calcite, secondary blocky anhydrite, saddle dolomites and sulphides in large (several mm) vugs. Asphaltene also occurs in interparticle pore spaces between coarse-crystalline matrix dolomite fabrics (Erickson et al., 1994)..

4.13 Porosity

Many diagenetic processes have affected the porosity and permeability of the Upper Stettler Formation and Crossfield Member with the most significant process being the extensive dolomitisation of the study area (Plate 14). Porosity and permeability values were obtained for facies from wells 2-11 from core analysis microfiche at the Core Research Centre in Calgary. Porosity values on average range from 4-5% for all the wells, with the lowest values at 1% and the highest values at 16% for wells 2-7, and <1% to 11.2 % for wells 8-11. Permeability is in the range of <.01 to 4.88 millidarcies (mD). These values are based on all the cumulative values within the wells and not solely on any specific facies, so that individual facies values may be higher or lower than average values. In terms of porosity, most of the primary porosity has been occluded or reduced through diagenetic alteration during the burial process. Secondary porosities are significantly more common, with increased porosity and permeability characteristics developed through the creation of vuggy, intercrystalline, and fracture porosities. The classification of both primary and secondary porosities is based on the scheme by Choquette and Pray (1970).

4.13.1 Primary Porosity

Primary porosity is considered to be any porosity that exists in a rock at the end of the depositional process (Moore, 1989b). It develops during either the predepositional phase (such as in the development of intragranular pores in fossils) or in the depositional phase (such as intergranular and growth framework porosity) (Flügel, 2004). Primary porosities observed in the Upper Stettler Formation and Crossfield Member includes: growth

66

PLATE 14: Porosity

(1)   Core photograph of fenestral porosity with slightly-compressed fenestrae in association with microbial mat (MM) sediments. Well 13-12-29-27W4 (2253.3m). Red arrow at bottom indicates up direction. Small arrow pointing to fenestral fabric.

(2)   Photomicrograph of fenestrae with blocky calcite cements (C) surrounded by peloidal micritic matrix sediments (xpl) (scale = 50μm). Well 10-9-66-21W5 (2400.5m). Red arrow pointing to fenestrae.

(3)   Core photograph of burrow porosity (B) that is selectively dolomitised and fractured. Well 10-13-26-8W5 (3582.6m). Red arrow at bottom of photograph indicates up direction.

(4)   Core photograph of moldic porosity from leached gastropods. Well 10-21-32-2W5 (2756.7m). Red arrow at bottom of photograph indicates up direction. Small arrows pointing to vugs from leached gastropods.

(5)   Photomicrograph of interparticle porosity in stylobrecciated mudstone with fluorescence (fl) ((scale = 100μm). Well 10-9-66-21W5 (2403.2m).

(6)   Photomicrograph of moldic porosity that has been occluded with mosaic calcite cement (C) in bioclastic floatstone (ppl) (scale = 50μm).

(7)   Core photograph of vuggy porosity in peloidal grainstone. Well 10-13-26-8W5 (3574.8m). Red arrow at bottom of photograph indicates up direction. Small arrow pointing to vug.

(8)   Photomicrograph of intercrystalline porosity between matrix dolomite fabric with fluorescence (fl) (scale = 100μm). Well 10-18-21-28W4. Red arrow pointing to intercrystalline pore space.

67
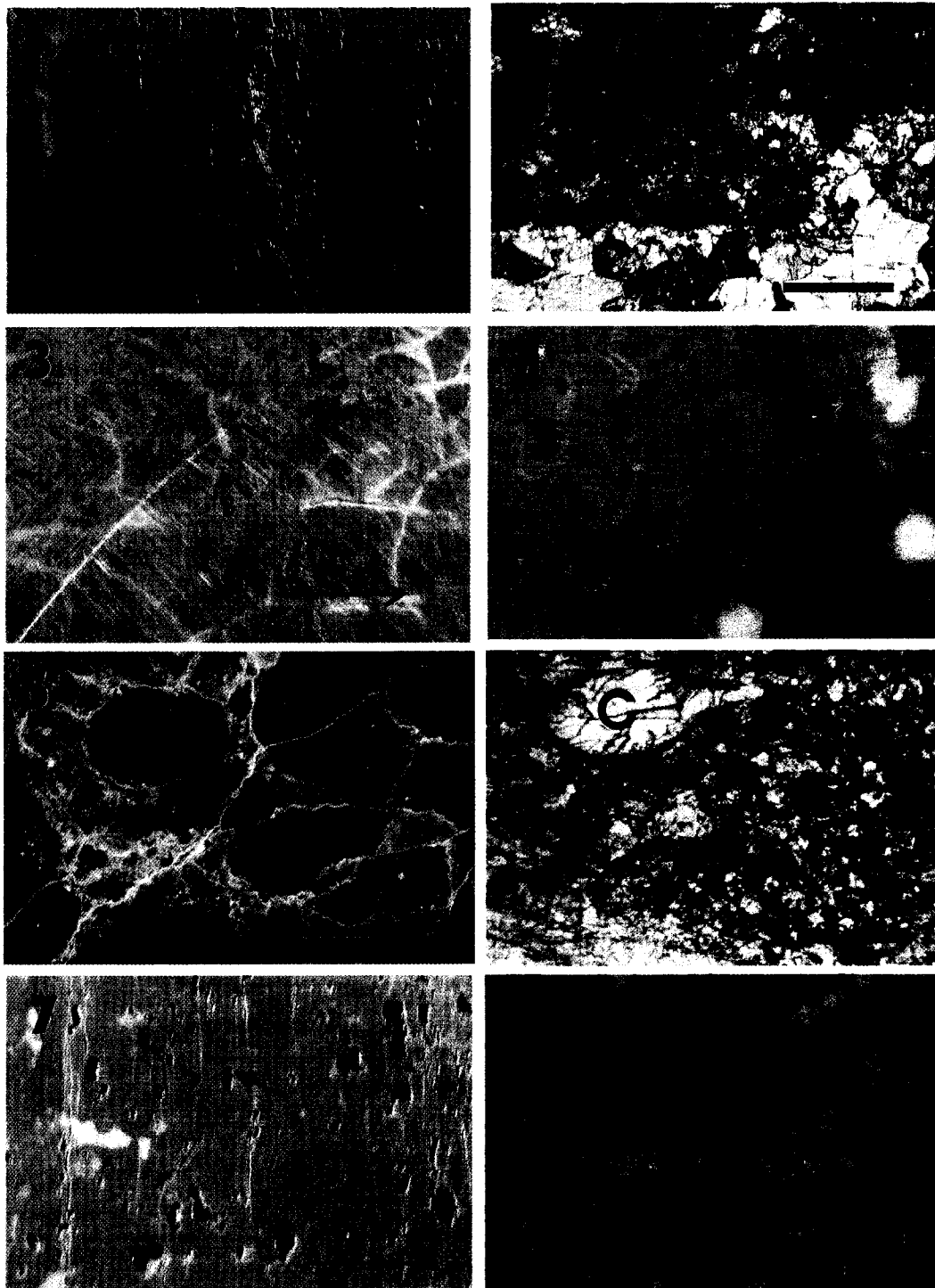
Plate 14: Porosity

framework, intraparticle, fenestral, and interparticle porosity (Plate 14). These porosity types are identified in limestone intervals within all the facies but primarily in wells 1, 8, & 9.

Within bioclastic facies, growth framework porosity (that has been subsequently filled with calcite cements) is seen mainly in stromatoporoid floatstones and bioclastic floatstone/rudstones within the stromatoporoid framework. Intraparticle porosity consists of the pore spaces within the individual skeletal frameworks of brachiopods, gastropods, ostracodes, and calcispheres in the study area. This intraparticle porosity was subsequently occluded with calcite cements or partly to completely micritised.

Fenestral porosity is the most significant primary porosity and it occurs in both laminated and algal mudstones in intertidal facies, forming as a result of degassing processes during microbial growth. This type of porosity has been affected by compaction, in that many of the fenestrae have been flattened. Cementation has also occurred, so that fenestrae are for the most part, filled with pore-lining dolomite and calcite cements. Within wells 2,5,6, and 9 however, the fenestrae are at least 40-50% occlusion-free.

Interparticle porosity is found within undolomitised peloidal grainstone facies between peloidal grains. Some of these grainstones have also been cemented with calcite spar between grains and the interparticle porosity has been destroyed. This is particularly noticeable in well 1.

4.13.2 Secondary Porosity

Secondary porosity is the porosity that develops at any time after the end of deposition. This secondary porosity is commonly created as a result of diagenesis by dissolution, dolomitisation or dedolomitisation, fracturing, or brecciation processes (Flügel, 2004). The identified secondary porosities in the Upper Stettler Formation and Crossfield Member are: burrow, moldic, fracture, vuggy, pin-point, intraparticle and intercrystalline (Plate 14).

Dolomitised burrow structures within mudstone facies are seen in most of the wells and appear most prevalent in wells 8-11. Burrow porosity has not only been affected by dolomitisation, but also appears to have been affected by mechanical compaction as the burrows are slightly flattened in most of the wells.

Moldic porosity was created as a result of dissolution processes affecting the internal fabrics within bioclast shells. This type of porosity is most apparent in well 7, where numerous gastropod shells within bioclastic floatstones are either occlusion-free or filled

69

with calcite cements. This porosity however is often occluded with calcite cements overall, and it occurs to a minor degree in bioclastic facies in all of the wells. Both moldic and burrow porosities are minor components within the Upper Stettler and Crossfield Member study area.

Intraparticle, intercrystalline, and pin-point porosities are prominent in pervasive dolomite matrix fabrics in all of the wells. Intraparticle and pin-point porosities often occur within dolomite rhombs, particularly the coarser matrix dolomites in wells 10 & 11. Dissolution and recrystallisation processes have been observed in these coarse-crystalline matrix dolomites resulting in the development of open spaces within dolomite rhombs. Intercrystalline porosity is one of the most abundant secondary porosity types and is identified in all of the dolomitised intervals within all of the wells. This porosity occurs between dolomite crystals within pervasive dolomite fabrics. In wells 10 & 11, intercrystalline porosity often appears asphaltene-stained. Facies in wells 8-11 have more extensive intercrystalline porosity in association with coarse-crystalline matrix dolomite, which is seen as sieve textures between dolomite crystals.

Fracture porosity is identified in all the wells (1-11) and within all the facies. Fractures are often infilled with blocky to equant calcite cements, secondary anhydrites and pore-lining dolomites. Many of the fractures should be considered microfractures and often appear without cement occlusion, particularly the late-stage horizontal fractures. The wider (a few centimetres), late-stage fractures in wells 10 & 11 are often occluded with secondary anhydrite or calcite containing inclusions of anhydrite.

The most prominent porosity within the study area is vuggy porosity. This porosity is relatively abundant in all the wells (1-11) and present within all of the facies. Vuggy porosity (and pinpoint porosity) are products of dissolution processes and generally occur as both small and large (several mm) unconnected vugs that are either occlusion-free or occluded with blocky calcite, anhydrite, saddle dolomite, and/or sulphides. Many of the vugs in wells 10 & 11 are asphaltene-stained, and when occluded with secondary anhydrite, they appear to have slightly paler reaction rims along the edges of the vugs.

70

Chapter V

Isotope Geochemistry of the Upper Stettler Formation and Crossfield Member

5.1 Introduction

The carbonates and evaporites of the Upper Stettler Formation and Crossfield Member were analysed for stable isotopic ratios of carbon ($^{13}C/^{12}C$), oxygen ($^{18}O/^{16}O$), sulphur ($^{34}S/^{32}S$) and radiogenic strontium ($^{87}Sr/^{86}Sr$). These values will be used in conjunction with petrographic evidence to determine the chemistry and source of dolomitising fluids within the study area. The following sections present the data obtained from these analyses with a brief description of the theory behind the chosen methods.

5.2 Stable Isotope Theory

Isotopes of an element differ from an isotope of the same element by the number of neutrons in the nucleus (Sharp, 2007). The observed differences in the isotopic compositions of oxygen and other elements of low atomic number (including H, C, N, and S) are caused by processes referred to as isotopic fractionation (Faure, 1991). There are three naturally occurring isotopes of Oxygen (^{16}O, ^{17}O, ^{18}O), two isotopes of carbon (^{13}C and ^{12}C), and four isotopes of sulphur (^{32}S, ^{33}S, ^{34}S, ^{36}S) (Sharp, 2007). The magnitude at which isotopic fractionation occurs is dependent on differences between the masses of the isotopes, the chemical bonds which are formed, and the temperature of the formation of these compounds in which the isotopes fractionate (Faure, 1991). Ratios of these elements forming from isotopic fractionation can occur as a result of (1) isotopic exchange reactions, (2) kinetic processes (Rollinson, 1993), and (3) natural physio-chemical processes such as evaporation, condensation, photosynthesis, and transformations (Moore, 2001). The fractionation factor (α) is the ratio between isotopic proportions with different phases of a particular system with these phases forming in equilibrium (Bowen, 1988). The fractionation factor is defined by the following equations (Hoefs, 2004):

$$\alpha^a_b = {}^R_a / {}^R_b \tag{1}$$

and

$$10^3 \ln \alpha^a_b = (A \times 10^6) / T^2 + B \tag{2}$$

71

In equation (1), R_a is the ratio of the heavy to the light element in a phase a, and R_b is the same in phase b, with a reaction in equilibrium at a specific temperature (Faure, 1991). Equation (2) further defines isotope fractionation by taking into account temperature variations for specific exchange reactions, where A and B are constants and T is the temperature in Kelvins (Faure, 1991). The values for both A and B (fractionation factors) for different mineral-water systems were determined and compiled by numerous workers over the last few decades (O'Neil, 1986; Northrop and Clayton, 1966, among many others).

Because of the difficulty in measuring differences in small ratios, the isotope composition is commonly expressed as the per mil difference in the isotope ratios of the standard (std) and the sample (spl). This is used to express differences in isotopes of sulphur, oxygen, and carbon that are analysed in this study, and it is written as (with sulphur as an example):

$$\delta^{34}S = (R_{spl} - R_{std}/ R_{std}) \times 10^3 \text{ ‰} \tag{3}$$

In this particular equation, R is the ratio of the heavy to the light isotope (Faure, 1991). The standard used to express sulphur isotope results is CDT (*Cañon Diablo Troilite*). The standards used to express oxygen and carbon isotope ratios are PDB (*Pee Dee Belemnitella*) from the Peedee Formation in South Carolina and SMOW (*standard mean ocean water*), with PDB generally used for carbonates of low-temperature origin (and in studies of diagenesis) (Sharp, 2007). The standard VPDB is a newer reference standard to replace PDB and it is also taken from the rostrum of a belemnite from the Pee Dee Formation. All the results for oxygen and carbon isotopes in this study are relative to VPDB. The conversion of SMOW and PDB scales for oxygen is:

$$\delta^{18}O_{SMOW} = 1.03091 (\delta^{18}O_{PDB}) + 30.91 \tag{4}$$

Isotopic fractionation occurs for a number of reasons, and in the case of diagenesis, ratios of stable isotopes can be used to identify the contributing source of fluids to diagenetic processes. Some of the suitable conditions and processes that affect isotopic fractionation during the diagenesis and dolomitisation of carbonates include (Brand and Veizer, 1981; Land, 1980):

72

(1)   The water-rock ratio (the openness of the system), in that an open-system would allow for the renewal of isotopes in fluids, whereas a closed system would involve a recycling effect between the fluids and associated rocks. With the dissolution of carbonates at depth, a closed system would only allow for small-scale dolomitisation processes, just as there is no influx of cations and anions, ^{18}O will not sufficiently enter the system either (Land, 1980).

(2)   Temperature variations that may contribute to the fractionation of a system, for example, temperature changes with depth.

(3)   The composition of diagenetic fluids and associated variations in salinity which are characteristic of these fluids. The exposure of carbonates with burial to increasing salinity conditions and also, the effect of dissolved evaporitic material contributes to more negative $\delta^{18}O$ and to a lesser degree, $\delta^{13}C$ values.

(4)   The secular variation of oceans over time and the related isotopic values of seawater from which the carbonates precipitated. The oxygen isotopic composition of carbonates becomes more depleted in $\delta^{18}O$ with the increasing age of the rocks (Veizer et al., 1999). In general, significant climate conditions affect the global ocean systems at any given time, and positive changes in $\delta^{18}O$ are often ascribed to changes in polar ice and the overall climate of the Earth at the time (Immenhauser et al., 2003).

(5)   Biological fractionation (vital effect) occurring when an organism develops out of equilibrium with the surrounding seawater, with the exception of brachiopods and some bivalves that tend to reflect conditions at the time of original precipitation (Brand and Veizer, 1981; Popp et al., 1986).

(6)   Changes in latitude, altitude, as well as seasonal variations also affect fractionation effects and the $\delta^{18}O$ composition of fluids (Tobin et al, 1999; Goodfriend, 1999; and Clarke and Jenkyns, 1999).

All of the above factors variably influence the isotopic composition of fluids and this has a direct effect on the isotopic composition of the minerals that precipitate from these fluids. The main fluids that contribute to the formation of dolomite include seawater, brines associated with evaporation from seawater, meteoric fluids, and water with an isotopic composition that has been altered through isotopic fractionation during water/rock reactions (Allan and Wiggins, 1993). Marine water at the time of the precursor mineral formation and each of theses fluids has a characteristic isotopic signature in relation to oxygen and carbon

and can therefore, be used to understand diagenetic processes that have occurred during secondary alteration events.

5.3 Carbon ($^{13}C/^{12}C$) and Oxygen ($^{18}O/^{16}O$) Isotope Results

A total of 83 samples were analysed for oxygen and carbon values and the data was collected with an isotope ratio mass spectrometer (IRMS) (Appendix 4). The following sections are the results of these analyses. The calcites examined include micrite, syntaxial calcite, blocky calcite (I & II), and late-stage blocky to equant fracture calcite. Other calcite cements (dogtooth, bladed, and drusy mosaic) present in the Upper Stettler Formation and Crossfield Member were not examined due to their close spatial relationship with the surrounding micrite, the samples would have been likely contaminated. In terms of dolomites, all the pervasive matrix dolomite phases, pore-lining dolomite, saddle dolomite, and dissolution-seam related dolomite were examined.

5.3.1 Calcites

(1) Limestone micrite (n=9) have values ranging from -3.96 to -7.28 ‰ (VPDB) for $\delta^{18}O$ and -1.14 to 1.27 ‰ (VPDB) for $\delta^{13}C$. These values are slightly depleted with respect to Late Devonian calcite phases that would have precipitated from Famennian seawater (Fig 5.1). Famennian seawater values are in the range of $\delta^{18}O$ = -4.5 (±0.5) ‰ and $\delta^{13}C$ = +2.0 (±0.5) ‰ (Hurley and Lohmann, 1989).

(2) Syntaxial calcite (n=3) have values ranging from -4.38 to -6.05 ‰ (VPDB) for $\delta^{18}O$ and 0.44 to 2.00 ‰ for $\delta^{13}C$ (VPDB).

(3) Blocky calcites I & II, and late-stage fracture calcite have values ranging from -5.65 to -11.13 ‰ (VPDB) for $\delta^{18}O$ and -0.39 to -22.60 ‰ for $\delta^{13}C$ (VPDB). These values indicate a steady depletion in $\delta^{13}C$ values with a less pronounced, but significant depletion in $\delta^{18}O$ values. Depleted values are representative of a continuum of blocky calcite cements that precipitated from shallow burial through to deep burial regimes. The most depleted calcite values are characteristic of late-stage blocky calcite cements that precipitated in vugs in association with saddle dolomite and late-stage secondary anhydrite. Blocky II calcites are interpreted to have occurred very late in the diagenetic history of the Upper Stettler Formation and Crossfield Member.

74
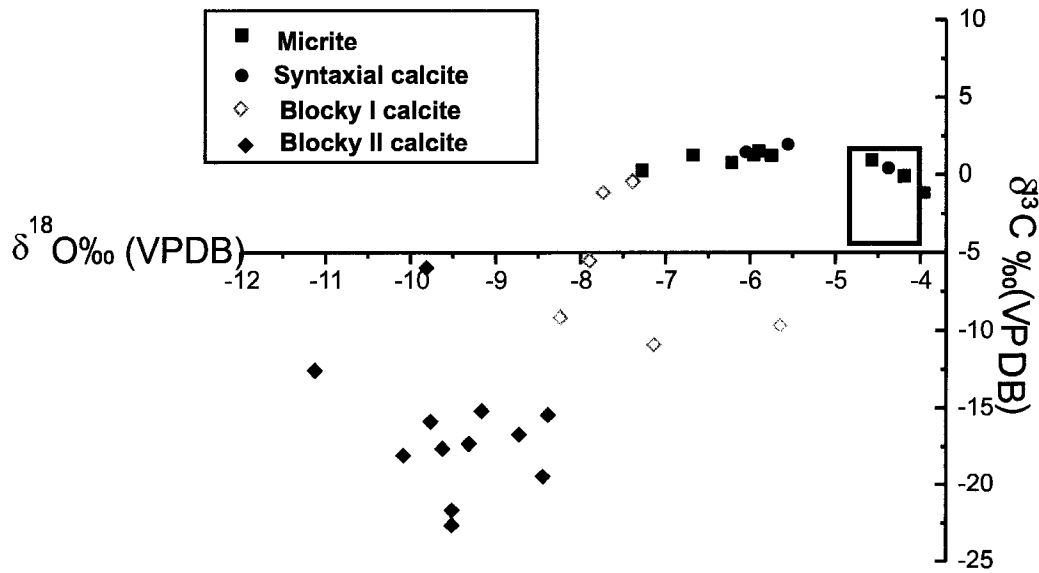
Figure 5.1: Plot of oxygen and carbon stable isotope results for calcite phases of micrite, syntaxial calcite, Blocky I calcite, and Blocky Ii calcite. Red box represents postulated calcite values precipitating in equilibrium with Famennian seawater. Values are from Machel et al. (1996).

75

5.3.2 Dolomites

(1) Dolomicrite (n=6) values range from -5.10 to -5.81 ‰ for $\delta^{18}O$ (VPDB) and -0.91 to 1.30 ‰ for $\delta^{13}C$ (VPDB). Dolomicrites have slightly lighter isotopic values with regard to both $\delta^{18}O$ and $\delta^{13}C$ (VPDB), and indicate a deviation from Famennian seawater values (Fig 5.2).

(2) Fine- to medium- crystalline matrix dolomites (n= 12) have similar values to dolomicrites with -2.82 to -6.17 ‰ for $\delta^{18}O$ (VPDB) and 0.22 to 1.08 ‰ for $\delta^{13}C$ (VPDB), with the closest value to carbonates precipitated in equilibrium with Famennian seawater of -2.82 ($\delta^{18}O$) and 0.22 ($\delta^{13}C$) (VPDB).

(3) Coarse- crystalline dolomite (n=25) has values which vary the most from the values of carbonates precipitated in equilibrium with Famennian seawater, but are still close to the other pervasive matrix dolomites in overall values. The values range from -4.42 to -8.32 ‰ for $\delta^{18}O$ (VPDB) and -1.14 to 1.19 ‰ for $\delta^{13}C$ (VPDB), with covariant depletion of slightly depleted carbon and more significantly depleted oxygen values.

(4) Dissolution-seam related dolomite (n=5) have similar compositions to the coarse-crystalline pervasive dolomite but with slightly higher carbon ($\delta^{13}C$) values.The composition range is from -4.49 to -6.51 ‰ for $\delta^{18}O$ (VPDB) and -1.09 to -2.14 ‰ for $\delta^{13}C$ (VPDB).

(5) Saddle dolomite cement (n=4) varies from -5.16 to -6.99 ‰ for $\delta^{18}O$ (VPDB) and -3.43 to -1.32 for ‰ for $\delta^{13}C$ (VPDB). Although many isotopic values cited for saddle dolomite have characteristically high depletions in $\delta^{18}O$ and to a slightly lesser degree in $\delta^{13}C$ values, these compositions correspond with other values cited for the Wabamun Group in Alberta (Mountjoy and Halim-Dihardja, 1991; Packard et al., 1992). The composition of the saddle dolomite cements are slightly depleted in $\delta^{13}C$ and are more significantly depleted in $\delta^{18}O$ (relative to Famennian seawater).

(6) Pore-Lining dolomite (n=1) yielded results similar to matrix dolomites, with -6.23 ‰ for $\delta^{18}O$ (VPDB) and 0.93 ‰ for $\delta^{13}C$ (VPDB) relative to carbonates precipitating from Famennian seawater. Only one sample was analysed for pore-lining dolomite due to its close spatial relationship with surrounding matrix dolomites. As a result, there is the possibility of contamination by other dolomite phases.

76

■ Dissolution-Seam Dolomite
◆ Dolomicrite
▲ Fine- to Medium- Crystalline Matrix Dolomite
▼ Coarse- Crystalline Matrix Dolomite
● Saddle Dolomite

$\delta^{18}O$ ‰ (VPDB)

$\delta^{13}C$ ‰ (VPDB)
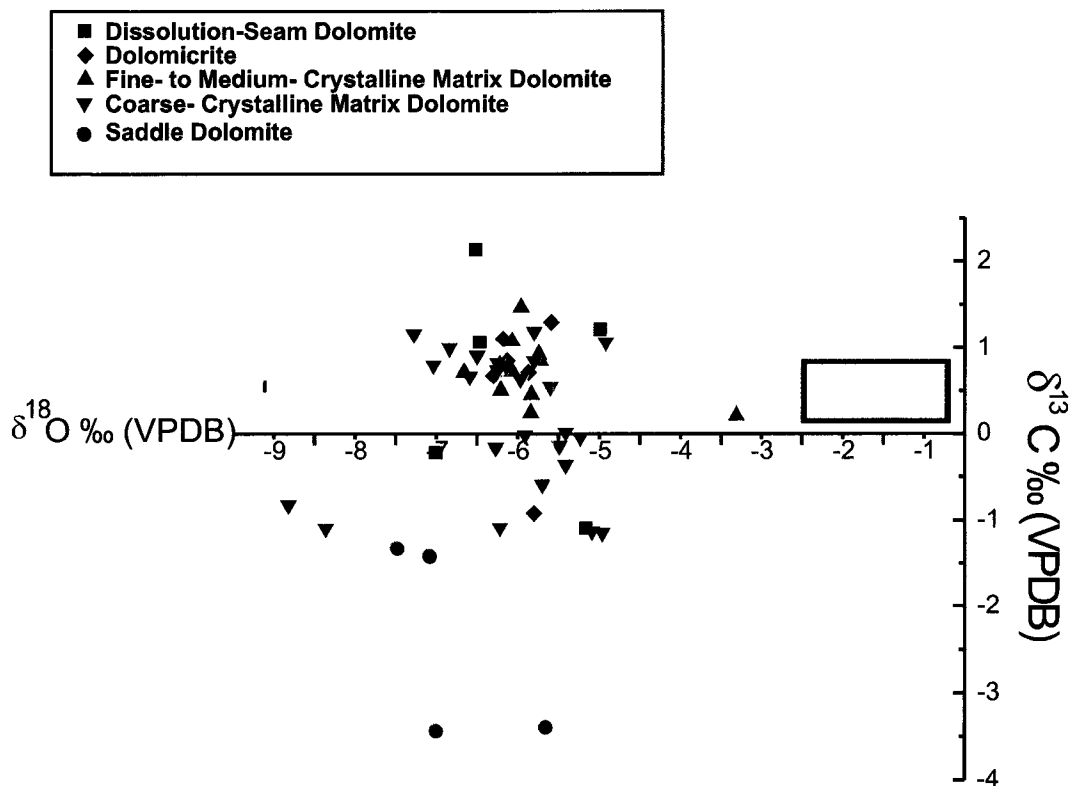
Figure 5.2: Plot of Oxygen and carbon isotope results for dolomite phases: dissolution-seam dolomite, dolomicrite, fine- to medium-crystalline matrix dolomite & coarse-crystalline matrix dolomite. Blue box represents postulated values of dolomite precipitating in equilibrium with Famennian seawater. Values from Machel et al. (1996).

77

5.4 Sulphur Isotopes

The $\delta^{34}S$ values of marine evaporites correspond with the isotopic composition of dissolved ocean sulphate at the time of their formation and are reported relative to the Cañon Diablo Troilite (CDT). The secular seawater curve for $\delta^{34}S$ values ranges from less than 10‰ to over 35‰, with the overall characteristics of the curve explained in terms of the addition or removal of reduced sulphur to the oceans (Sharp, 2007). Marine evaporites that have formed as inorganic precipitates from these oceans will therefore be a reflection of seawater compositions at the time of formation (with slightly displaced values through fractionation processes of 0 to +2.4‰) (Strauss, 1999). Factors that affect the sulphur compositions of the ocean at any given period are consequently reflected in the evaporites that precipitate during that particular period. Variations in the ocean values of $\delta^{34}S$ occur as a result of:

(1) The dissolution of older evaporitic material that may have been previously buried and then exposed through uplift and subsequently weathered. The sulphur in these evaporites will increase the ocean values of $\delta^{34}S$ significantly (Bottrell and Newton, 2006).

(2) The effects of high biological activity (by sulphate-reducing bacteria), wherein sulphate-reducing bacteria tend to produce sulfides depleted in $\delta^{34}S$ during their metabolism, resulting in the removal of depleted $\delta^{34}S$ sulphur as sedimentary sulphides (Canfield, 2001). Overall, this will increase the $\delta^{34}S$ of oceans (and evaporites formed from these oceans) (Sharp, 2007). Bacterial sulphate reduction (BSR) and thermochemical sulphate reduction (TSR) are significant processes in the reduction of sulphates, with $\delta^{34}S$ variations from TSR reactions reported by Machel (2001) as +2.4 to +24.1 ‰ in relation to ocean values.

(3) Weathering processes lower the $\delta^{34}S$ of the oceans, evaporites precipitating from these oceans would therefore have lower values (Sharp, 2007).

The secular ocean curve is developed from the compiled values of evaporites from specific time periods, which indicate that values in the late Proterozoic are similar to that of today (in the mid-range of values) and $\delta^{34}S$ values were high in the Cambrian through the Devonian, decreasing to a minimum in the Permian (Veizer et al., 1980). Claypool et al. (1980) suggest a considerable decrease in $\delta^{34}S$ in the early Devonian with a sharp rise into the late Devonian, with values in the Famennian up to +30 ‰ to +34 ‰.

78

5.4.1 Sulphur (^{34}S/ ^{32}S) Isotope Results

A total of 17 samples were examined for sulphur isotope ratios. Of this total, results were obtained for: native sulphur (n=2), primary anhydrite (n=7), and secondary anhydrite (n=8) (Table 5.1). The results indicated a progressive increase in ‰ δ^{34}S (CDT) values from primary anhydrites to secondary anhydrites (Fig 5.3). One primary anhydrite sample was close to the seawater curve, with the other 6 samples as slightly enriched in comparison to Devonian seawater. Native sulphur samples were also enriched, with one native sulphur sample having the highest value of 29.7 ‰ δ^{34}S (CDT), suggesting it formed significantly later in the diagenetic process. The progressively higher values for secondary anhydrite suggests a continuous process of secondary precipitation through intermediate to late diagenesis.

5.5   Strontium (^{87}Sr/^{86}Sr) Theory

In contrast to stable isotopes, a radiogenic isotope is a daughter isotope that is produced from the decay of a radioactive parent isotope (Banner, 2004). There are four isotopes of strontium: ^{84}Sr, ^{88}Sr, ^{87}Sr, ^{86}Sr, with ^{84}Sr being the most rare isotope and ^{88}Sr the most common (Allan and Wiggins, 1993). ^{86}Sr is non-radiogenic, and ^{87}Sr is radiogenic and formed from the radioactive decay of ^{87}Rb (Faure, 1991). Prior to diagenetic processes, fluids in carbonates should reflect or have similar ratios to that of marine water during original precipitation of the carbonate mineral. If the carbonate mineral has not been contaminated through the interaction of clays that have a high ^{87}Rb content (^{87}Sr is the daughter product of ^{87}Rb), then the original ^{87}Sr incorporated into the carbonate mineral will remain constant (Moore, 1989). Interaction with certain non-carbonate phases may therefore be a useful indicator of fluid pathways. Non-carbonate phases can significantly contaminate carbonate isotopic signatures however and purity is an important consideration when analysing carbonates (Bailey et al., 2000).

The ^{87}Sr/^{86}Sr ratio is derived from seawater at the time of original precipitation, and this seawater is influenced by the effects of chemical weathering on the continents and in ocean basins, and has therefore varied through time in response to global tectonics (Moore, 1989). Strontium can be used for the dating and correlation of sediments as seawater curves have been developed by numerous workers to indicate the relative ratios of ^{87}Sr/^{86}Sr for seawater throughout the Phanerozoic (Denison et al., 1997; Veizer et al., 1999; Brand, 2004). If the value of a carbonate differs from that of the original marine signature for any particular

79

Table 5.1: Sulphur $\delta^{34}S$ CDT

Sample	Depth	Well #	Phase	Sulphur Values
SR115NS	3581.48m	Well 11	Sulphur	26.1
SR095NS	2519.53m	Well 9	Sulphur	29.7
SR064PA	2387.12m	Well 6	Anhydrite	26.4
SR410PA	2619.54m	Well 4	Anhydrite	26.1
SR023PA	2647.28m	Well 2	Anhydrite	26.7
SR034PA	2247.19m	Well 3	Anhydrite	26.2
SR117PA	3582.59m	Well 11	Anhydrite	26.6
SR015PA	2406.06m	Well 1	Anhydrite	22.1
SR082PA	3636.98m	Well 8	Anhydrite	26.5
SR078SA	2756.74m	Well 7	Secondary Anhydrite	24.6
SR101SA	2571.80m	Well 10	Secondary Anhydrite	27.1
SR514SA	2589.10m	Well 5	Secondary Anhydrite	26.1
SR092SA	2513.71m	Well 9	Secondary Anhydrite	27.8
SR432SA	2644.65m	Well 4	Secondary Anhydrite	27.6
SR314SA	2258.93m	Well 3	Secondary Anhydrite	26.8
SR613SA	2397.91m	Well 6	Secondary Anhydrite	27.5
SR029SA	2653.07m	Well 2	Secondary Anhydrite	26.7

Table 5.2: Strontium $^{87}Sr/^{86}Sr$ Results

Sample	Depth	Well #	Phase	Strontium Values
R092SA	2513.71m	Well 9	Anhydrite	0.708042±14
R031PA	2245.45m	Well 3	Anhydrite	0.708158±13
R214VC	2663.24m	Well 2	Blocky Calcite	0.710289±18
R428VC	2639.47m	Well 4	Blocky Calcite	0.708747±11
R106LC	2575.97m	Well 10	Blocky Calcite	0.708408±10
R113LC	3575.86m	Well 11	Blocky Calcite	0.709956±15
R113FD	3575.86m	Well 11	Pore-Lining Dolomite	0.709690±70
R059LD	2584.22m	Well 5	Dolomicrite	0.708229±10
R415FD	2624.81m	Well 4	Fine- to Medium Crystalline Matrix Dolomite	0.710872±10
R518FD	2591.03m	Well 5	Fine- to Medium Crystalline Matrix Dolomite	0.708426±15
R078SF	2756.74m	Well 7	Fine- to Medium Crystalline Matrix Dolomite	0.708330±18
R093PG	2515.62m	Well 9	Fine- to Medium Crystalline Matrix Dolomite	0.708448±11
R109PG	2583.69m	Well 10	Fine- to Medium Crystalline Matrix Dolomite	0.708394±16
R037FD	2251.24m	Well 3	Coarse-Crystalline Matrix Dolomite	0.710222±10
R615PG	2401.77m	Well 6	Coarse-Crystalline Matrix Dolomite	0.709492±13
R087FD	3659.18m	Well 8	Coarse-Crystalline Matrix Dolomite	0.709211±10
R112SG	3574.75m	Well 11	Coarse-Crystalline Matrix Dolomite	0.710532±26
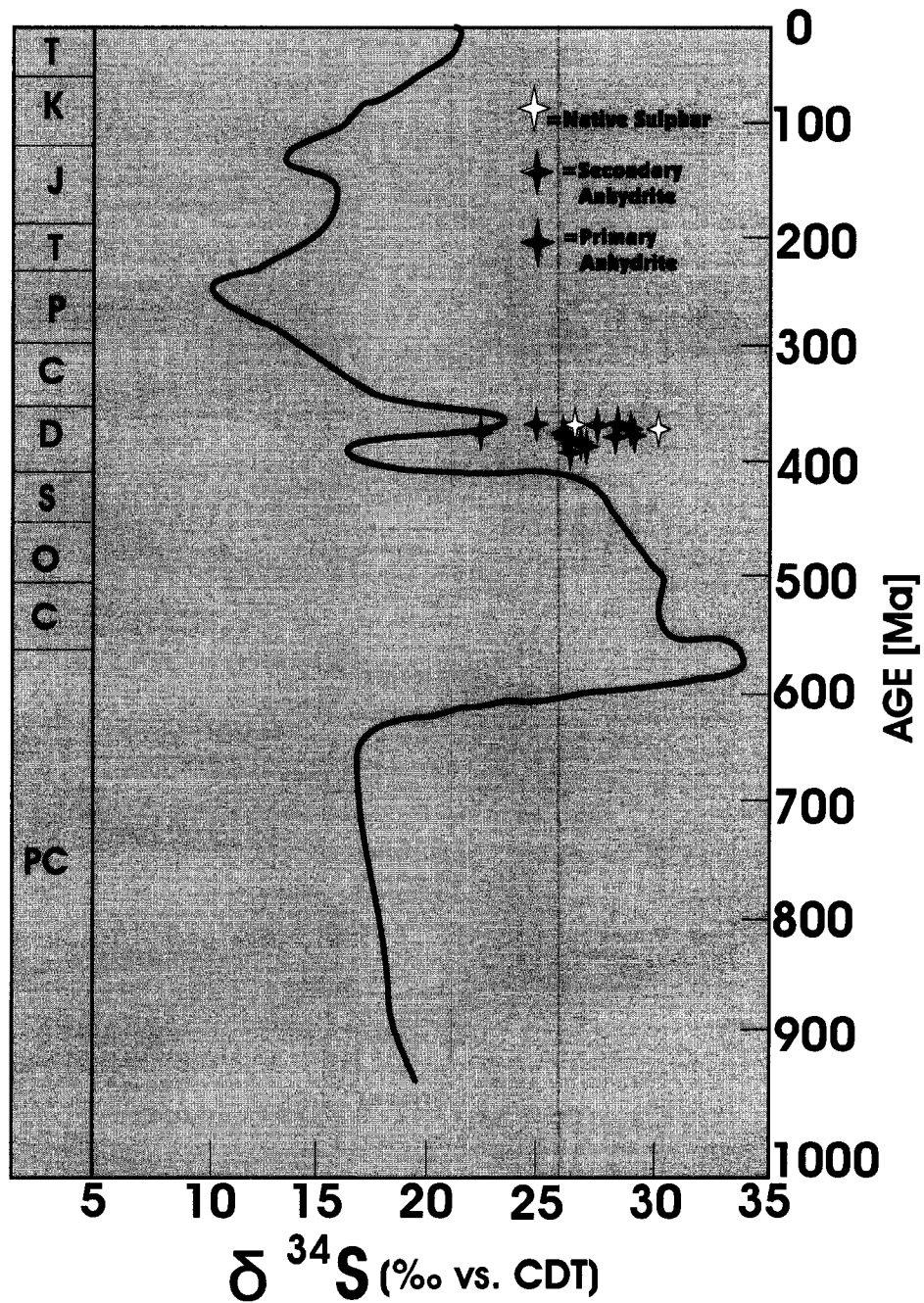
Figure 5.3: Sulphur isotope results against age and seawater curve for evaporite phases of primary & secondary anhydrite and elemental sulphur. Curve modified from Claypool et.al 1980 and Botrell and Newton, 2005)

81

time period, then this difference can be attributed to diagenetic alteration by younger seawater or to diagenesis by non-marine fluids. The $^{87}Sr/^{86}Sr$ ratio can therefore be used to date diagenetic events such as dolomitisation (if seawater is the source of the fluids) and no recrystallisation has occurred since this event (Moore, 1989).

5.5.1 Strontium ($^{87}Sr/^{86}Sr$) Isotope Results

A total of 17 samples were analysed for strontium ($^{87}Sr/^{86}Sr$) ratios (Table 5.2) and were plotted against Famennian seawater values (Fig 5.4). Strontium values for carbonates precipitating from Famennian seawater are estimated at 0.70805 to 0.70830 (Veizer et al., 1999). The values for primary anhydrites (n=2) are 0.70804 and 0.70816. These values are roughly coeval with Famennian seawater values. Blocky calcite values (n=4) range from 0.70841 to 0.71029 with values that are within the range of Famennian seawater and values that are significantly enriched with respect to Famennian seawater. These values reflect the different stages of precipitation of calcite cements within the Upper Stettler Formation and Crossfield Member. Dolomites (n=11) range from 0.70823 to 0.71087, with slightly enriched to significantly enriched isotopic values. The most radiogenic samples are the medium-crystalline and coarse-crystalline matrix dolomites that may have been the product of recrystallisation processes that produced overall coarser dolomite fabrics. The fine-crystalline matrix dolomites and dolomicrites appear to have precipitated in fluids closer to Famennian seawater values. Recrystallisation processes may therefore have essentially reset the original signatures of medium- and –coarse- crystalline matrix dolomites whereas the fine-crystalline dolomites represent closer to original precipitation conditions. An alternative explanation is that the coarse-crystalline matrix dolomites may have precipitated from more radiogenic pore fluids with increasing depth. The one sample of saddle dolomite is also characteristically more radiogenic than Famennian seawater.
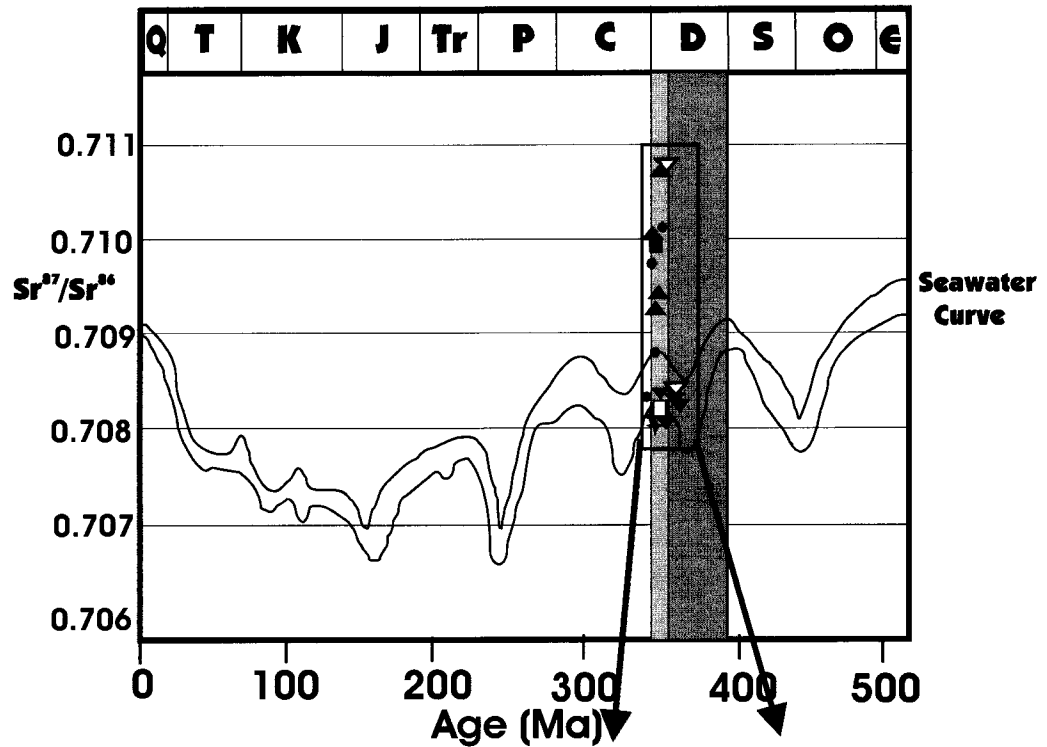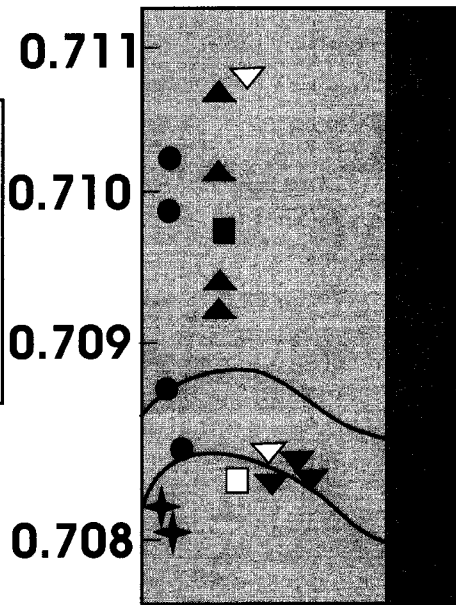
Figure 5.4: $^{87}Sr/^{86}Sr$ results for calcite, dolomite, and anhydrite phases against age and seawater curve. Paler grey sections are Famennian of Late Devonian.

83

Chapter VI

Discussion and Interpretation:
Diagenesis in the Upper Stettler Formation and Crossfield Member

6.1   Introduction

The diagenesis and dolomitisation of the Upper Stettler Formation and Crossfield Member began soon after deposition and continued into the deep burial realm. The diagenetic features observed in the study area through the use of petrography and isotope geochemistry are discussed in the following sections. An outline of the diagenetic processes that occur from deposition through to deep burial is explained in terms of burial depths, timing, and the composition of pore-fluids. The interpretation of this diagenetic history and the relationships between diagenetic events is summarised in the form of a paragenetic sequence (Fig 6.1).

6.2   Early Diagenesis

Shortly after deposition there is evidence of the possibility of early lithification in sediments deposited in supratidal and upper intertidal environments. Finely laminated sediments have little intercalation between laminations and although there exists minor truncations of evaporite cements, for the most part, laminae are intact (James and Choquette, 1990). In the upper intertidal realm, there is evidence of intraclastic material in fine peloidal mudstones that is further suggestive of early lithification (Erickson et al, 1994). In lower intertidal through subtidal settings, there is however, little evidence of early lithification.

Cementation is limited to minor calcite cements (which will be discussed in the following sections) within lower intertidal through shallow subtidal realms but this cementation does not occur on an extensive scale within either depositional setting. The precipitation of evaporites is documented within some upper intertidal areas that may have been periodically exposed. The formation of evaporites in supratidal settings, with extensive precipitation of primary anhydrite and gypsum, is commonly deposited as nodules or thin laminations.

Micritisation is the earliest diagenetic feature that can be observed within all of the wells (1-11) (Plate 4-1). These micritisation processes are limited to bioclastic and peloidal grainstones through floatstone/rudstones that are interpreted to have developed in the lower

84
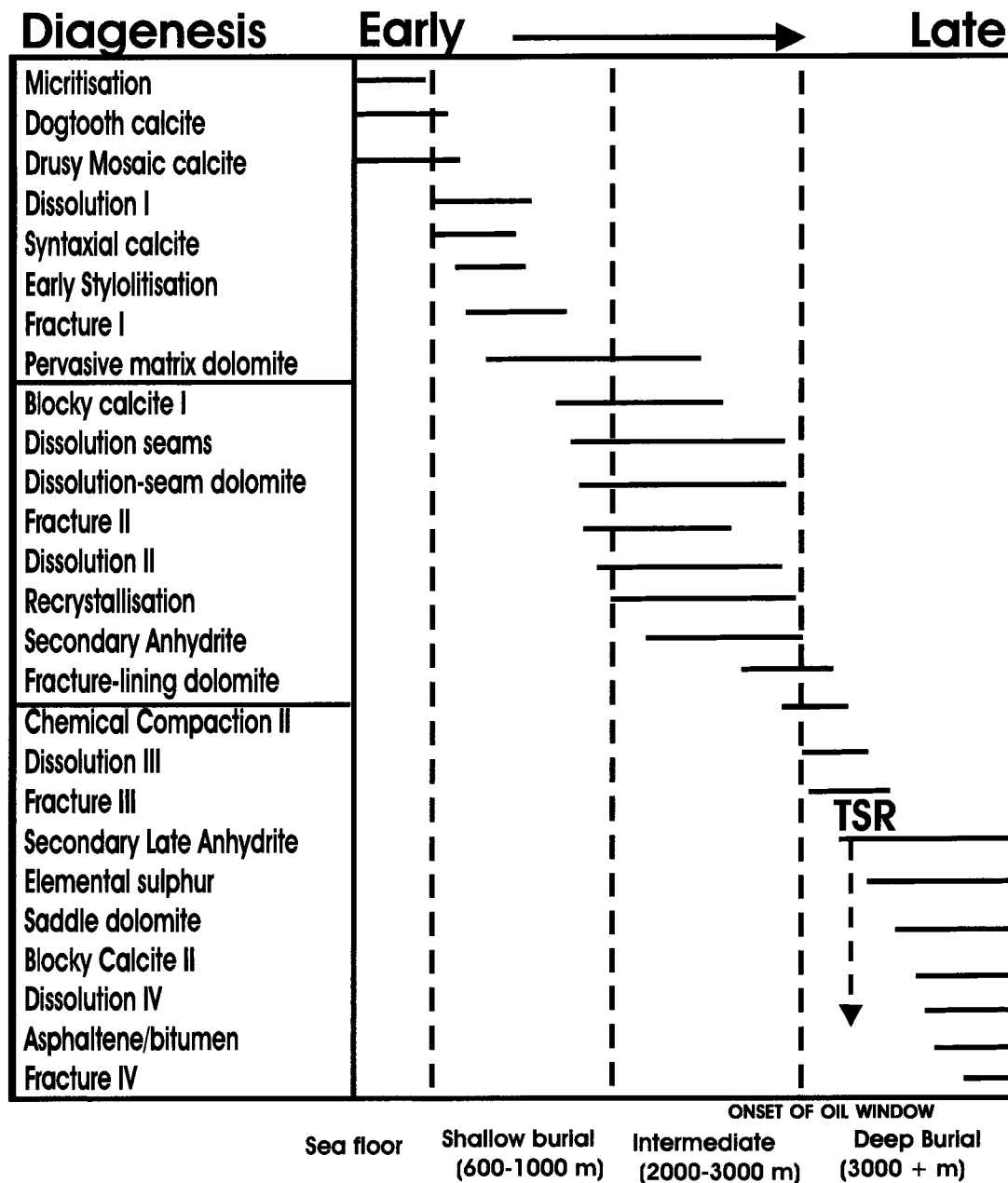
Figure 6.1: Paragenetic sequence of early through late diagenetic events and calcite, dolomite, and anhdyrite/gypsum phases in the Upper Stettler Formation and Crossfield Member. Depth adapted from Machel (1999).

85

intertidal through shallow subtidal depositional realms. Micritisation features include micritic envelopes developed around bioclastic material, clumping of peloidal grains, and the complete micritisation of bioclastic material.

Neomorphic alteration of aragonitic and high-magnesium calcite within bioclasts occurred early in the diagenetic history. Two other significant neomorphic alterations occurred within the study area and were continuous processes throughout the diagenetic history of the Upper Stettler Formation and Crossfield Member: (1) the first detailed nemorphism is the pseudomorphic alteration of anhydrite to gypsum and gypsum to anhydrite, and (2) the recrystallisation of fine- to medium-crystalline matrix dolomites (Plate 4). Both of these processes will be discussed in greater detail in the following sections.

6.3   Calcite Cementation

With the exception of blocky calcite cements that precipitated throughout the diagenetic history of the study area, there are few examples of other types of calcite cements. Other calcite cements are minor to rare and in many cases, are only visible within the Giroux Lake area (well 1). The only calcite cements that were geochemically sampled for isotopic analysis are the blocky and the syntaxial calcites. The other calcite cements that have been identified were too fine to be sampled without risk of contamination. As a result, the timing of dogtooth calcite, bladed to equant calcites, and drusy mosaic calcites are derived solely from petrographic evidence from limited undolomitised strata.

6.3.1   Dogtooth, Drusy Mosaic, and Bladed to Equant Cements

Dogtooth cement is very fine-crystalline and evident along the edges of fossil fragments in interparticle pore spaces and can be characterised as meteoric, marine-phreatic or shallow burial (Flügel, 2004). This type of cement most likely developed in the shallow subsurface in conjunction with the precipitation of drusy mosaic calcites within interparticle pore spaces. Both cements infill interparticle/intraparticle pore spaces within fossil molds created from shallow dissolution processes (Plate 8). Unfortunately, the lack of isotopic data makes a more precise determination of timing difficult.

Bladed to equant cements are typically marine cements (Carpenter and Lohmann, 1989), however this can also be interpreted to be a burial cement (Choquette and James, 1990). This cement precipitates in vugs with blocky I calcite cement, and as a result, it is

86

interpreted to have precipitated at moderate burial at early/intermediate stages in the burial history.

6.3.2 Syntaxial Calcite Cement

Syntaxial calcite cements are typically cloudy and twinned in the Upper Stettler and Crossfield (Plate 8). Generally, syntaxial cements precipitated in marine vadose or phreatic environments tends to be cloudy (and may be inclusion-rich), whereas syntaxial cements formed with burial depth are clear (Flügel, 2004). However, the growth of syntaxial cements has also been interpreted to be of meteoric, marine, or deep-burial origin (Walker et al., 1990). The cloudy nature of the crystals of syntaxial calcite in the Upper Stettler and Crossfield suggest that it precipitated from marine or meteoric-marine waters. The isotopic signatures of oxygen and carbon for syntaxial cements ($\delta^{18}O$ = -4.38 to -6.05 ‰ VPDB and $\delta^{13}C$ = 0.44 to 2.00 ‰ VPDB) suggest that it precipitated in fluids that were slightly depleted in $\delta^{18}O$ from typical Famennian seawater (Famennian seawater: $\delta^{18}O$ = -4.5 and $\delta^{13}C$= +2.0 ‰), but are consistent with precipitation from Famennian seawater for $\delta^{13}C$ values. The signatures suggest that the syntaxial cements have precipitated from Famennian seawater and the slightly lighter $\delta^{18}O$ values are the result of modified pore fluids with shallow burial. Evidence for shallow burial is further corroborated with the identification of syntaxial cements forming between bent/broken bioclasts. Precipitation between bent/broken bioclasts indicates that some mechanical compaction had occurred with burial prior to the precipitation of syntaxial cements. The syntaxial crystals have also been affected by mechanical compaction processes with the development of mechanically twinned crystals.

6.3.3 Blocky Calcites I – II

Volumetrically, blocky calcites are the most abundant calcite cement and have precipitated during various stages in the diagenetic history of the Upper Stettler and Crossfield (Fig 6.2). Blocky I calcites precipitated in the intermediate burial stages of the units, developing in dissolution vugs and fractures (Plate 8). This calcite is often relatively clear and inclusion-free (although there are some examples of rare anhydrite replacement), and forms medium through coarse (up to 800μm) crystals. Isotopically, they are depleted in $\delta^{18}O$ (values of -5.65 to -7.90 ‰ VPDB) and more significantly depleted in $\delta^{13}C$ (values of - 0.39 to -10.90 ‰ VPDB). With increased temperature associated with burial, $\delta^{18}O$ values tend to become isotopically lighter (Coniglio et al., 1994). The $\delta^{18}O$ values of the cements are probably depleted as a result of increasing temperatures from precipitation at

87
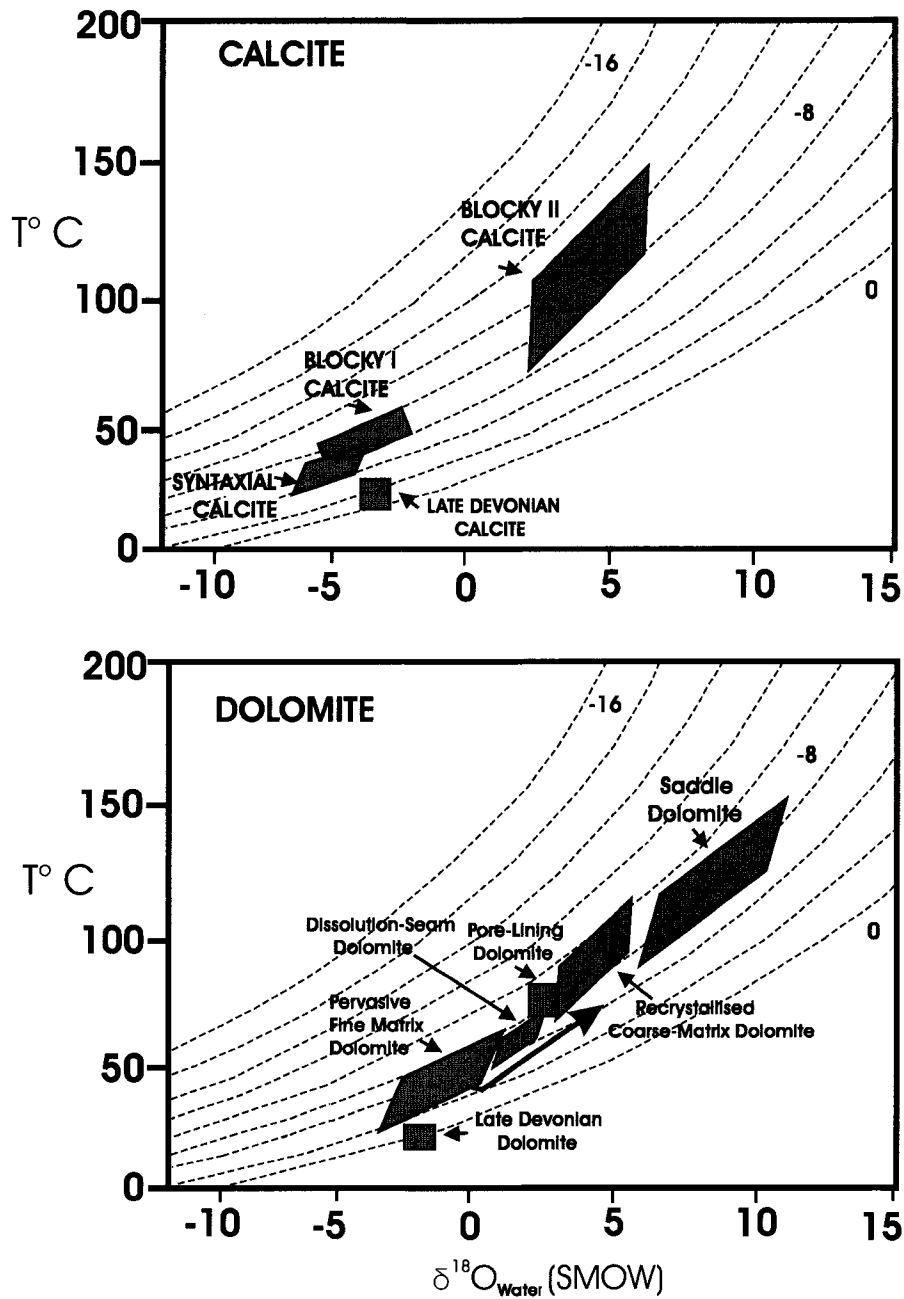
Figure 6.2: Oxygen Isotope composition of fluid versus
formation temperature for calcite and dolomite. Isochore lines
are oxygen composition of phases in (VPDB). Red Arrow shows
recrystallisation pathway. The isotopic fractionaltion curves are
derived from Friedman and O'Neil (1977).

intermediate depths through the burial process. Depletion in $\delta^{13}C$ is often an indication of the effects of increased organic matter with burial (Yang et al., 1995). The progressive depletion of $\delta^{13}C$ values is therefore most likely an indication of the interaction of sediments during burial with pore fluids that have a higher organic content. The strontium $^{87}Sr/^{86}Sr$ values (0.70841 – 0.70875) for blocky I calcite are slightly more enriched than that of Famennian seawater (values of 0.70805 to 0.70830 fromVeizer, 1997), which indicates that original signatures have not been significantly altered, suggesting that the blocky I calcites precipitated fairly early in the diagenetic history of the Upper Stettler Formation and Crossfield Member.

Blocky II calcite cements are interpreted to be late-stage burial cements and represent the latest diagenetic cement in the Upper Stettler and Crossfield. They are vug and fracture-occluding cements that are typically cloudy, asphaltene-stained, and coarser than blocky calcite I (forming up to 1.2 mm crystals). These calcites are often identified replacing secondary anhydrites and in association with elemental sulphur and saddle dolomite cements. The isotopic composition of the cements is significantly depleted in both oxygen and carbon ($\delta^{18}O$ = -8.24 to -11.13‰ VPDB and $\delta^{13}C$ = -9.14 to -22.60 ‰ VPDB) (Fig 5.1). In terms of strontium ^{87}Sr, blocky II calcites represent one of the most radiogenic phases (with values of 0.70996 to 0.71029) relative to the typical strontium $^{87}Sr/^{86}Sr$ values of Famennian seawater.

Depleted $\delta^{18}O$ may be a result of increased temperatures with burial in conjunction with changes in the $\delta^{18}O$ of the formation fluids from which the calcites precipitated from (Mountjoy et al., 1999). The $\delta^{13}C$ values of calcite cements can be used to identify the influence of meteoric fluids to the pore fluids, the oxidation of thermogenic or biogenic CH_4, whether or not CO_2 from microbial processes or the maturation of organic matter affected pore fluids, or whether thermochemical sulphate reduction occurred (Machel and Cavell, 1999).The significantly depleted $\delta^{13}C$ of the blocky II calcite is most likely related to high-temperature TSR processes [as a reflection of the generation of CO_2 by the oxidation of hydrocarbon gases (Krouse et al., 1988)]. Temperatures at which the calcite cement precipitated were probably greater than 150°C, as this is the minimum temperature at which late-stage calcites replace late diagenetic anhydrites in wells that have been affected by TSR reactions (Heydari and Moore, 1989). The strontium $^{87}Sr/^{86}Sr$ ratios further support precipitation from pore fluids mixed with low fluxes of increasingly radiogenic fluids that may be the result of tectonic loading and basin evolution or compactional processes related to the Late Devonian- Early Mississippian Antler Orogeny, but more likely related to the Laramide Orogeny in the Late Cretaceous to Early Tertiary. This rationale is based on

studies of similar Devonian carbonates in the Alberta Basin that have precipitated vug-occluding late-stage blocky calcites with comparable isotopic signatures and petrographic characteristics (Machel and Cavell, 1999; Buschkuehle and Machel, 1999).

6.4   Dolomitisation

Dolomitisation is one of the most significant diagenetic events to occur in the Upper Stettler Formation and Crossfield Member (Plates 9 & 10). In terms of diagenetic alteration, it has affected all the facies in wells 1-11 and is an important factor in understanding the changes in porosity and permeability that have occurred in the study area. Ultimately, porosity and permeability characteristics are greatly affected not only by pervasive matrix dolomitisation processes but also by the development of dolomite cements that have precipitated throughout the burial process.

6.4.1   Characteristics of Pervasive Matrix Dolomite

It is likely that all of the matrix dolomite in wells 2-11 was precipitated from a similar dolomitisation mechanism early on in the diagenetic history of the Upper Stettler Formation and Crossfield Member. The criteria for early pervasive dolomitisation events occurring in the shallow burial diagenetic realm and the characteristic features of these matrix dolomites include:

(1) Dolomitisation occurs in sediments that are relatively unlithified, and the degree of preservation of the original fabrics (such as fenestrae and peloidal grains) is quite significant in the dolomicrite and fine- to medium- crystalline matrix samples. The preservation of precursor depositional fabrics indicates that the dolomitisation of sediments occurred prior to any fabric-destructive diagenetic processes associated with increased burial.

(2) The development of sub-parallel, anastomosing microstylolites that were subsequently healed by matrix dolomitisation processes suggests that the sediments underwent shallow burial prior to dolomitisation. However, subsequent fabric-destructive episodes of stylolitisation and the development of dissolution seams cross-cut dolomite matrix fabrics and indicate that most major chemical compaction events occurred with increasing depth and after the pervasive dolomitisation of the precursor matrix.

(3) Matrix dolomite is relatively fine- to medium- crystalline and ranging from (<10 μm – 200μm) with the mean size range of <100μm. Coarse- crystalline dolomite ranges from 200μm to 450μm and is most significant in wells 8-11, these coarse- crystalline dolomites

90

indicate that recrystallisation processes have occurred with burial and they will be further discussed in section 6.7.

(4) The fabric of the matrix dolomite ranges from planar-s to nonplanar, is typically non-luminescent to very dully luminescent and is pale to dull green to non-fluorescent. Replacement of precursor limestone is generally mimetic, with most original depositional structures preserved. Within the coarse- crystalline dolomites, dolomitisation is often fabric-destructive and the identification of precursor fabrics is difficult (precursor fabrics are especially difficult to determine in wells 8, 9, and 11).

(5) The isotopic (oxygen and carbon) composition of the dolomites ranges from $\delta^{18}O$ of -4.79 to -6.17 ‰ (VPDB) (with one outlier of -2.82 ‰) and $\delta^{13}C$ values of 0.22 to 1.47 ‰ (VPDB) (mean value of -5.33 and with one outlier of -0.91) for all of the dolomicrite and fine-crystalline dolomite matrix samples. These values are slightly more depleted isotopically than Famennian carbonates precipitating in equilibrium with seawater (the values would also be expected to be slightly more positive as a result of the effects of evaporation). The amount of depletion is likely the result of recrystallisation processes that have affected the matrix dolomite during subsequent burial diagenesis. Coarse-crystalline matrix dolomites reflect this recrystallisation by a further depletion in oxygen isotopic values and a slight depletion in carbon values. The composition of coarse-crystalline dolomites range from -4.22 to -8.32 ‰ (VPDB) for $\delta^{18}O$ (with a mean value of -5.65) and from -1.14 to 1.19 ‰ (VPDB) for $\delta^{13}C$ values (Fig 5.2).

(6) Strontium $^{87}Sr/^{86}Sr$ values of the matrix dolomites indicate that the dolomicrite and fine-crystalline dolomite precipitated from Famennian (or evaporated) seawater, these values are close to values for Famennian seawater of 0.70805 to 0.70830 (Veizer et al., 1999) (Fig 5.4). The primary evaporite values are also close to Famennian seawater values which further suggests that the dolomicrite and fine-crystalline matrix dolomite precipitated from Famennian seawater. Coarse-crystalline and medium-crystalline matrix dolomites are slightly more radiogenic and in conjunction with oxygen/carbon values, may further confirm that recrystallisation processes have diagenetically altered matrix dolomites during the burial process.

6.4.2 Pore-Lining Dolomite Cement

Pore-lining dolomite is a very minor phase in the Upper Stettler Formation and Crossfield Member. It typically occurs in wells 2 through 10 as a pore-lining cement in

91

fenestrae and as a intermediate vug-occluding cement. The isotopic composition of this cement is relatively depleted with regard to oxygen values but is in a similar range to values of coarse-crystalline dolomites [$\delta^{18}O$ = -4.42 to -8.32 ‰ and $\delta^{13}C$= -1.14 to 1.19 ‰ (VPDB)] (Fig 5.2). The oxygen values suggest that this cement precipitated at some depth, but the carbon values indicate fluids that have not been affected by deep burial processes and organic reactions. The carbon values are similar to what would be expected from Famennian seawater (Veizer et al., 1999), and as a result, the lack of diagenetic alteration of carbon values with depth combined with slightly depleted oxygen values are suggestive of an intermediate burial after initial pervasive dolomitisation episodes that reflect values associated with the timing of coarse-crystalline matrix dolomite. There is also the possibility that the correlation of these dolomites with coarse-crystalline matrix dolomites may be a result of contamination during extraction as a result of the close spatial relationship between the two dolomite types.

6.4.3 Dissolution-Seam Associated Dolomite

This dolomite began to precipitate after the first episodes of pervasive dolomitisation and continued to precipitate with continued burial. Its occurrence with dissolution-seams of insoluble residues of clays, organics, and iron-rich residues indicates that chemical compaction had already started to alter the sediments. Chemical compaction begins to affect sediments at subsurface burial depths of at least 10's to 100's metres (Tucker, 1988). The destruction of fine- to medium- crystalline matrix dolomite by dissolution-seam dolomite indicates that this dolomite must have developed with some depth and after initial pervasive dolomitisation had occurred.

The oxygen and carbon isotopic compositions of dissolution-seam dolomite ($\delta^{18}O$ = - 4.66 to -6.51 ‰ and $\delta^{13}C$ = -1.09 to 2.14 ‰ VPDB) suggest that it occurred during multiple pressure solution events throughout the diagenetic history of the study area. Oxygen and carbon values (Fig 5.2) reflect two trends: first, relatively early burial signatures with slightly depleted values from Famennian seawater, and secondly, more significantly altered carbon values that suggest interaction with more carbon-depleted fluids with slightly higher organic content. Isotopic values are notably higher in well 10 outside of the Crossfield trend whereas Crossfield trend wells tend to have values more compatible with Famennian seawater. This discrepancy is most likely the result of the greater diagenetic alteration in the wells west of the Crossfield trend that has been observed both petrographically and geochemically in all of

92

the wells 8 through 11. This dolomite therefore developed in more than one stage in the diagenetic history of the Upper Stettler and Crossfield, but for the most part, it is an intermediate to late diagenetic event that occurred with deeper burial. Its isotopic signature suggests however, that it is not one of the latest diagenetic features in the diagenetic history of the study area.

6.4.4   Saddle Dolomite Cement

Saddle dolomite is a late-stage diagenetic cement in wells 5 through 8 and 10 & 11 (Fig 6.1). This dolomite is also significantly more abundant in wells 10 & 11. In all of these wells, saddle dolomite is a fracture and vug-occluding phase that is commonly associated with blocky calcite and secondary blocky anhydrite, and is often asphaltene-stained. The significance of this cement is that it typically precipitates at high temperatures, and is often associated with sulphide mineralization and hydrocarbon occurrences (Radke and Mathis, 1980), further substantiating that it is a high temperature and/or late burial cement. The texture of saddle dolomites occurring in the Upper Stettler Formation and Crossfield Member are predominantly coarse (up to 2mm crystals), subhedral to anhedral crystals, with undulose extinction and curved crystal faces. The presence of saddle dolomite is an indication of the high temperatures of precipitation, suggested temperatures of 60 - 150°C or within the oil window (Searl, 1989), and the high salinity of pore fluids (Machel, 1987).

The oxygen and carbon isotopic values for saddle dolomite samples are relatively similar to that of pervasive dolomites, but with slightly more depleted oxygen ($\delta^{18}O$) values [mean of -6.30 ‰ (VPDB)] and more significantly depleted carbon ($\delta^{13}C$) values [mean of -2.40 ‰ (VPDB)]. Lower values are expected with higher salinity pore fluids associated with burial (Machel, 1987). The formation of hydrocarbons and TSR reactions in the presence of organic matter will lower the overall SO_4^{2-} content of the fluids, increasing the alkalinity and aiding in the precipitation of saddle dolomite (Davies, 2000). These factors will also contribute to the overall depleted oxygen and carbon isotope values.

6.5   Dolomite Recrystallisation Features

Characteristics of recrystallisation fabrics include: (1) a negative shift in $\delta^{18}O$ and an enrichment in $^{87}Sr/^{86}Sr$ values (Al-Aasm and Packard, 2000), (2) an increase in overall crystal size and nonplanar over planar crystal faces (Kupecz et al., 1995), (3) crystal

93

overgrowths (identified with CL) and etched cores (Al-Aasm, 2000), (4) Increasing dolomite stoichiometry and ordering with increased depth (Kupecz et al., 1995).

There are two distinctive size ranges of pervasive matrix dolomite crystals, the first size range (<10 – 200µm) and the second size range (>200µm- 450µm) are indicative of crystallisation from different types of pore fluids. Typical coarse-crystalline dolomite in the study area has etched cores and partially-dissolved edges, and appears to have bright, clear rims and cloudy cores under both CL and Epi-Fluorescence. The $^{87}Sr/^{86}Sr$ ratios plotted against $\delta^{18}O$ indicate that coarse-crystalline dolomites have undergone a degree of recrystallisation in contact with more radiogenic pore fluids that are enriched in ^{87}Sr (Figure 6.3). In this same plot, oxygen values are isotopically heavier with increasing ^{87}Sr enrichment. Two possible explanations may be given for this: (1) with increased burial (typically $\delta^{18}O$ values would become lighter) the more positive values may be an indication of relatively low water-rock interaction in which recrystallisation processes are occurring. The dilution of pore waters with slightly-increased $\delta^{18}O$ compositions may be reflected in the recrystallised dolomite, (2) the system may have been affected by isotopic re-equilibration during recrystallisation that was essentially a continuous process after early pervasive dolomitisation and occurred through to deep burial (Erickson et al., 1994).

6.6   Well Comparison of Diagenetic Alteration

The dolomitisation of wells along the Crossfield trend (wells 2-7) were compared with the wells west of the Crossfield trend (wells 8-11) in terms of the degree of dolomitisation observed and the nature of the dolomite fabrics (Fig 6.4). The following differences were observed:

(1) Dolomite crystal sizes tend to be coarser, with predominantly coarse-crystalline dolomites in wells 8-11. The dolomite fabric in these wells also tends to be planar-e, whereas in wells 2-7, the typical fabric is planar-s to nonplanar.

(2) There are undolomitised intervals within wells 8- 11 (particularly in wells 8-10), that may be indicative of the edges of a variable dolomitisation front that has developed through episodic dolomitisation processes. In contrast, all of wells 2-7 have been completely dolomitised and there are no intervals of undolomitised strata.

(3) Within wells 8-11, there is significantly less anhydrite observed in the Upper Stettler evaporites in comparison to wells within the Crossfield trend (2-7).

94
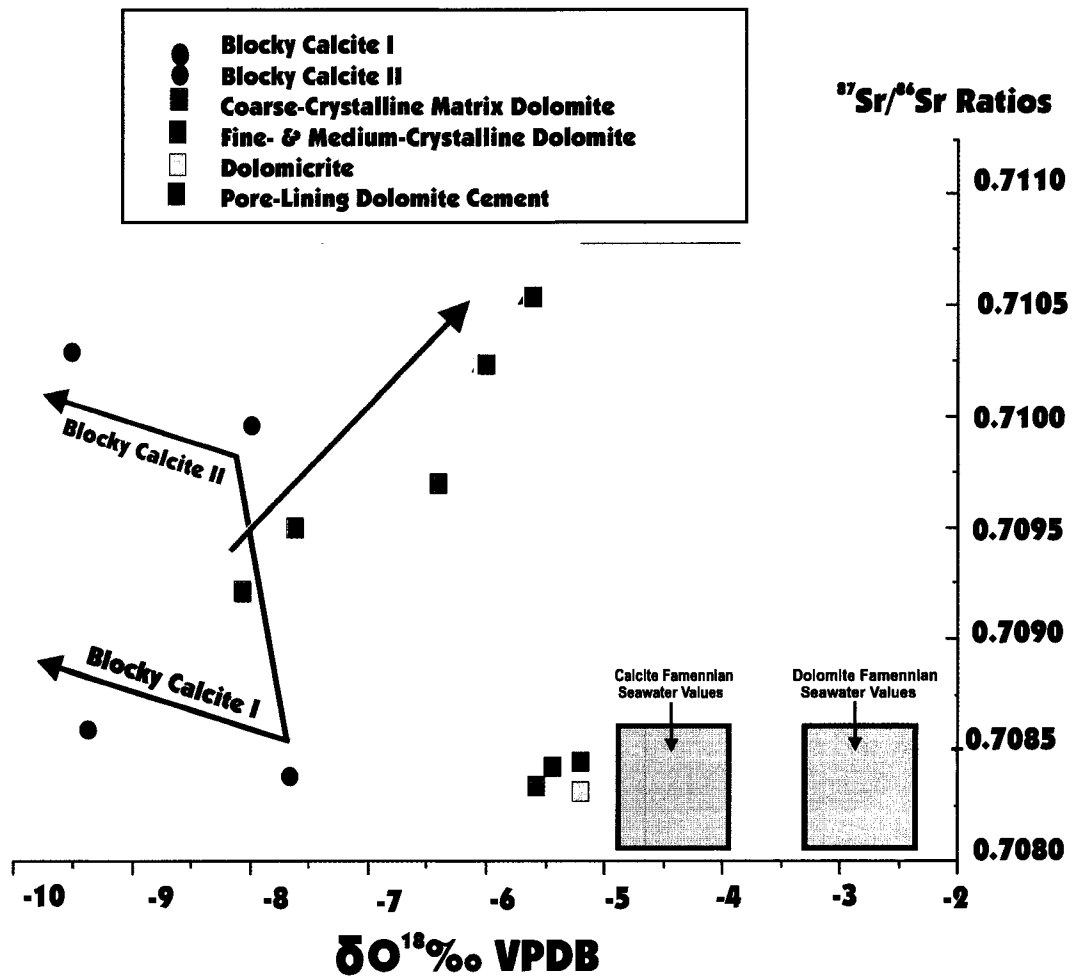
Figure 6.3: $^{87}Sr/^{86}Sr$ results versus oxygen isotope composition. Blue and red boxes represent precipitation in equilibrium with Famennian seawater. Light blue arrow shows recrystallisation pathway, dark blue & red arrows indicate blocky calcites - red arrow indicates precipitation from more radiogenic pore fluids with depleted oxygen values. Famennian seawater values from Machel et al. (1996).

95
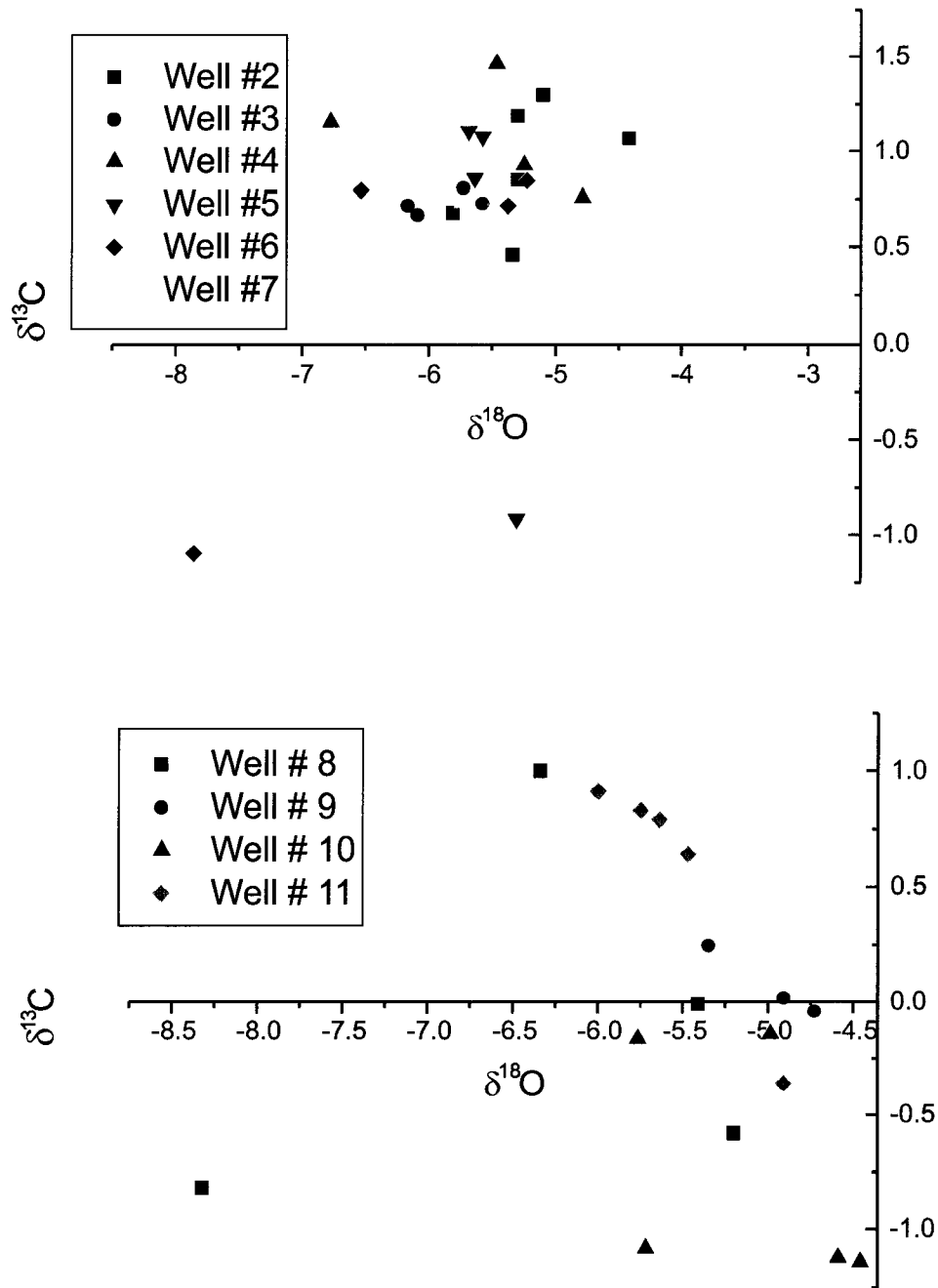
Figure 6.4: Comparison of oxygen and carbon values of Pervasive
Matrix Dolomites for facies from two groups of wells - wells 2-7 in
Crossfield Trend and wells 8-11 in Panther River/Moose Mtn/Burnt
Timber/Benjamin Ghost regions.

96

(4) The oxygen and carbon isotope values show some variation between wells 2-7 and 8-11 (Figure 6.3). Isotopic values show slightly more depleted $\delta^{18}O$ and $\delta^{13}C$ in wells 8-11 indicating more progressive diagenetic alteration and recrystallisation with burial in these wells.

(5) Porosity characteristics within pervasive matrix fabrics in well 8-11 indicate the presence of more extensive dissolution processes with increased vuggy porosity that cross-cuts matrix dolomite fabrics. Within these vugs are asphaltene-stained cements of late-stage sulphides, saddle dolomite, and blocky II calcite. Within wells 2-7, vugs within matrix dolomite fabrics are commonly not asphaltene-stained and with the exception of well 4, there is a limited occurrence of elemental sulphur.

(6) There is an abundance of H_2S within the wells outside of the Crossfield trend in comparison with the region where wells 2 to 7 are drilled (Eliuk, 1984). This disparity may be directly related to the degree of TSR reactions occurring within these wells.

Characteristics of greater diagenetic alteration and dolomites precipitated from modified pore waters are more evident in wells 8-11 than along the Crossfield trend. In well 11 in particular, significant generations of fractures suggest that this well at least has been exposed to larger-scale tensional or compressional processes. These networks of compressional fractures are relatively well-developed in well 11 and probably developed with significant burial. The timing of late-burial fracturing may be related to episodes of compression associated with the Laramide Orogeny (Al-Aasm and Clarke, 2004; Erickson et al., 2004)

6.7   Dolomitisation Models

Most modern dolomite precipitation is penecontemporaneous, and forms patchy concentrations comprising units less than 1m thick. In contrast, ancient dolomites are found to be much more laterally extensive and can form units that are hundreds of metres thick (Warren, 1989). Several conditions must be met in order for large-scale dolomitisation, similar to those formed in ancient settings to occur (Morrow, 1990): (1) There must be a sufficient supply of Mg^{2+} ions available for the development of any significant amount of dolomite; (2) A delivery mechanism is necessary to transfer the Mg^{2+} ions to the site of dolomitisation; and, (3) The composition of the dolomitising fluids must be conducive to dolomitisation ie. the fluids must be able to overcome any kinetic inhibitions to

97

dolomitisation (Machel, 2004). Any proposed dolomitisation models for large-scale dolomitisation processes will be viable only if the above conditions are met.

Proposed models for dolomitisation involve many different types of fluids, including marine brines, continental brines, normal seawater, and modified seawater (from evaporation, sulphate reduction, or mixing with meteoric water) (Warren, 1989). There are a number of proposed dolomitisation models for large-scale dolomitisation processes that involve each of these fluid types. These dolomitisation models will be discussed briefly in the following sections, and a mechanism will be suggested for the dolomitisation of the Upper Stettler Formation and Crossfield Member. The dolomitisation models that will be discussed include: (1) Sabkha (evaporative) model; (2) Seepage-Reflux model; (3) Seawater (Kohout) models; (4) Mixing-zone models; (5) Burial Compaction models and hydrothermal/tectonic models. The basic description of these models is taken from Machel and Mountjoy (1986), Tucker and Wright (1990), Warren (1989 & 2000), Morrow (1990), Machel (2004), and Flügel (2004).

6.7.1 Sabkha Model

Modern dolomitisation in the Arabian Gulf sabkhas involves flood (marine) recharge processes during the winter and spring through storm, wind, and tidal action on to supratidal flats (Tucker and Wright, 1990). Dolomitisation occurs along tidal channels and lagoons, in areas that have been exposed to the maximum flux of seawater through the sabkha and due to intense evaporation, hypersaline brines develop (Warren, 1989; Müller et al., 1990). Since areas of dolomite growth follow both the strandline and inland along tidal channels, whilst forming seaward in the vicinity of tombolo islands, a specific pattern of growth develops (Warren, 1989). Although this is not an agreed upon mechanism based on possible mass-balance problems (Hardie, 1987), a dolomitisation mechanism referred to as "evaporative pumping" may result after the flood recharge on to the sabkha leads to the downward movement of water through the sediments (Hsü and Siegenthaler, 1969). This downward flow connects with seaward-flowing groundwater. Evaporative pumping occurs when evaporation takes place from the capillary zone above the water table, which induces an upward flow in groundwater to the capillary zone, until the water-table falls below the capillary zone (Sanford and Wood, 2001). It has been suggested that there exists two different fluid sources for sabkha dolomitisation, a seawater source on the seaward side and a continental source on the landward side (Mckenzie et.al, 1980). Changes in porewater

98

chemistry are the result of the evaporation and precipitation of minerals and the mixing of marine-derived fluids with these continental brines (Hardie, 1987).

Dolomite precipitated in sabkha environments has some of the following characteristics:

(1) Although there is dispute over whether dolomite develops as a primary mineral, or as a secondary replacement of fine-grained aragonite muds (Hardie, 1987), most sabkha dolomite is considered to be of secondary origin (Machel and Mountjoy, 1986).

(2) The crystal size of the dolomite is typically fine (1-20μm) and tends to increase inland across the sabkha (Tucker and Wright, 1990) and although there are rare sources of calcium-deficient dolomite (Gunatilaka et al., 1987), most sabkha dolomite is calcian-rich and poorly-ordered (Patterson and Kinsman, 1982).

(3) Typical dolomite (protodolomites) form in thin beds or crusts replacing aragonitic and gypsum sediments and are associated with a variety of evaporite minerals (mainly calcium sulphates) (Machel and Mountjoy, 1986).

(4) Due to repeated eustatic and/or relative sea –level changes, sabkha sediments are commonly formed in distinctive shallowing-upward cycles with undolomitised shallow-marine or lagoonal sediments at the base, overlain by dolomitised intertidal sediments grading into sulphate-rich dolomitised supratidal sediments (Machel, 2004).

(5) The $\delta^{18}O$ of sabkha waters (of marine origin) tend to vary and become isotopically lighter with distance from the lagoon (following evaporation trends). This pattern is explained by the circulation of waters within the lagoon and the influence of wind strength and direction on salinity distribution (Mckenzie et al, 1980).

6.7.2   Seepage-Reflux Models

This model is quite similar to the mechanism associated with the sabkha model but the reflux model is often used to explain the thicker, larger-scale dolomitisation patterns (associated with evaporites) in the ancient record (Warren, 1989). Seepage-reflux models simply involve the evaporation of marine water as it passes landward across a hypersaline lagoon, increasing the density of the evaporated waters. These dense hypersaline fluids infiltrate underlying sediments and move seaward by seepage (reflux) through the underlying beds (Morrow, 1990). Reflux systems develop as a result of differences in fluid density created by the development of spatial salinity differences (Jones and Xiao, 2005). This density instability is what causes the brine to displace the underlying marine waters that are

99

of lower density (Shields and Brady, 1995). If the platform is isolated due to a barrier (such as a reef mound), this barrier can effectively aid in the generation of brines due to the increased isolation and subsequent evaporation of seawater (Jones and Xiao, 2005).

Suitable fluids that are conducive to the dolomitisation of the underlying sediments occurs as a result of the precipitation of gypsum and anhydrite (that effectively removes sulphate from the fluid source) in conjunction with the large source of Mg^{2+} ions in the evaporated seawater (Morrow, 1990).

Dolomites suggested to have developed from seepage-reflux systems typically have some of the following characteristics:

(1) They are often found in close stratigraphic association with platform interior evaporites (Adams and Rhodes, 1960). The top of the dolomite body lies beneath a widespread, evaporitic horizon (Warren, 2000).

(2) Dolomites created by reflux mechanisms tend to be fine to medium crystalline [10-100μm (Warren, 2000)], matrix-selective (and mimetic-replacive), non-luminescent (Melim and Scholle, 2002) and may be inter-grown with abundant gypsum and anhydrite in layers and nodules (Machel, 2004).

(3) The dolomite body that develops in reflux models is both asymmetric and tabular and extends downward from the platform surface, thinning basinward and with increasing depth (Jones and Xiao, 2005).

(4) If not reset by the effects of burial, the $\delta^{18}O$ values of reflux dolomites (along with trace elements of Sr and Na) tends to increase away from the evaporite dolomite contact or the source of the refluxing brines (Warren, 2000). The overall isotopic signature of the dolomite would however, be expected to be relatively enriched with respect to both trace elements and $\delta^{18}O$, as a result of precipitating from evaporated seawater (Tucker and Wright, 1990).

6.7.3 Seawater/Tidal Pumping (Kahout) Models

There are many seawater-type models that have been used to explain widespread dolomitisation processes and these models essentially describe dolomites that have formed from marine to slightly modified seawater in marine settings. The basis of the models is that seawater itself is capable of dolomitising sediments provided there exists an efficient pumping mechanism to move the fluids through the carbonate sediments (Land, 1985; Flügel, 2004). Mechanisms that have been used to explain seawater dolomitisation include

100

tidal pumping through the pumping of large amounts of seawater through sediments (Caballo et al., 1987).

Kohout convection occurs (in water depths ranging from 1-3 km) as a result of the creation of a horizontal density gradient between cold marine waters that are adjacent to a carbonate platform and geothermally heated groundwater within the platform (Flügel, 2004). Seawater is drawn into the platform margin, displacing less dense (and warmer) porewaters within the platform which subsequently emerge as springs on the platform (or platform edge) (Tucker and Wright, 1990).

Characteristics of dolomitisation from seawater to slightly-modified seawater are similar to that of a mixed origin and include:

(1) Seawater dolomitisation typically occurs at shallow-intermediate depths within predicted temperatures at these depths (Machel, 2004).

(2) Some more recent dolomites from Florida indicate that initial dolomite precipitates are fine crystals (1-5μm) that are Ca-rich, poorly-ordered, and euhedral (Caballo et al., 1987). Dolomite textures are somewhat variable (although they are typically fine-crystalline) due to the wide range of precipitation conditions for seawater models.

(3) Since the dolomite has precipitated from seawater, the strontium values of the dolomites should reflect seawater at the time of precipitation (Allan and Wiggins, 1993). Stable isotope composition of dolomite would be relatively light [positive values of both $\delta^{18}O$ (+2.0 to +4.0 ‰ PDB approximately) and $\delta^{13}C$ are seen in most examples, albeit these dolomites are typically from the more recent geologic past], also reflecting marine waters at the time of precipitation (Warren, 2000).

(4) Ancient units of dolomite produced from seawater are often part of a stacked peritidal, platform succession. Although seawater could transport dolomitising fluids to more central areas of the platform, dolomitisation would typically occur further from the central portions of large platforms (Warren, 2000).

(5) Dolomites precipitated mostly from seawater or slightly-modified seawater, typically do not have spatially-associated evaporitic assemblages (Nicolaides, 1997).

101

6.7.4 Mixing Zone Models

The idea behind mixing-zone models (or dorag dolomitisation) is that by mixing seawater with freshwater the resulting fluid will be more conducive to dolomitisation as the high Mg/Ca ratio is still maintained but the kinetic obstacles associated with the high ionic strength of seawater is overcome (Badiozamani, 1973). In this particular model, the main supplier of Mg^{2+} is seawater and active groundwater movement acts as the pump to drive dolomitising fluids through sediments (Tucker and Wright, 1990). In general, mixing-zone models are only viable models in humid areas, as there is not sufficient fresh water to form an extensive mixing zone in arid regions and the flow rates are also too sluggish to supply the required magnesium (Warren, 1989).

Some characteristics of dolomites formed in mixing zone environments include:

(1) Dolomites produced in mixing zones are rarely associated with evaporites (or their pseudomorphs) (Warren, 1989).

(2) The textures of dolomites in a zone of mixing of seawater with phreatic meteoric waters determined by Land (1973) consists of relatively fine (8-25μm), subhedral to euhedral crystals that are replacing micrite or infilling void spaces. The isotopic composition in this particular study was $\delta^{18}O = -1.0$ ‰ and $\delta^{13}C = -8.4$ ‰. These are relatively low carbon values that are a reflection of heavier groundwater and slightly depleted oxygen values that are in the range of typical seawater signatures. In general, there is a positive covariance between $\delta^{18}O$ and $\delta^{13}C$ compositions (Allan and Matthews, 1982).

(3) Lu and Meyers (1998) suggested a mixing-zone model for the mixing of evaporative brines and meteoric fluids in a study in Nijar, Spain. In this particular study, dolomite textures and sizes are variable (indicating that the chemistry of the dolomitising fluids developed during the mixing process is an important control on the type of dolomite produced, and as a result, may be highly variable). Dolomites varied from <10-100μm, forming as both replacements and cements, with isotopic signatures in the range of $\delta^{18}O = -1.0$ to +4.2 ‰ PDB and $\delta^{13}C = -4.0$ to +2.0 ‰ PDB. In other words, the types of dolomite precipitated in mixing-zones are highly dependent on the fluid compositions of each of the contributing fluid sources.

(4) Dolomites tend to develop best along the edges of sedimentary basins, but when evaporitic sediments are in the vicinity, dolomitisation may also be significant in the areas connected to these evaporitic facies (Warren, 2000). Mixing-zone dolomites also tend to occur on paleotopographic highs, where there is the possibility of freshwater lenses (Warren, 1989).

102

(5) There is a common association with meteoric diagenetic features such as moldic porosity and pre-compaction isopachous calcite spar cement and other vadose cements (Taberner and Santisteban, 1987).

(6) In several studies on mixing-zone dolomites, crystals have been determined to be inclusion-rich in the early stages of precipitation, and develop a zoned texture as the chemistry of the porewater evolves during later diagenetic stages (Folk and Land, 1975; Machel and Mountjoy, 1986).

6.7.5 Burial Compaction & Hydrothermal/Tectonic Models

In burial compaction models, the main mechanism is the compactional dewatering of basinal shales and the expulsion of Mg^{2+}- rich fluids into adjacent shelf-edge and platform carbonates (Flügel, 2004). The source of the Mg^{2+} is from porewater (usually a seawater-derivative) and changes in clay minerals that occur with increasing depth (Tucker and Wright, 1990). Compaction (resulting from burial and tectonic compression) tends to cause fluid flow pathways for fluids to travel either laterally or upward, and hydrodynamic head and density differences create lateral and downward flow of formation fluids (Allan and Wiggins, 1993).

Tectonic (or squeegee) models are essentially another type of burial compaction model. In this model, metamorphic fluids are expelled from the crustal sections that are affected by tectonic loading causing movement of fluids towards the basin margins. These fluids may then mix with burial compaction and/or topography driven flow resulting in fluid mixing (Machel, 2004).

Hydrothermal models involve the interaction of buried units with circulating groundwater which can be explained by convection cells, where dense hypersaline brines are recirculated from great depths associated with crustal rocks to shallow depths by convection cells (Lovering, 1969; Morrow, 1990). The movement of hydrothermal fluids may be also associated with tectonic compression and sedimentary loading (Qing and Mountjoy, 1994). Machel and Lonnee (2002) further suggest that a fluid should not be termed hydrothermal but rather geothermal if it has not formed at a higher than ambient temperature (as the driving mechanisms and sources of these fluids should not be considered in the definition). Regardless of definition, hydrothermal models are essentially burial dolomitisation models (and not a separate model) with the added distinction that they are significantly involved in the mineralisation of ore deposits (ie. MVT deposits) (Berger and Davies, 1999).

103

Characteristics of burial compaction and tectonically-associated dolomitisation processes and dolomite textures include:

(1) The texture of dolomites tends to be sparry, nonplanar, and with saddle morphologies (suggesting temperatures of precipitation that are higher than 50˚C). Oxygen isotope values of these dolomites shows a marked depletion (due to high-temperature precipitation) and carbon isotopes may also show depletion as a result of hydrocarbon processes and the effects of thermochemical sulphate reduction (TSR) (Warren, 2000).

(2) Other characteristic features seen as a result of burial dolomitisation include: healed microfractures, relict stylolites within dolomite mosaics, dolomite fronts cutting across bedding in limestones, and textures where seams of dolomite enclose millimetre to decimetre patches of limestone as a result of dolomitisation along stylolites (Zenger, 1983).

(3) There is no specific shape of dolomite bodies, as dolomitising fluids can flow laterally or be cross-formational. Faults and fractures tend to produce narrow, linear dolomite bodies whereas lateral flow (often produced from dewatering of a nearby basin) may produce much more extensive tabular bodies (Allan and Wiggins, 1993).

(4) In Alberta, there are several examples of fracture and fault-controlled burial dolomitisation and compaction associated with dewatering (Mountjoy and Halim-Dihardja, 1991; Green and Mountjoy, 2005; Machel and Anderson, 1989; Nesbitt and Muehlenbachs, 1994). All of these examples produce coarse-crystalline dolomites, although the amount of dolomite that can occur is significantly variable. In compaction associated with dewatering models (such as Machel and Anderson, 1989 and Nesbitt and Muehlenbachs, 1994), only a limited amount of dolomitisation can occur as the fluid source itself is limited. However, the fracture and fault-controlled burial models allow for greater fluids to pass along conduits and hence, greater dolomitisation potential.

(5) Fluids produced as a result of squeegee compaction (tectonic loading) may produce very hot and fast-flowing fluids that may recrystallise existing dolostones along its pathway (Machel and Cavell, 1999; Machel 2004), however, dolomites that are produced in this way become highly resistant to future recrystallisation processes (Machel et al., 1996).

6.8 A Dolomitisation Model for the Upper Stettler Formation and Crossfield Member

Based upon the above definitions of the dolomitisation models in conjunction with a petrographic and isotopic examination of the Upper Stettler Formation and Crossfield Member, a seepage-reflux model most adequately explains the pervasive dolomitisation of the study area.

In terms of the other models, the following characteristics were not compatible with information obtained for the Upper Stettler Formation and Crossfield Member:

(1) The Upper Stettler Formation and Crossfield Member have an abundance of evaporites (gypsum and anhydrite) in all of the wells examined which is a characteristic feature of sabkha models and evaporative depositional settings in general. However, the growth of evaporites and the patterns of dolomitisation are much more widespread in occurrence both vertically (much greater than 1.5m) and laterally, wherein the study area sediments are not found in the typical sabkha pattern of 1-1.5 metre thick precipitation patterns along tidal channels.

(2) There is no evidence of a progressive increase in crystal size inland which is an important characteristic of the sabkha model.

(3) The isotopic composition of the matrix dolomites does not indicate a pattern of lighter oxygen values with sediments from the shallow subtidal inland towards lagoonal sediments characteristic of sabkha models.

(4) Although it is not impossible, both seawater and mixing-zone models do not tend to have spatially-associated evaporites involved in the precipitation of dolomite. Since the presence of evaporites is substantial within the Upper Stettler and Crossfield, these models are likely not suitable for an explanation of the pervasive dolomitisation of the study area.

(5) The mixing-zone model is often explained with the mixing of fluids on a paleotopographic high which did not exist in the study area, and there are also no characteristic meteoric signatures and cements indicating a mixing zone of marine and meteoric fluids.

(6) Burial and hydrothermal dolomitisation tend to produce less widespread dolomitisation, with the exception of lateral flows due to compaction during burial. Hydrothermal dolomitisation however, typically develops in the vicinity of fractures acting as fluid conduits. As a result, it is doubtful that the early pervasive matrix dolomites were produced in these types of models. Burial and hydrothermal dolomitisation may have diagenetically altered the early pervasive dolomites during the burial process however,

105

creating recrystallised textures as well as contributed to the formation of late-stage saddle dolomite cements.

(7) The effects of burial compaction are clearly evident in the Upper Stettler and Crossfield, in the form of significantly depleted oxygen and carbon values and the precipitation and dissolution of late-stage cements of blocky calcite, anhydrite, and saddle dolomite. The formation of thick dissolution seams with planar-e dolomite is another significant feature associated with burial compaction. Also, the recrystallisation of early formed pervasive dolomite is directly related to the effects of burial, with the dissolution and reprecipitation of fabrics.

(8) A late-stage fracture network is apparent in some of the wells (mostly in 8-11) that are partially occluded with secondary anhydrites, which could have acted as conduits for hydrothermal fluids during episodes of compression associated with the Laramide Orogeny. This observation is also supported by Erickson et al. (1994). This observation however, does not adequately explain the widespread occurrence of pervasive dolomites in the Upper Stettler and Crossfield.

Although there are obvious petrographic and geochemical characteristics to support burial dolomitisation, a more inclusive model is needed to explain the widespread occurrence of pervasive matrix dolomites in all of the wells (2-11) in the Upper Stettler Formation and Crossfield Member. The most suitable mechanism to explain the pervasive dolomitisation is the episodic movement of refluxing brines through the shallow subsurface as a result of gravity and density differences between the dense evaporative brines and the lighter pore fluids in the underlying sediments. The following observations support this model based on the isotope geochemistry and petrographic characteristics of the dolomicrite and fine- to medium-crystalline dolomite in the study area:

(1) The close spatial relationship of the dolomitised sediments with the overlying Upper Stettler evaporites raises the possibility of the development of evaporitic brines. There is a notable difference in the amount of anhydrite in the overlying evaporites in wells 8 to 11 in comparison to wells 2 to 7 within the Crossfield trend. Wells 8 to 11 have intervals of undolomitised strata surrounded by pervasively dolomitised units. The presence of undolomitised strata may be directly related to the amount of anhydrite in the Stettler evaporites, and that the source of the refluxing brines is further east of the Crossfield trend (which in comparison to wells 8-11) have been completely dolomitised.

(2) There is a subtle gradient towards the west as a result of subsidence in the Prophet Trough and the development of a foreland basin as a result of convergence and loading

106

associated with the Antler Orogeny (Erickson et al., 1994). It has been suggested that this gradient would further enhance the flow of Stettler hypersaline brines with dolomitising potential.

(3) The presence of undolomitised strata between dolomitised units may also support the idea of episodic brines travelling through the underlying sediments. The development of 'fingers' of dolomite are supportive of the reflux model, with the development of the edges of the dolomite front further west of the Crossfield trend and visible in wells in the Panther River/Burnt Timber/Moose Mountain areas. Reflux brines generate a tabular body that is thickest closer to the brine source and that thins out basinward (Jones and Xiao, 2005). This is clearly visible in the dolomitisation patterns of the strata west of the Crossfield trend.

(4) Differences in porosity are also apparent within the two groups of wells. Wells outside of the Crossfield trend also have higher porosity and permeability than wells in the Crossfield trend. This difference in porosity may simply be a function of TSR reactions and higher dissolution rates in wells 8-11, however it has been suggested by Jones and Xiao (2005) that within reflux models, the highest porosity tends to develop in the most distal regions of the dolomitising flow path. The rationale for this conclusion about the path of refluxing brines is that closer to the brine source, the development of overdolomitisation occurs with the precipitation of dolomite cements (Jones and Xiao, 2005).

(5) Matrix dolomites are typically fine-crystalline and fabric-selective (mimic replacement), and non-luminescing within the study area. The dolomite fabric is similar to the type of dolomite typically formed from refluxing brines (Warren, 2000).

(6) The oxygen and carbon isotopes are slightly more depleted than what would be expected from evaporated Famennian seawater, however these slightly lighter values may be a reflection of recrystallisation processes that occurred with burial. Refluxing brines could still produce dolomites with the isotopic signatures of the matrix dolomites in the Upper Stettler and Crossfield.

(7) In terms of strontium values ($^{87}Sr/^{86}Sr$), the dolomicrite and fine-crystalline dolomites reflect values that would be expected if the dolomites had precipitated from seawater or modified seawater during the Famennian.

(8) The idea of episodic brines pervasively dolomitising the Upper Stettler and Crossfield is supported by the presence of cycles of evaporites throughout the study area, which is also observed by Erickson et al. (1994).

107

With all of these observations, the concept of episodic refluxing brines most adequately explains the pervasive dolomitisation of the Upper Stettler and Crossfield Member.

6.9 Anhydrite Formation

Primary anhydrite/gypsum were deposited as fine-grained laths in laminated and nodular mosaic fabrics as supratidal sediments in the Upper Stettler Formation and Crossfield Member (Plates 6 & 7). Many of these anhydrites show enterolithic structures with precipitation. The growth of anhydrites at the centre of nodules within anhydrite sheets creates these enterolithic structures as a result of the buckling and convolution of the sheets in their attempt to find space between the confining layers of the host sediment (Shearman and Fuller, 1969). With burial (after approximately 200-300 m), primary gypsum is recrystallised to anhydrite. Replacement of gypsum with secondary intermediate burial anhydrite is a continuous process that is identified as translucent, grey-white blocky anhydrite that forms in dissolution vugs and replaces primary fabrics within earlier depositional nodules. The final stage of anhydrite precipitation forms milky white, pile-of-brick type fabrics and secondary blocky textures within dissolution vugs in association with blocky II calcite, elemental sulphur, and saddle dolomite. Some of these late-stage secondary anhydrites replace translucent secondary intermediate-type fabrics, but many of the anhydrites occluding vugs probably precipitated directly from dissolved precursor anhydrites. This pile-of-brick anhydrite represents the latest diagenetic anhydrite in the Upper Stettler and Crossfield Member, and it is an important contributing factor to TSR reactions.

Strontium ($^{87}Sr/^{86}Sr$) analysis indicates that primary and recrystallised anhydrites were precipitated from Famennian seawater, this is further supported with the $\delta^{34}S$ values for anhydrite that also suggest precipitation from Famennian seawater (Figs 5.3 & 5.4). The strontium $^{87}Sr/^{86}Sr$ values are 0.70804 – 0.70816 and $\delta^{34}S$ values range from +21.1 to +27.8 ‰ (CDT).

6.10 Sulphide Mineralisation and Thermochemical Sulphate Reduction (TSR)

The process of the reduction of sulphate by hydrocarbons occurs either by bacteria [bacterial sulphate reduction (BSR)] or inorganically [Thermochemical sulphate reduction (TSR)]. Each of these processes is important in specific diagenetic thermal regimes, with

108

BSR occurring in diagenetic settings from 0 to 60-80° C and TSR occurring with significantly higher temperatures of 100-140° C, and some temperatures as high as 160-180° C (Machel, 2001). Bacterial sulphate reduction (BSR) can be represented by the following reaction (Nöth, 1997):

$$2CH_3O + SO_4^{2-} \rightarrow 2HCO_3^- + H_2S \qquad (6.1)$$
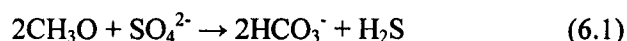
In this reaction, anaerobic bacteria use sulphate as an oxidant in metabolic processes to oxidise organic matter, which results in the production of small amounts of H_2S (<3%) (Nöth,1997). Baumgartner et al. (2006) discussed current views on the role of sulphate reducing bacteria (BSR) in depositional environments with microbial mat systems, and summarised that in contrast to past views that BSR's are mainly anaerobic, there is increasing evidence that sulphate reducing bacteria not only survives in the oxic zones of microbial mats, but has some of the highest rates of sulphate reduction during oxic conditions (Baumgartner et al., 2006). During early diagenesis or with shallow to intermediate burial, although the amount of reactive iron and organic matter for metabolic functions is relatively low (in comparison to shales for example), the generation of iron sulphides may be related to BSR reactions (Machel et al., 1997). Although sulphate reduction occurs mainly through TSR reactions in the Crossfield in the deep burial realm, the minor presence of pyrite in spatial proximity to laminated microbial mat sediments, indicates that BSR reactions may have occurred in the study area prior to deep burial, but the very rare nature of its occurrence may also indicate other mechanisms have contributed to its precipitation. Petrographic and isotopic evidence indicate that the main sulphate reducing mechanism occurred with significant depth by TSR reactions.

Thermochemical sulphate reduction (TSR) can be related by the following reaction (Nöth, 1997; Machel 2001):

Hydrocarbons + SO_4^{2-}

$\rightarrow$ altered hydrocarbons + solid bitumen + HCO_3^- (CO_2) + H_2S (HS⁻) + heat

(6.2)
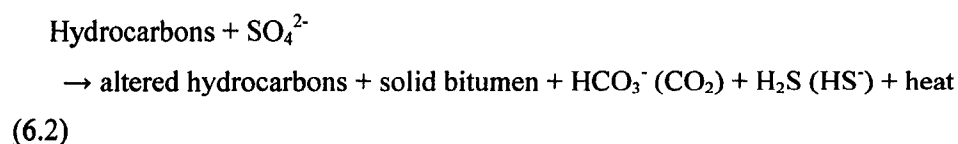
In this reaction, organic matter is oxidised and dissolved sulphate (SO_4^{2-}) (such as from anhydrites) is reduced to form hydrogen sulphide, bicarbonate ions and carbon dioxide and numerous organic sulphur compounds (Nöth, 1997). The prerequisite conditions for TSR

109

reactions are temperatures >100°C, the presence of organic matter, and a supply of sulphate from host rocks.

Isotopic data combined with trends in depth and temperature indicate that the genesis of H_2S and CO_2 in Devonian rocks is directly related to the thermal reduction of sulphate that is originally derived from Devonian anhydrite (Hutcheon, 1999). The by-products of TSR reactions involving the reduction of anhydrite is the creation of H_2S, and consequently, the $\delta^{34}S$ of the H_2S will approach that of the sulphate (Hunt, 1996).

Within the Upper Stettler, sediments are generally tight and non-porous, and as a result the facies that have petrologic and geochemical evidence for TSR reactions are predominantly within facies deposited within the Crossfield Member. In the Upper Stettler and Crossfield, the following isotopic and petrographic characteristics suggest that TSR reactions have occurred with increased temperatures at depth:

(1) The main precipitates commonly associated with TSR reactions include saddle dolomite cements, blocky calcite cements, and sour gas (Buschkuehle and Machel, 1999; Machel, 1987). All of these products are late-stage features within the facies of many of the wells in the study area, but particularly in wells 2 -5 and 8-11.

(2) The presence of elemental sulphur resulting from the reduction of secondary "pile of brick" type anhydrites that typically form at depth from solution rather than as the recrystallisation of gypsum cement are an indication of TSR (Machel, 2001) (Plate 12). The elemental sulphur and presence of bitumen and asphaltene staining late-stage cements, coarse-crystalline matrix dolomites, and lining the edges of dissolution vugs indicates that the elemental sulphur is probably a reactive product of TSR. The existence of elemental sulphur in the system suggests that overall, there are limited hydrocarbons for reaction processes to continue (Machel, 1987). If this is the case, although TSR reactions occurred within the study area, they were probably not a widespread and continuous phenomena with depth in all of the wells.

(3) Along the same line of reasoning, variations in the H_2S content of gas (since it is essentially a limiting agent in reduction reactions) will affect the degree of TSR reactions. In a study by Eliuk (1984), the amount of H_2S in gases from Olds-Crossfield and Limestone-Burnt Timber wells were examined. Variations in the H_2S content of gas ranged from 1.4 to 45% in the Olds-Crossfield (in the vicinity of wells 2-7) and 13 to 67% in the Limestone-Burnt Timber area (where wells 8-11 are located). The presence of higher H_2S content in the Limestone-Burnt Timber area was suggested by Eliuk (1984) to be a function of the amount of porosity and the amount of available anhydrite. Another factor affecting the total H_2S

110

content of gas is that there is the potential for loss or oxidation after generation, which may occur when H_2S forms at maximum depth and is then exposed to uplift (Yang et al., 2001). Uplift may result in fracturing that allows H_2S to escape (Yang et al., 2001). In the Upper Stettler and Crossfield, the amount of H_2S in gas is more significant in wells 8-11, where products of TSR reactions occur in greater abundance. In terms of the necessity for porosity to exist in conjunction with anhydrite, wells 8-11 clearly have higher porosity through episodes of dissolution associated with TSR processes. The dissolution of anhydrites from TSR processes can occur from an increase in the overall acidity of the pore fluids from the formation of products of TSR such as H_2SO_4 and HCO_3. Increased acidity of the pore fluids will further dissolve carbonate phases, creating more porosity for the migration of hydrocarbons, resulting in more anhydrite dissolution and the further creation of porosity (Erickson et al., 1994).

(4) The presence of reaction rims on anhydrite has been documented by Krouse et al. (1988) and Erickson et al. (1994) as related to TSR reactions. The reaction rims surrounding anhydrite nodules consists of porous dolomite separated from late-stage cements by black, carbonaceous residues (Krouse et al., 1988) (Plate 6). The dissolution process producing porous dolomite rims are interpreted by Krouse et al. (1988) to be related to TSR reactions because: (i) the dolomite and TSR-associated anhydrite appear to have been exposed to similar dissolution processes, (ii) the proximity of the dolomite to other reaction products of TSR, and (iii) as mentioned in the previous section, there is a direct correlation with porosity-thickness in the Crossfield Member and the concentration of H_2S gas in the reservoir. In wells 8-11 of the study area in particular, there are several examples of these types of reaction rims. Although the rims are not a significant petrographic characteristic found in association with TSR reactions in the Upper Stettler and Crossfield, the presence of them further corroborates that TSR has diagenetically altered the study area.

(5) The isotopic evidence for the occurrence of TSR in the Upper Stettler and Crossfield can be seen in the $\delta^{34}S$ values for both anhydrites and the elemental sulphur. Compositions of anhydrite cements (+22.1 to +27.8‰) are coeval with marine seawater at the time of precipitation, and the elemental sulphur (+26.1 & +29.7‰) is similar to these marine values, suggesting that the source of elemental sulphur involved in TSR reactions is most likely the original anhydrite precipitated from marine waters. This interpretation is corroborated by a study undertaken on the Burnt Timber and Crossfield East by Yang et al., (2001), that revealed similar isotopic results.

111

(6) In terms of carbon and oxygen isotopes, the late-stage blocky II calcites precipitated in vugs and fractures in association with secondary anhydrites also indicate that TSR has occurred, with negative $\delta^{13}C$ values suggestive of the contributions of organic carbon to the precipitating fluids as a result of the oxidation of hydrocarbons (Fig 5.1). The values for $\delta^{18}O$ are also significantly depleted which are a reflection of precipitation from formation fluids that have a substantial contribution of oxygen from isotopically heavier dissolved anhydrites [anhydrites precipitated from evaporated seawater typically have $\delta^{18}O$ values of 12.0 to 19.2 ‰ VSMOW (Yang et al., 2001)].

Based upon the above premises, TSR reactions occurred at depth within the examined wells from the Upper Stettler Formation and Crossfield Member. These reactions are not widespread however, and appear to be more localised and concentrated in wells 2 through 5 along the Crossfield trend and in wells 8 to 11 in the Burnt Timber/Panther River/Moose Mountain region. Current burial depths for the Upper Stettler and Crossfield range from 2265-2755m in the Crossfield trend and 2615-3670m west of the Crossfield trend. The localisation of these processes suggests that any TSR reactions probably occurred within a relatively isolated or closed-system. Another important observation about the occurrence of TSR reactions is that they are significantly more apparent in the wells west of the Crossfield trend (8-11), and occur almost exclusively in facies from the Crossfield Member with relative absence from Upper Stettler facies. The lack of TSR reactions is a reflection of the presence of non-porous facies within the Upper Stettler.

6.11   Effect of Diagenesis and Dolomitisation on Porosity and Permeability

Interpretations of porosity and permeability characteristics are based on both petrography and quantitative core analyses from the Core Research Centre in Calgary.

Within the facies of the Upper Stettler and Crossfield, there appears to be variable porosity and permeability characteristics based on the grain-size of the precursor fabrics. The facies with fine-grained precursor fabrics are tighter (such as supratidal facies in the Upper Stettler laminates and mudstones in intertidal and shallow subtidal settings). The best porosity is preserved in coarser facies, such as peloidal and fenestral grainstones in intertidal and shallow subtidal realms and the stromatoporoid and bioclastic floatstone/rudstones in intertidal/subtidal realms.

In terms of secondary porosity, the most important types in the Upper Stettler and Crossfield were created through diagenetic dissolution processes with increased burial.

112

Intercrystalline, fracture, and vuggy porosities, resulting from these processes are the most abundant effective porosity types in the study area (Plate 14). The precipitation of secondary cements however, has reduced the effectiveness of these pore spaces for fluid retention and for fluid transport through permeable pore networks. In wells 8-11, where there is greater evidence of the effects of dissolution, intercrystalline porosity between coarse-crystalline recrystallised dolomites is relatively high in dolomitised facies. There are intervals of undolomitised strata within these wells also that have low propensity for fluid retention or transport. In contrast, the dolomitisation and subsequent recrystallisation of strata within intervals in the wells has effectively enhanced the porosity and permeability potential of the wells overall.

The most important processes affecting the porosity and permeability of the Upper Stettler and Crossfield include the following: (1) precipitation of vug and fracture-occluding cements of blocky calcite I & II, secondary-intermediate blocky anhydrites, late-stage pile-of-brick and blocky anhydrites, saddle dolomite, and pore-lining dolomite, (2) pervasive matrix dolomitisation, (3) the recrystallisation of early matrix dolomites forming coarse-crystalline dolomites, and, (4) the effects of mechanical and chemical compaction with depth.

Anhydrite cementation is one of the most important porosity-destroying processes during diagenesis (Jones and Xiao, 2005; Ehrenberg, 2006). In the Upper Stettler and Crossfield, intermediate and late-stage anhydrite cements have effectively reduced porosity and permeability by the occlusion of dissolution vugs and microfractures. In association with anhydrite dissolution, TSR reactions are capable of generating porosity (Machel, 2004). These TSR reactions, possibly because they are not widespread and apparent in all of the wells (1-11) do not significantly contribute to the creation of porosity in the Upper Stettler and Crossfield.

In a sedimentary basin, the average porosity tends to decrease with increasing burial depth (Bjørlykke, 1993). In terms of mechanical and chemical compaction, both of these processes continue to destroy porosity characteristics as the sediments are buried. Initially, mechanical compaction (usually in the first 300m) causes significant porosity through dewatering of sediments and grain compaction causing the realignment and breakage of grains and bioclasts (Hiatt and Kyser, 2000). After significant mechanical compaction has occurred, pressure solution processes associated with chemical compaction further reduces porosity. The dissolution of calcium carbonate occurs during pressure solution where it reprecipitates in open pores (Hiatt and Kyser, 2000). Since carbonates have retrograde

113

solubility, this will continue to occur up to temperatures of 400°C with burial (Hiatt and Kyser, 2000). As a result, chemical compaction is one of the principle destructive forces of porosity in carbonate rocks (Choquette and James, 1990).

The early dolomitisation of carbonate muds tends to enhance permeability characteristics of reservoirs as this enhancement results in an increase in the crystal size of the precursor mudstones, creating more permeable replacement fabrics, so permeability in coarser-grained precursor fabrics (such as grainstones) will not be as enhanced by dolomitisation processes (Jones and Xiao, 2005). The higher permeability in dolostones in comparison with associated limestones is therefore interpreted as reflecting the replacement of microporous lime muds with dolomite that has intercrystalline macroporosity (Ehrenberg et al., 2006). By contrast, the precipitation of dolomite or anhydrite cement in interparticle spaces will decrease permeability characteristics.

Based on the diagenetic evolution that has occurred in the Upper Stettler Formation and Crossfield Member during the burial process, the following observations can be made:

(1) Initially, porosity and permeability networks were enhanced with the onset and multiple occurrence of early pervasive dolomitisation from reflux brines.

(2) The development of porosity with very shallow burial is fabric-selective, with enhanced porosity in fine-crystalline sediments initially, followed by decreased porosity with increased depth as fine-crystalline sediments are more greatly affected by mechanical compaction processes. Porosity creation with burial and early dolmitisation is not as significant in medium- to coarse-grained sediments, which is purely a factor of initial grain size prior to burial.

(3) Chemical compaction processes and in particular, pressure solution are porosity-destructive events with continual burial, dissolving phases and resulting in reprecipitation of new phases as pore-occluding cements.

(4) As early matrix dolomites are recrystallised, their overall porosity is enhanced, but it is counteracted by the increase in precipitation of secondary intermediate and late-stage cements of blocky calcite, anhydrite, pore-lining dolomite and saddle dolomite.

(5) Late-stage dissolution processes have increased porosity in wells 8-11, which have higher corresponding H_2S contents.

(6) TSR reactions have not significantly enhanced porosity and permeability characteristics and tend to have had a more localised effect in specific facies within the Crossfield Member.

114

(7) Late-stage vuggy and fracture porosity that is not fabric-selective are the most important secondary porosity types within the study area. Intercrystalline and pin-point porosity is also significant in the creation of permeable networks within sediments. All of these porosity types are apparent to a greater extent in the dolomitised intervals in wells outside of the Crossfield trend (ie. 8-11).

(8) The differences in the basic porosity and permeability characteristics between undolomitised and dolomitised intervals within wells 8-11 in some cases may act as an aquitard for fluid flow. This is due to the basic difference in porosity and permeability characteristics between compressed limestones and dolostones, wherein overlying limestones may inhibit fluid flow pathways.

In summary, porosity and permeability characteristics initially increased with shallow burial and early pervasive dolomitisation processes, and then significantly decreased with burial as a result of the effects of mechanical and chemical compaction. The recrystallisation of early matrix dolomites to coarse-crystalline dolomites and the creation of sucrosic/sieve textures through TSR processes resulted in slightly enhanced porosity during the burial process. In terms of porosity destruction, with the exception of pressure solution processes, the most significant destruction of porosity is from late cementation events that precipitated anhydrites and blocky calcites in vugs and fractures.

6.12 Diagenetic Model for Upper Stettler Formation and Crossfield Member

The diagenetic history of the Upper Stettler Formation and Crossfield Member is characterised by several main diagenetic processes: (1) early pervasive dolomitisation, (2) blocky calcite cementation, (3) recrystallisation of early matrix dolomites, (4) neomorphism of anhydrites/gypsum and the precipitation and dissolution of secondary anhydrite, (5) hydrocarbon emplacement, sulphide mineralisation, and minor TSR reactions, and (6) the precipitation of saddle dolomite cements. The following stages describe the diagenetic alteration of the Upper Stettler Formation and Crossfield Member with increasing burial depth from shallow marine through to deep burial.

Stage 1: The Upper Stettler Formation and Crossfield Member carbonates and evaporites were deposited in a series of shallowing-upward cycles on west to northwesterly carbonate ramps during the Famennian (Late Devonian). Farther west (basinward), the Upper Stettler laminated and nodular anhydrites and Crossfield peloidal mudstones and bioclastic floatstones/rudstones grade into shallow subtidal facies of massive mudstones and peloidal

115

grainstones. Stromatoporoid (*Labechiid*) patch reefs also grew on basinward sections of the ramp creating lagoonal systems in shallow intertidal regions. Evaporites, in the form of primary fine-crystalline gypsum and anhydrites precipitated in supratidal settings as laminated and nodular mosaics of anhydrite/gypsum by evaporated seawater.

Stage 2: Micritisation processes and early neomorphic alteration occurred penecontemporaneously with deposition of the Upper Stettler Formation and Crossfield Member. Some lithification occurred in Upper Stettler laminated evaporites. Early calcite cementation with shallow burial includes drusy mosaic calcite and rare dogtooth cements precipitating in interparticle/intraparticle pore spaces.

Stage 3: With shallow burial, mechanical compaction of peloidal grains, minor bending/breakage of bioclasts and the minor flattening of burrows occurs. Within 10's metres of burial, chemical compaction and stylolitisation begins with the development of sub-parallel anastomosing microstylolites. Episodic refluxing Mg^{2+}-rich evaporative brines flow down through shallow-buried sediments as a result of density differences and gravity along a gradient towards the west resulting from subsidence and the creation of a foredeep in the southern part of the Prophet Trough associated with the Antler Orogeny (development of gradient from Erickson et al., 1994). Dissolution associated with chemical compaction creates interparticle porosity and vugs within pervasive matrix fabric. Precipitation of syntaxial calcite cements that form as overgrowths on crinoidal fragments and surrounding dissolved matrix. Beginning of recrystallisation of gypsum to anhydrite at depths greater than 200-300m (depth from Choquette and James, 1990), transformations continue with increased depth. Early fracture I cross-cut pervasive dolomites.

Stage 4: Intermediate burial: increasing chemical compaction and dissolution with burial, development of dissolution-seam dolomite cross-cutting pervasive matrix dolomite fabrics. Development of low-amplitude, parallel and horsetail stylolites. Blocky calcite I and bladed calcite cements forming in vugs. Recrystallisation begins of fine-crystalline matrix dolomites which continues with burial. Precipitation of secondary anhydrites associated with dissolution and reprecipitation in vugs and fractures.

Stage 5: Chemical compaction and dissolution continues, producing high-amplitude stylolites [at depths greater than 600m (Al-Aasm et al., 2002)] and fitted fabrics. With

116

continued burial, recrystallisation of fine-crystalline to coarse-crystalline dolomites continues and dissolution of secondary (intermediate anhydrites) occurs with increased chemical compaction. Precipitation of pore-lining dolomites along fenestrae and within vugs. Fracture II cross-cuts matrix dolomites (and some recrystallised matrix dolomite) and blocky I calcite cements.

Stage 6: Late burial: Dissolution with increased compaction. Precipitation of secondary anhydrite in vugs and along fractures. Thermochemical sulphate reactions (TSR) occurs with the dissolution of anhydrites and the precipitation of elemental sulphur. Continued dissolution of anhydrites, changing chemical composition of pore fluids. Precipitation of late-stage blocky
calcite II partially replacing secondary anhydrites and elemental sulphur. Asphaltene staining of late-stage calcites, secondary anhydrites, and saddle dolomites. Late-stage horizontal fracturing.

117

Fig 6.5: Diagenetic Model
Stage 1&2: Deposition & Early Marine Diagenesis
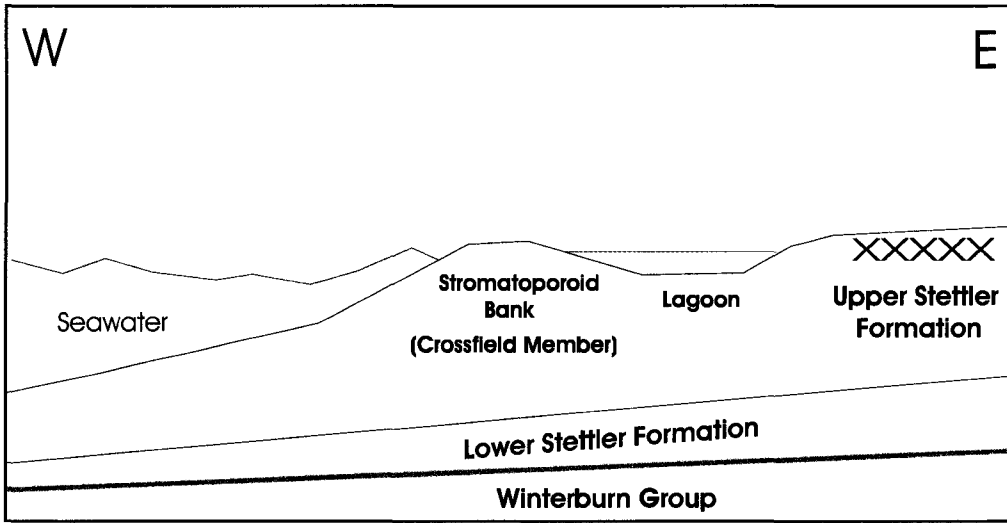
Early Diagenetic Features: (1) Micritisation, (2) Neomorphism, (3) Primary evaporites,
(4) Early calcite cements drusy mosaic/dogtooth.

Stage 3: Shallow Burial (10's-600 m)I
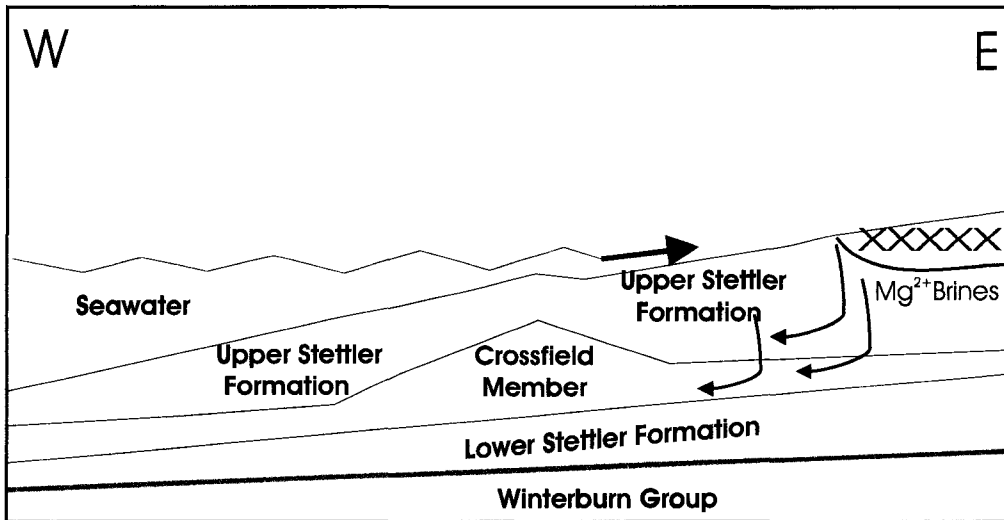
Shallow Burial: (1) Early pervasive dolomitisation -Brine source east of study area,
(2) Mechanical compaction (black arrow),(3) Early stylolitisation, (4) Syntaxial calcite cements,
(5) Neomorphism of gypsum to anhydrite, (6) Cross-cutting fractures with
increasing overburden. Black arrows indicate reflux pathway and blue arrow indicates periodic
marine influx.

118

Stage 4 & 5: Intermediate Burial (600-2000m)

W   **E**

BIG VALLEY LIMESTONES

Upper Stettler Formation

Upper Stettler Formation   Crossfield Member

Lower Stettler Formation

Winterburn Group- Graminia silts
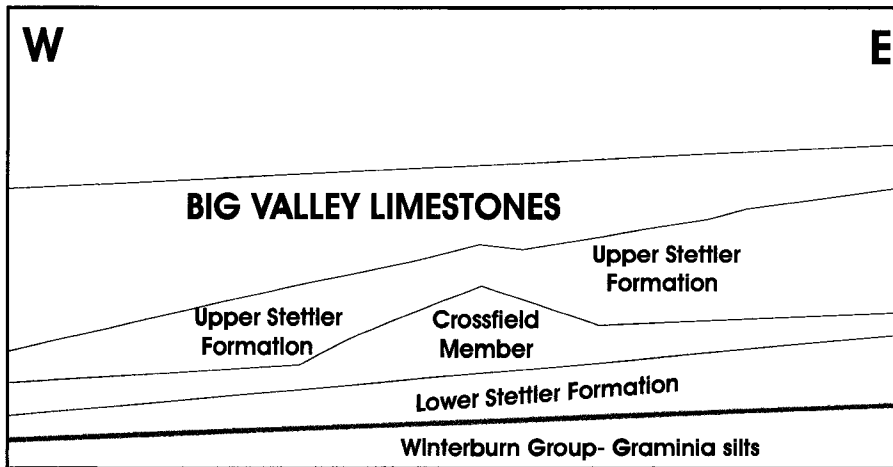
Stage 4: (1) Increased mechanical/chemical compaction with dissolution ,(2) Blocky I & bladed calcites forming in vugs, (3) Recrystallisation of early matrix dolomites begins, (4)Precipitation of secondary anhydrites from pore-fluids and recrystallisation of earlier evaporites, (5) Pore-lining dolomite

Stage 6: Deep Burial (2000 +m)

W   **E**

BIG VALLEY LIMESTONES

Upper Stettler Formation

Upper Stettler Formation   CrossfieldMember   TSR

TSR   Lower Stettler Formation

Winterburn Group- Graminia silts

With Increasing Burial
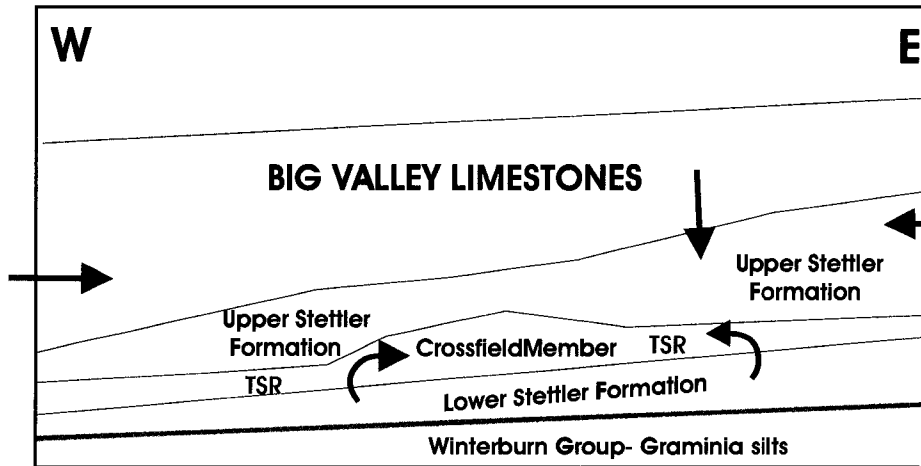
Stage 5 & 6: (1)Dissolution related to chemical compaction & TSR, (2) Secondary Anhydrite precipitating from pore fluids,(3) Elemental sulphur
 (3) Saddle dolomite, (4) Blocky II calcite,(5) Asphaltene-staining, (6) Late-stage compressional fracturing (Laramide), (6) Interaction with anhydrites from L.Stettler. Solid black arrows represent compression and tectonic loading. Blue arrows represent interaction with fluids containing dissolved Lower Stettler anhydrites.

119

CHAPTER VII

CONCLUSIONS

Based on petrographic and isotopic evidence, the following conclusions can be made about the dolomitisation and diagenesis of the Upper Stettler Formation and Crossfield Member:

(1)   Six main lithofacies were identified, which include: nodular and laminated mudstones, peloidal mudstone-wackestones, peloidal (fenestral) grainstone/packstones, bioclastic floatstone/rudstones, stromatoporoid floatstones, and dolostones. These lithofacies were deposited in shallowing-upward cycles, in subtidal, intertidal, and supratidal depositional settings on a carbonate ramp.

(2)   Dolomitisation is one of the most significant processes in the diagenetic history of the study area. The main types of dolomite identified are: dolomicrite, fine- to medium-crystalline dolomite, coarse- crystalline dolomite, dissolution-seam associated dolomite; pore-lining dolomite, and saddle dolomite.

(3)   Early episodic pervasive dolomitisation resulted from refluxing evaporitic brines beginning in the Famennian. These dolomites have strontium isotopic signatures reflecting precipitation from modified Famennian seawater. The oxygen and carbon isotopic values are slightly depleted from Famennian seawater, which may be simply a reflection of the slight modification of values with burial.

(4)   Calcite phases include precipitation early in the diagenetic history during shallow burial through to late-stage cements that represent the latest cementation event in the Upper Stettler Formation and Crossfield Member.

(5)   Recrystallisation of early matrix dolomites occurred with increasing depth and dissolution processes, resulting in the precipitation of planar-e to nonplanar coarse-crystalline dolomite with radiogenic strontium and depleted oxygen and carbon isotopic signatures, reflecting changes in pore water chemistry with recrystallisation.

(6)   Evaporite precipitation is an important component for the pervasive dolomitisation of the Upper Stettler and Crossfield. Early precipitated laminated and nodular mosaic gypsum/anhydrite is diagentically altered to its more stable form with continued depth. The inclusions of anhydrite within gypsum indicate that the conversion of anhydrite back to gypsum possibly occurred as the result of uplift during the diagenetic history of the study area. Anhydrite replaces gypsum at depths greater than 200-300m, and with continued

120

burial, the development of recrystallised anhydrite occurs at intermediate burial. Late-stage anhydrite forms out of solution from dissolved earlier stages rather than as a neomorphic replacement of gypsum. Furthermore, it is commonly associated with saddle dolomite, elemental sulphur, blocky II calcite, and asphaltene/bitumen.

(7)   Mechanical and chemical compaction has compressed fabrics throughout the study area, and pressure solution (chemical compaction) is one of the most significant causes of diagenetic alteration. Alteration resulted in the formation of broken/bent bioclasts, and slightly-flattened peloids, burrow, and fenestrae and the development of thick dissolution seams containing insoluble residues of clays and organics and associated dolomites.

(8)   Pore-lining dolomite is a rare dolomite phase and develops with intermediate burial along vugs. The formation of saddle dolomite in late-stage vugs, along with blocky II calcite, anhydrite, native sulphur, and asphaltene/bitumen are indicative of the presence of thermochemical sulphate reactions (TSR) at depth.

(9)   The porosity and permeability of the Upper Stettler Formation and Crossfield Member was enhanced at shallow burial with the early pervasive dolomitisation of the study area that increased crystal sizes, enhancing pore throats. With continued burial, there was a significant loss in effective porosity and permeability by the effects of mechanical compaction (dewatering, reorientation of grains, and closer grain-packing) and subsequently by chemical compaction processes, particularly pressure solution. The precipitation of secondary anhydrites, blocky I and II calcite, and saddle dolomite were significant as porosity destructive mechanisms within vugs and fractures.

(10)   Several geochemical and textural differences exist between the wells within the Crossfield trend (wells 2-7) and those in the Panther River/Moose Mountain/Burnt Timber/Benjamin Ghost regions (wells 8-11). These differences are functions of porosity, TSR reactions, H_2S content, anhydrite concentration, and distance from the source of the episodic refluxing brines.

(11)   Pore water chemistry was possibly influenced by interaction with fluids from the underlying Lower Stettler Formation with slightly enriched $\delta^{18}O$ values. The diagenesis of the Upper Stettler Formation and Crossfield has also been affected by extensional and compressional forces associated with the Antler and Laramide orogenies, respectively. This can be seen in the fracture networks at depth in wells 8-11 and the altered pore water fluids that precipitated late-stage blocky II calcites.

121

REFERENCES

Adams, J.E. and Rhodes, M.L. 1960. Dolomitization by seepage refluxion. Bulletin of the American Association of Petroleum Geologists, 44: 1912-1920.

Al-Aasm, I.S. 2000. Chemical and isotopic constraints on recrystallization of sedimentary dolomites from the Western Canada Sedimentary Basin. Aquatic Geochemistry, 6: 227-248.

Al-Aasm, I.S. and Clarke, J.D. 2004. The effect of hydrothermal fluid flow on early diagenetic dolomitization: An example from the Devonian Slave Point Formation, northwest Alberta *In* Deformation, fluid flow, and reservoir appraisal in foreland fold and thrust belts. AAPG Hedberg Series, 1: 297-316.

Al-Aasm, I.S., Lonnee, J., Clarke, J. 2002. Multiple fluid flow events and the formation of saddle dolomite: case studies from the Middle Devonian of the Western Canada Sedimentary Basin. Marine and Petroleum Geology, 19: 209-217.

Al-Aasm, I.S., Taylor, B.E., and South, B. 1990. Stable isotope analysis of multiple carbonate samples using selective acid extraction. Chemical Geology (Isotope Geoscience Section), 80: 119-125.

Al-Aasm, I.S. and Packard, J.J. 2000. Stabilization of early-formed dolomite: a tale of divergence from two Mississippian dolomites. Sedimentary Geology, 131: 97-108.

Allan, J.R. and Matthews, R.K. 1982. Isotope signatures associated with early meteoric diagenesis. Sedimentology, 29: 797-817.

Allan, J.R. and Wiggins, W.D. 1993. Dolomite Reservoirs: Geochemical Techniques for Evaluating Origin and Distribution. AAPG Continuing Education Course Note Series #36: 110pp.

Andrichuk, J.M. 1958. Stratigraphy and facies analysis of Upper Devonian reefs in Leduc, Stettler, and Redwater areas, Alberta. Bulletin of American Association of Petroleum Geologists, 42: 1-93.

Andrichuk, J.M. 1960. Facies analysis of Upper Devonian Wabamun Group in west-central Alberta, Canada. Bulletin of the American Association of Petroleum Geologists, 44: 1651-1681.

Andrichuk, J.M. and Wonfor, J.S. 1954. Late Devonian geologic history in Stettler area, Alberta, Canada. Bulletin of the American Association of Petroleum Geologists, 38: 2500-2536.

Azmy, K., Veizer, J., Misi, A., Flávio de Oliveira, T., Sanches, A.L., Dardenne, M.A. 2001. Dolomitization and isotope stratigraphy of the Vazante Formation, São Francisco Basin, Brazil. Precambrian Research, 112: 303-329.

Badiozamani, K. 1973. The dorag-dolomitization model – application to the Middle Ordovician of Wisconsin. Journal of Sedimentary Petrology, 43: 965-984.

Bailey, T.R., McArthur, J.M., Prince, H., Thirwall, M.F. 2000. Dissolution methods for strontium isotope stratigraphy: whole rock analysis. Chemical Geology, 167: 313-319.

Bathurst, R.G.C. 1966. Boring algae, micrite envelopes and lithification of molluscan biosparites. Geological Journal, 5: 15-32.

Banner, J.L. 2004. Radiogenic isotopes: systematics and applications to earth surface processes and chemical stratigraphy. Earth-Science Reviews, 65: 141-194.

Baumgartner, L.K., Reid, R.P., Dupraz, C., Decho, A.W., Buckley, D.H., Spear, J.R., Przehop, K.M., Visscher, P.T. 2006. Sulfate reducing bacteria in microbial mats: changing paradigms, new discoveries. Sedimentary Geology, 185: 131-145.

Berger, Z. and Davies, G. 1999. The development of linear hydrothermal dolomite (HTD) reservoir facies along wrench or strike slip fault systems in the Western Canada Sedimentary Basin. CSPG Reservoir, 26: 34-38.

Bjørlykke, K. 1993. Fluid flow in sedimentary basins. Sedimentary Geology, 86: 137-158.

Boggs, S. 1995. Principles of Sedimentology and Stratigraphy. Prentice-Hall Inc., NJ, 774p.

Bottomley, D. and Veizer, J. 1992. The nature of groundwater flow in fractured rocks: Evidence from the isotopic and chemical evolution of recrystallized fracture calcites from the Canadian Precambrian Shield. Geochimica et Cosmochimica Acta, 56: 369-388.

Bottrell, S.H. and Newton, R.J. 2006. Reconstruction of changes in global sulphur cycling from marine sulphate isotopes. Earth-Science Reviews 75: 59-83.

Bowen, R. 1988. Isotopes in the Earth Sciences. Elsevier, NY: 647pp.

Brand, U. 2004. Carbon, oxygen, and strontium isotopes in Paleozoic carbonate components: An evaluation of original seawater chemistry proxies. Chemical Geology, 204: 23-44.

Brand, U. and Veizer, J. 1981. Chemical diagenesis of a multicomponent carbonate system – 2 Stable isotopes. Journal of Sedimentary Petrology, 51: 987-997.

Buxton, T.M. and Sibley, D.F. 1981. Pressure solution features in a shallow buried limestone. Journal of Sedimentary Petrology, 51: 19-26.

Burrowes, O.G. and Krause, F.F. 1987. Overview of the Devonian System: Subsurface of Western Canada Basin In Devonian Lithofacies and Reservoir Styles in Alberta (Eds: Krause, F.F. and Burrowes, O.G.), 13th CSPG Core Conference, 1-20.

Buschkuehle, B.E. and Machel, H.G. 1999. Diagenesis and paleofluid flow in the Devonian Southesk-Cairn carbonate complex in Alberta, Canada. Marine and Petroleum Geology, 19: 219-227.

Canfield, D.E. 2001. Isotope fractionation by natural populations of sulphate-reducing bacteria. Geochimica et Cosmochimica Acta, 65: 1117-1124.

Carballo, J.D., Land, L.S., and Miser, D.E. 1987. Holocene dolomitization of supratidal sediments by active tidal pumping, Sugarloaf Key, Florida. Journal of Sedimentary Petrology, 57: 153-165.

Carpenter, S.J. and Lohmann, K.C. 1989. $\delta^{18}O$ and $\delta^{13}C$ variations in Late Devonian marine cements from the Golden Spike and Nevis reefs, Alberta, Canada. Journal of Sedimentary Petrology, 59: 792-814.

Chilingar, G.V., Bissell, H.J. and Wolf, K.H. 1967. Diagenesis of carbonate rocks in Diagenesis In Sediments (Eds: Larsen, G. and Chilingar, G.V.): 179-322.

Choquette, P.W. and James, N.P. 1990. Limestones- the burial diagenetic environment in Diagenesis (Eds: McIlreath, I.A. and Morrow, D.W). Geoscience Canada Series 4, 75-111.

Choquette, P.W. and Pray, L. 1970. Geologic nomenclature and classification of porosity in sedimentary carbonates. American Association of Petroleum Geologists Bulletin, 54: 207-250.

Churcher, P.L. and Majid, A.H. 1989. Similarities between the Tangent-Wabamun play of the Alberta Basin and the Albion-Scipio type play of the Michigan Basin. Bulletin of Canadian Petroleum Geology, 37: 241-245.

Clarke, L.J. and Jenkyns, H.C. 1999. New oxygen isotope evidence for long-term Cretaceous climate change in the Southern Hemisphere. Geology, 27: 699-702.

Claypool, G.E., Holser, W.T., Kaplan, I.R., Sakai, H., and Zak, I. 1980. The age curves of sulphur and oxygen isotopes in marine sulphate and their mutual interpretation. Chemical Geology, 28: 199-260.

Coniglio, M., Sherlock, R., Williams-Jones, A.E., Middleton, K. and Frape, S.K. 1994. Burial and hydrothermal diagenesis of Ordovician carbonates from the Michigan Basin, Ontario, Canada. Special Publication of the International Association of Sedimentologists, 21: 231-254.

Davies, G.R. 2000. Hydrothermal Dolomite Reservoir Facies – Global and Western Canadian Perspectives. Graham Davies Geological Consultants, Ltd. Report: 195pp.

Denison, R.E., Koepnick, R.B., Burke, W.H., Heatherington, E.A., Fletcher, A. 1997. Construction of the Silurian and Devonian seawater $^{87}Sr/^{86}Sr$ curve. Chemical Geology, 140: 109-121.

Dickson, J.A. 1966. Carbonate identification and genesis as revealed by staining. Journal of Sedimentary Petrology, 36: 491-505.

Dravis, J.J. and Yurewicz, D.A. 1985. Enhanced carbonate petrography using fluorescence microscopy. Journal of Sedimentary Petrology, 55: 795-804.

Dunham, R.J. 1962. Classification of carbonate rocks In Classification of carbonate rocks, a symposium (Ed: W.E. Ham). American Association of Petroleum Geologists, Memoir 1: 108-121.

Ehrenberg, S.N. 2006. Porosity destruction in carbonate platforms. Journal of Petroleum Geology, 29: 41-52.

Ehrenberg, S.N., Eberli, G.P., Keramati, M. and Moallemi, S.A. 2006. Porosity-permeability relationships in interlayered limestone-dolostone reservoirs. AAPG Bulletin, 90: 91-114.

Eliuk, L.S. 1984. A hypothesis for the origin of Hydrogen Sulphide in Devonian Crossfield Member Dolomite, Wabamun Formation, Alberta, Canada, In Carbonates in Subsurface and Outcrop (Eds: Eliuk, L.S.), CSPG Core Conference, 245-289.

Eliuk, L.S. and Hunter, D.F. 1987 Wabamun Group structural thrust fault fields: the Limestone-Burnt Timber example, In Devonian Lithofacies and Reservoir Styles in Alberta (Eds: Krause, F.F. and Burrowes, O.G.), 13th CSPG Core Conference: 39-62.

Embry, A.F and Klovan, J.E. 1971. A late Devonian reef tract on northeastern Banks Island, N.W.T. Bulletin of Canadian Petroleum Geology, 19: 730-781.

Erickson, G., Jamieson, J., and Packard, J. 1994. Regional Evaluation of the Wabamun Group in the Foothills Subsurface (t.1-40, R27W4-15W5). PanCanadian and Geosgil & WR May & Associates. Consultants Rept on file with PanCanadian Petroleum Ltd, 60pp.

Faure,G. 1991. Inorganic Geochemistry. Macmillan Publishing, NJ: 626pp.

Flügel, E. 2004. Microfacies of Carbonate Rocks: Analysis, Interpretation and Application. Springer-Verlag, Berlin: 976pp.

124

Folk, R.L. 1965. Some aspects of recrystallization in ancient limestones *in* Dolomitization and Limestone Diagenesis (Eds: Pray, L.C and Murray, R.C.): 14-48.

Folk, R.L. 1987. Detection of organic matter in thin sections of carbonate rocks using a white card. Sedimentary Geology, 54: 193-200.

Folk, R.L. and Land, L.S. 1975. Mg/Ca ratio and salinity: two controls over crystallization of dolomite. American Association of Petroleum Geologists Bulletin, 59: 60-68.

Fowler, M.G., Stasiuk, L.D., Hearn, M. and Obermajer, M. 2001. Devonian hydrocarbon source rocks and their derived oils in the Western Canada Sedimentary Basin. Bulletin of Canadian Petroleum Geology, 49: 117-148.

Friedman, L, and O'Neil, J.R. 1977. Compilation of stable isotopic fractionation factors of geochemical interest: U.S. Geological Survey, Professional Paper 440-KK, 12p.

Fuller, J.G. and Porter, J.W. 1969. Evaporites and Carbonates; Two Devonian Basins of Western Canada. Bulletin of Canadian Petroleum Geology, 17: 182-193.

Geldsetzer, H.H. and Meijer Drees, N.C. 1984. Upper Devonian surface and subsurface lithostratigraphic units, west central Alberta and east central British Columbia *In* Carbonates in Subsurface and Outcrop (Eds: Eliuk, L.S.), CSPG Core Conference, 225-237.

Goodfriend, G.A. 1999. Terrestrial stable isotope records of Late Quaternary paleoclimates in the eastern Mediterranean region. Quaternary Science Review 18: 501-513.

Green, D.G. and Mountjoy, E.W. 2005. Fault and conduit controlled burial dolomitization of the Devonian west-central Alberta Deep Basin. Bulletin of Canadian Petroleum Geology, 53: 101-129.

Gregg, J.M. and Sibley, D.F. 1984. Epigenetic dolomitization and the origin of xenotopic dolomite texture. Journal of Sedimentary Petrology, 54: 908-931.

Gunatilaka, A., Saleh, A., Al-Temeemi, A., Nassar, N. 1987. Calcium-poor dolomite from the sabkhas of Kuwait. Sedimentology, 34: 999-1006.

Halbertsma, H.L. 1994. Devonian Wabamun Group *In* Geological Atlas of the Western Canada Sedimentary Basin, G.D. Mossop and I. Shetson (comp.), Canadian Society of Petroleum Geologists and Alberta Research Council, Calgary, Alberta. 16pp. URL: WWW.ags.gov.ab.ca/publications/ATLAS_WWW/ATLAS [April 2005].

Halbertsma, H.L. and Meijer-Drees, N.C. 1987. Wabamun Limestone Sequences in North-Central Alberta *In* Devonian Lithofacies and Reservoir Styles in Alberta (Eds: Krause, F.F. and Burrowes, O.G.), 13th CSPG Core Conference: 21-37.

Halim-Dihardja, M.K. 1986. Diagenesis and sedimentology of the Late Devonian (Famennian) Wabamun Group in the Tangent, Normandville, and Eaglesham fields, north-central Alberta. Unpublished M.Sc. Thesis, McGill University Dept. of Geological Sciences, 192pp.

Hardie, L. 1987. Dolomitization: A critical view of some current views. Journal of Sedimentary Petrology, 57: 166-183.

Harwood, G. 1988. Microscopic techniques: II. Principles of sedimentary petrology *In* Techniques in Sedimentology (Eds: Tucker, M.). Blackwell Scientific Publications, Oxford: 108-173.

Heydari, E. 1997. Hydrotectonic models of burial diagenesis in platform carbonates based on formation water geochemistry in North American sedimentary basins *In* Basin-Wide Diagenetic

125

Patterns: Integrated Petrologic, Geochemical, and Hydrologic Considerations, SEPM Special Publication, 57: 53-79.

Heydari, E. and Moore, C.H. 1989. Burial diagenesis and thermochemical sulphate reduction, Smackover Formation, southeastern Mississippi salt basin. Geology, 17: 1989.

Hiatt, E.E. and Kyser, K. 2000. Links between depositional and diagenetic processes in basin analysis: porosity and permeability evolution in sedimentary rocks *In* Fluids and Basin Evolution (Ed: Kyser, K.). Mineralogical Association of Canada short course 28: 63-92.

Hoefs, J. 2004. Stable Isotope Geochemistry. Springer-Verlag, Berlin: 239pp.

Hsü, K.J. and Siegenthatler, C. 1969. Preliminary experiments on hydrodynamic movement induced by evaporation and their bearing on the dolomite problem. Sedimentology, 11-25.

Hunt, J.M. 1996. Petroleum Geochemistry and Geology. W.H. Freeman and Company, NY: 743pp.

Hurley, N.F. and Lohmann, K.C. 1989. Diagenesis of Devonian reefal carbonates in the Oscar Range, Canning Basin, Western Australia. Journal of Sedimentary Petrology, 59: 127-146.

Hutcheon, I. 1999. Controls on the distribution of non-hydrocarbon gases in the Alberta Basin. Bulletin of Canadian Petroleum Geology, 47: 573-593.

Hutcheon, I., Cody, J., and Yang, C. 2000. Fluid flow in the Western Canada Sedimentary Basin – A biased perspective based on geochemistry *In* Fluids and Basin Evolution (Ed: Kyser, K.). Mineralogical Association of Canada Short Course 28: 197-208.

Immenhauser, A., Porta, G.D., Kenter, J.A.M, Bahamonde, J.R. 2003. An alternative model for positive shifts in shallow-marine carbonate $\delta^{13}C$ and $\delta^{18}O$. Sedimentology 50: 953-959. Johnston, D.I. and Chatterton, B.D. 2001. Upper Devonian (Famennian) conodonts of the Palliser Formation and Wabamun Group, Alberta and British Columbia, Canada *In* Palaeontographica Canadiana, CSPG-GSA, 19: 1-59.

Johnston, D.I. and Chatterton, B.D. 2001. Upper Devonian (Famennian) conodonts of the Palliser Formation and Wabamun Group, Alberta and British Columbia, Canada *In* Palaeontographica Canadiana, CSPG-GSA, 19: 1-59.

Jones, G.D and Xiao, Y. 2005. Dolomitization, anhydrite cementation, and porosity evolution in a reflux system: Insights from reactive transport models. AAPG Bulletin, 89: 577-601.

Jones, G.D., Whitaker, F.F., Smart, P.L., Sanford, W.E. 2002. Fate of reflux brines in carbonate platforms. Geology, 30: 371-374.

Kaylor, D.F. 1988. Facies and Diagenesis of the Upper Devonian Palliser Formation, Front Ranges of the Southern Rocky Mountains, Alberta and B.C. Unpublished M.Sc. Thesis, Mcgill University Dept. of Geological Sciences, 140pp.

Kasprzyk, A. 2003. Sedimentological and diagenetic patterns of anhydrite deposits in the Badenian evaporite basin of the Carpathian Foredeep, southern Poland. Sedimentary Geology, 158: 167-194.

Kent, D.M. 1994. Paleogeographic evolution of the cratonic platform – Cambrian to Triassic *In* Geological Atlas of the Western Canada Sedimentary Basin, G.D. Mossop and I. Shetson (comp.), Canadian Society of Petroleum Geologists and Alberta Research Council, Calgary, Alberta. 16pp. URL: WWW.ags.gov.ab.ca/publications/ATLAS_WWW/ATLAS [April 2005].

Krouse, H.R. and Coplen, T.B. 1997. Reporting of relative sulphur isotope-ratio data. Pure & Applied Chemistry, 69: 293-295.

Krouse, H.R., Viau, C.A., Eliuk, L.S., Ueda, A. and Halas, S. 1988. Chemical and isotopic evidence of thermochemical sulphate reduction by light hydrocarbon gases in deep Devonian reservoirs. Nature, 333: 415-419.

Kupecz, J.A., Montanez, I.P., Gao, G. 1995. Recrystallization of dolomite with time *In* Carbonate Microfabrics (Eds: Rezak, R. and Lavoie, D.L.). Elsevier, NY: 187-194.

Land, L.S. 1973. Holocene meteoric dolomitization of Pleistocene limestones, North Jamaica. Sedimentology, 20: 411-424.

Land, L.S. 1980. The isotopic and trace element Geochemistry of dolomite: the state of the art *In* Concepts and Models of Dolomitization, SEPM Special Publication 28 (Eds:Zenger, D.H, Dunham, J.B., and Ethington, R.L.): 87-110.

Land, L.S. 1985. The origin of massive dolomite. Journal of Geologic Education, 33: 112-125.

Lonnee, J. and Al-Aasm, I.S. 2000. Dolomitization and fluid evolution in the Middle Devonian Sulphur Point Formation, Rainbow South Field, Alberta: petrographic and geochemical evidence. Bulletin of Canadian Petroleum Geology, 48: 262-283.

Lovering, T.S. 1969. The origin of hydrothermal and low temperature dolomite. Economic Geology, 64: 743-754.

Lu, F.H. and Meyers, W.J. 1998. Massive dolomitization of a late Miocene carbonate platform: a case of mixed evaporative brines with meteoric water, Nijar, Spain. Sedimentology, 45: 263-277.

Machel, H.G. 1987. Saddle dolomite as a by-product of chemical compaction and thermochemical sulphate reduction. Geology, 15: 936-940.

Machel, H.G. 1987b. Some aspects of diagenetic sulphate-hydrocarbon redox reactions *In* Diagenesis of Sedimentary Sequences (Ed: Marshall, J.D.). Geological Special Publication, 36: 15-28.

Machel, H.G. 1997. Recrystallization vs neomorphism, and the concept of 'significant recrystallization' in dolomite research. Sedimentary Geology, 113: 161-168.

Machel, H.G. 2001. Bacterial and thermochemical sulphate reduction in diagenetic settings – old and new insights. Sedimentary Geology 140: 143-175.

Machel, H.G. 2004. Concepts and models of dolomitization: a critical reappraisal *In* The Geometry and Petrogenesis of Dolomite Hydrocarbon Reservoirs (Eds: Braithwaite, C.J.R., Rizzi, G., & Darke, G.). Geological Society, London, Special Publications, 235: 7-63.

Machel, H.G. and Anderson, J.H. 1989. Pervasive subsurface dolomitization of the Nisku Formation in central Alberta. Journal of Sedimentary Petrology, 59: 891-911.

Machel, H.G. and Cavell, P.A. 1999. Low-flux, tectonically-induced squeegee fluid flow ("hot flash") into the Rocky Mountain Foreland Basin. Bulletin of Canadian Petroleum Geology, 47: 510-533.

Machel, H.G., Cavell, P.A., and Patey, K.S.1996. Isotopic evidence for carbonate cementation and recrystallization, and for tectonic expulsion of fluids into the Western Canada Sedimentary Basin. Geological Society of America Bulletin, 108: 1108-1119.

127

Machel, H.G. and Hunter, I.G. 1994. Facies models for Middle to Late Devonian shallow-marine carbonates, with comparisons to modern reefs: a guide for facies analysis. Facies, 30: 155-176.

Machel, H.G. and Lonnee, J. 2002. Hydrothermal dolomite – a product of poor definition and imagination. Sedimentary Geology, 152: 163-171.

Machel, H.G. and Mountjoy, E.W. 1986. Chemistry and environments of dolomitization – A reappraisal. Earth-Science Reviews, 23: 175-222.

Machel, H.G. and Mountjoy, E.W. 1987. General constraints on extensive pervasive dolomitization – and their application to the Devonian carbonates of Western Canada. Bulletin of Canadian Petroleum Geology, 35: 143-158.

Machel, H.G., Riciputi, L.R., Cole, D.R. 1997. Ion microprobe investigation of diagenetic carbonates and sulfides in the Devonian Nisku Formation, Alberta, Canada *In* Basin-wide Diagenetic Patterns: Integrated Petrologic, Geochemical, and Hydrologic Considerations. SEPM Special Publication, 57: 157-165.

Martin, L. 2004. Well Map of Giroux Lake for ConocoPhillips Canada URL :WWW .ConcocoPhillips.ca

Martindale, B. 2005. Personal Communication.

Martindale, B., Packard, J. and Al-Aasm, I.S. 2004. The Wabamun Crossfield Member in Southern Alberta (est. 4.9. Tcfe resource) – An example of reflux dolomitisation of peritidal carbonates *In* Dolomites: The Spectrum: Mechanisms, Models, Reservoir Development, CSPG Seminar and Core Conference, Calgary, Alberta, Canada.

McKenzie, J.A., Hsü, K.J., Schneider, J.F. 1980. Movement of subsurface waters under the sabkha, Abu Dhabi, UAE, and its relation to evaporative dolomite genesis *In* Concepts and Models of Dolomitization (Eds: Zenger, D.H., Dunham, J.B., Ethington, R.L.). Special Publication Society of Economic Paleontologists and Mineralogists, 28: 11-30.

Melim, L.A. and Scholle, P.A. 2002. Dolomitization of the Capitan Formation forereef facies (Permian, west Texas and New Mexico): seepage reflux revisited. Sedimentology, 49: 1207-1227.

Metherell, R.G. and Workman, L.E. 1969. Sedimentary features of the Crossfield Member. Bulletin of Canadian Petroleum Geologists, 17: 444-459.

Moore, P.F. 1989a. The Kaskaskia sequence: reefs, platforms and foredeeps. The Lower Kaskaskia sequence – Devonian *In* Western Canada Sedimentary Basin: A Case History. Eds: Ricketts, B.D.:139-165.

Moore, C.H. 1989b. Carbonate Diagenesis and Porosity. Elsevier, NY: 338pp.

Moore, C.H. 2001. Carbonate Reservoirs: Porosity evolution and diagenesis in a sequence stratigraphic framework. Developments in Sedimentology 55, Elsevier Science, Amsterdam: 444 pp.

Morrow, D.W. 1990. Dolomite – Part 2: Dolomitization Models and Ancient Dolostones *In* Diagenesis (Eds: McIlreath, I.A. and Morrow, D.W.). Geoscience Canada Series 4: 125-139.

Morrow, D.W and McIlreath, I.A. 1990. Diagenesis – general introduction *In* Diagenesis (Eds: McIlreath, I.A. and Morrow, D.W.). Geoscience Canada Series 4: 1-9.

Mountjoy, E.W. and Halim-Dihardja, M.K. 1991. Multiple phase fracture and fault-controlled burial dolomitization, Upper Devonian Wabamun Group, Alberta. Journal of Sedimentary Petrology, 61:

590-612.

Mountjoy, E.W., Machel, H.G., Green, D., Duggan, J., Williams-Jones, A.E. 1999. Devonian matrix dolomites and deep burial carbonate cements: A comparison between the Rimbey-Meadowbrook reef trend and the deep basin of west-central Alberta. Bulletin of Canadian Petroleum Geology, 47: 487-509.

Mountjoy, E.W., Qing, H., and McNutt, R.H. 1992. Strontium isotopic composition of Devonian dolomites, Western Canada Sedimentary Basin: significance of sources of dolomitizing fluids. Applied Geochemistry, 7: 59-75.

Müller, D.W., McKenzie, J.A., Mueller, P.A.1990. Abu Dhabi sabkha, Persian Gulf, revisited: Application of strontium isotopes to test an early dolomitization model. Geology, 18: 618-621.

Murray, R.C. and Pray, L.C. 1967. Dolomitisation and limestone diagenesis: An introduction *In* Dolomitization and Limestone Diagenesis (Eds: L.C. Pray and R.C. Murray), Special Publication 13: 1-14.

Nesbitt, B.E. and Muehlenbachs, K. 1994. Paleohydrogeology of the Canadian Rockies and origins of brines, Pb-Zn deposits and dolomitization of the Western Canada Sedimentary Basin. Geology, 22: 243-246.

Nikolaides, S. 1997. Marine-derived dolomite in the shallowly buried temperate Port Campbell Limestone (Miocene), Otway Basin, Australia. Sedimentology, 44: 143-157.

Northrop, D.A. and Clayton, R.N. 1966. Oxygen-isotope fractionations in systems containing dolomite. Journal of Geology, 74: 174-196.

Nöth, S. 1997. High H_2S contents and other effects of thermochemical sulphate reduction in deeply buried carbonate reservoirs: a review. Geologische Rundschau, 86: 275-287.

O'Neil, J.R. 1986. Theoretical and experimental aspects of isotopic fractionation *In* Stable Isotopes in High Temperature Geologic Processes. Reviews in Mineralogy, 16: 1-35.

Ostrom, J.N. 1985. Lithofacies Analysis of the Upper Devonian Crossfield Member, Stettler Formation, Olds Area, Southwestern Alberta. Unpublished B.Sc. Thesis, University of British Columbia, 89pp.

Packard, J. 2005. Personal Communication.

Packard, J. and Mcnab, G. 1994. Reservoir potential of the eastern margin of the Garrington-Okotoks Wabamun gas trend. Consultants Rept on file with Pan Canadian Petroleum Ltd.

Packard, J., Pellegrin, G.J., Al-Aasm, I.S., Samson, I., and Gagnon, J. 1990. Diagenesis and dolomitization associated hydrothermal karst in Famennian Upper Wabamun ramp sediments, northwestern Alberta *In*
The Development of Porosity in Carbonate Reservoirs (Eds: Bloy, G.R. and Hadley, M.G). CSPG Short Course Notes: 1-19.

Patterson, R.J. and Kinsman, D.J.J. 1982. Formation of diagenetic dolomite in coastal sabkha along Arabian (Persian) Gulf. The American Association of Petroleum Geologists Bulletin, 66: 28-43.

Peterhänsel, A. and Pratt, B.R. 2001. Nutrient-triggered bioerosion on a giant carbonate platform masking the postextinction Famennian benthic community. Geology, V.29, Issue 12: 1079-1082.

Popp, B.N., Anderson, T.F., Sandberg, P.A. 1986. Brachiopods as indicators of original isotopic compositions in some Paleozoic limestones. Geological Society of America Bulletin, 97: 1262-1269.

Price, R.A. 1994. Cordilleran Tectonics and the Evolution of the Western Canada Sedimentary Basin *In* Geological Atlas of the Western Canada Sedimentary Basin, G.D. Mossop and I. Shetson (comp.), Canadian Society of Petroleum Geologists and Alberta Research Council, Calgary, Alberta. 19pp. URL: WWW.ags.gov.ab.ca/publications/ATLAS_WWW/ATLAS [April 2005].

Qing, H. and Mountjoy, E.W. 1994. Formation of coarsely-crystalline, hydrothermal dolomite reservoirs in the Presqu'ile Barrier, Western Canada Sedimentary Basin. AAPG Bulletin, 78: 55-77.

Raasch, G.O. 1956. Late Devonian and/or Mississippian Faunal Succession in Stettler Area, Alberta. Journal of Alberta Society of Petroleum Geologists, 4: 112-118.

Radke, B.M. and Mathis, R.L. 1980. On the formation and occurrence of saddle dolomite. Journal of Sedimentary Petrology, 50: 1149-1168.

Randazzo, A.F. and Zachos, N.G. 1983. Classification and description of dolomitic fabrics of rocks from Floran aquifer, U.S.A. Sedimentary Geology, 37: 151-162.

Reid, R.P. and Macintyre, I.G. 2000. Microboring versus recrystallization: further insight into the micritization process. Journal of Sedimentary Research, 70: 24-28.

Richards, B.C. 1989. Upper Kaskaskia sequence: Uppermost Devonian and Lower Carboniferous *In* Western Canada Sedimentary Basin: A Case History. (Eds: Ricketts, B.D.): 165-202.

Rollinson, H. 1993. Using Geochemical Data: Evaluation, Presentation, Interpretation. Longman Group, UK: 353pp.

Ross, G.M, Patchett, P.J., Hamilton, M., Heaman, L., DeCelles, P.G., Rosenberg, E., and Giovanni, M.K. 2005. Evolution of the Cordilleran orogen (southwestern Alberta, Canada) inferred from detrital mineral geochronology, geochemistry, and Nd isotopes in the foreland basin. GSA Bulletin, 117: 747-763.

Sanford, W.E. and Wood, W.W. 2001. Hydrology of the coastal sabkhas of Abu Dhabi, United Arab Emirates. Hydrogeology Journal, 9: 358-366.

Schreiber, B.C. and Helman, M.C. 2005. Criteria for distinguishing primary evaporite features from deformation features in sulphate evaporites. Journal of Sedimentary Research, 75: 525-533.

Searl, A.1989. Saddle dolomite: a new view of its nature and origin. Mineralogical Magazine, 53: 547-555.

Sharp, Z. 2007. Principles of Isotope Geochemistry. Pearson, Prentice-Hall, NJ: 344pp.

Shearman, D.J. and Fuller, J.G. 1969. Anhydrite diagenesis, calcitization, and organic laminates, Winnipegosis Formation, Middle Devonian, Saskatchewan. Bulletin of Canadian Petroleum Geology, 17: 496-525.

Shields, M.J. and Brady, P.V. 1995. Mass balance and fluid flow constraints on regional-scale dolomitization, Late Devonian, Western Canada Sedimentary Basin. Bulletin of Canadian Petroleum Geology, 43: 371-392.

Shinn, E.A. and Robbin, D.M. 1983. Mechanical and chemical compaction in fine-grained shallow water limestones. Journal of Sedimentary Petrology, 53: 595-618.

Sibley, D.F. and Gregg, J.M. 1987. Classification of dolomitic rock textures. Journal of Sedimentary Petrology, 57: 957-965.

Strauss, H. 1999. Geological evolution from isotope proxy signals – sulphur. Chemical Geology, 161: 89-101.

Stoakes, F.A. 1992. Wabamun Megasequence, In Devonian-Early Mississippian Carbonates of the Western Canada Sedimentary Basin: A Sequence Stratigraphic Framework, SEPM Short Course #28: 225-239.

Taberner, C. and Santisteban, C. 1987. Mixed-water dolomitization in a transgressive beach-ridge system, Eocene Catalan Basin, NE Spain In Diagenesis of Sedimentary Sequences (Ed: Marshall, J.D.). Geological Society Special Publication 36: 123-139.

Tobin, K.J., Steinhauff, D.M., Walker, K.R.1999. Ordovician meteoric carbon and oxygen isotopic values: implications for the latitudinal variations of ancient stable isotopic values. Palaeogeography, Palaeoclimatology, Palaeoecology, 150: 331-342.

Tucker, M.E. 2001. Sedimentary Petrology. Blackwell Science Ltd, Oxford: 262pp.

Tucker, M.E. and Wright, V.P. 1990. Carbonate Sedimentology. Blackwell Scientific Publications, Oxford: 482pp.

Veizer, J., Holser, W.T., and Wilgus, C.K. 1980. Correlation of $^{13}C/^{12}C$ and $^{34}S/^{32}S$ secular variations. Geochimica et Cosmochimica Acta, 44: 579-587.

Veizer, J., Ala, D., Azmy, K., Bruckschen, P., Buhl, D., Bruhn, F., Carden, G., Diener, A., Ebneth, S., Godderis, Y., Jasper, T., Korte, C., Pawellek, F., Podlaha, O., Strauss, H. 1999. $^{87}Sr/^{86}Sr$, $\delta^{13}C$ and $\delta^{18}O$ evolution of Phanerozoic seawater. Chemical Geology, 161: 59-88.

Walker, K.R., Jernigan, D.G., and Weber, L.J. 1990. Petrographic criteria for the recognition of marine, syntaxial overgrowths, and their distribution in geologic time. Carbonates and Evaporites, 5: 141-151.

Walker, R.G. 1992. Facies, facies models and modern stratigraphic concepts In Facies Models (Eds: Walker, R.G. and James, N.P.): 1-14.

Wanless, H.R. 1979. Limestone response to stress: pressure solution and dolomitisation. Journal of Sedimentary Research, 49: 437- 462.

Warren, J.K. 1989. Evaporite Sedimentology. Prentice Hall Inc., N.J.: 285p.

Warren, J. 2000. Dolomite: occurrence, evolution and economically important associations. Earth-Science Reviews, 52: 1-81.

Wenbin, T. 1998. Origins of replacement dolomites, Upper Devonian Leduc, Nisku, and Wabamun Formations, Southeastern Alberta, Western Canada Sedimentary Basin. Unpublished Phd Thesis, Mcgill University Dept. of Geological Sciences, 242pp.

Wonfor, J.S. and Andrichuk, J.M. 1956. The Wabamun Group in the Stettler Area, Alberta. Journal of the Alberta Society of Petroleum Geologists, 4: 99-111.

Wood, W.W., Sanford, W.E., and Al Habshi, A.R.S. 2002. Source of solutes to the coastal sabkha of Abu Dhabi. Geological Society of America Bulletin, 114: 259-268.

131

Worden, R.H., Smalley, P.C., Fallick, A.E. 1997. Sulfur cycle in buried evaporites. Geology, 25: 643-646.

Workman, L.E. and Metherell, R.G. 1969. Geology Crossfield East and Lone Pine Creek Gas Fields, Alberta. Bulletin of Canadian Petroleum Geology, 17: 92-108.

Wright, V.P. 1992. A revised classification of limestones. Sedimentary Geology, 76: 177-185.

Wright, G.N, McMechen, M.E. and Potter, D.E. 1994. Structure and Architecture of the Western Canada Sedimentary Basin *In* Geological Atlas of the Western Canada Sedimentary Basin, G.D. Mossop and I. Shetson (comp.), Canadian Society of Petroleum Geologists and Alberta Research Council, Calgary, Alberta. 19pp. URL: WWW.ags.gov.ab.ca/publications/ATLAS_WWW/ATLAS [April 2005].

Yang, C., Hutcheon, I. and Krouse, H. 2001. Fluid inclusion and stable isotope studies of thermochemical sulphate reduction from Burnt Timber and Crossfield East gas fields in Alberta, Canada. Bulletin of Canadian Petroleum Geology, 49: 149-164.

Yang, W., Spencer, R.J., and Krouse, H.R. 1995. Stable isotope and major element compositions of fluid inclusions in Devonian and Cambrian dolomite cements, western Canada. Geochimica et Cosmochimica Acta, 59: 3159-3172.

Zenger, D.H. 1983. Burial dolomitization in the Lost Burro Formation (Devonian), east-central California, and the significance of late diagenetic dolomitization. Geology, 11: 519-522.

APPENDIX I

Well Locations

North of Crossfield Trend:

Well #1: 10-9-66-21W5 (Giroux Lake)

Along Crossfield Trend:

Well #2: 11-23-25-29W4 (Jeff Lake/Crossfield)
Well #3: 13-12-29-27W4 (Inverness Acme)
Well #4: 10-18-21-28W4 (Canoxy Okotoks)
Well #5: 5-22-32-1W5 (Amerada Olds)
Well #6: 10-23-30-28W4 (Primewest)
Well #7: 10-21-32-2W5 (Northstar Garrington)

West of Crossfield Trend:

Well #8: 7-23-31-9W5 (Burnt Timber)
Well #9: 5-19-30-10W5 (Panther River)
Well #10: 10-5-23-6W5 (Moose Mountain)
Well #11: 10-13-26-8W5 (Benjamin Ghost)

133

APPENDIX II

Abbreviations & Symbols:

Mdst - Mudstone
Wkst - Wackestone
Grnst - Grainstone
Pkst - Packstone
Rdst- Rudstone
Flst - Floatstone

• Peloids
／ Intraclasts
Algae
✦ Crinoids
▾ Brachiopods
⑬ Stromatoporoids
⌧ Bivalves
◭ Gastropods
◈ Fossil Fragments
◔ Burrows

o Nodules
⊘ Fenestrae
ᴧ Stylolites
≈ Wavy Laminations
= Parallel Laminations

V Vuggy Porosity
c Chert
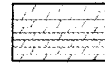
 - Dolostone
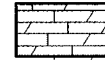
 - Dolomitised Limestone
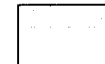
 - Anhydritic Nodular and
Laminated Dolomudstones
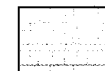
 - Limestone

 - Missing Core

134

APPENDIX III: Graphic Core Logs

GIROUX LAKE
Well #1: 10-9-66-21W5

Depth (m)

Columns: Allochems | Sedimentary Structures | Lithology (Mdst/Wkst/Pkst/Grst/Flst/Rudst)

Depths (top to bottom): 2415, 2409, 2403, 2397, 2391, 2385, 2379, 2373, 2367, 2361, 2355, 2349, 2343, 2337, 2331, 2325, 2319

135
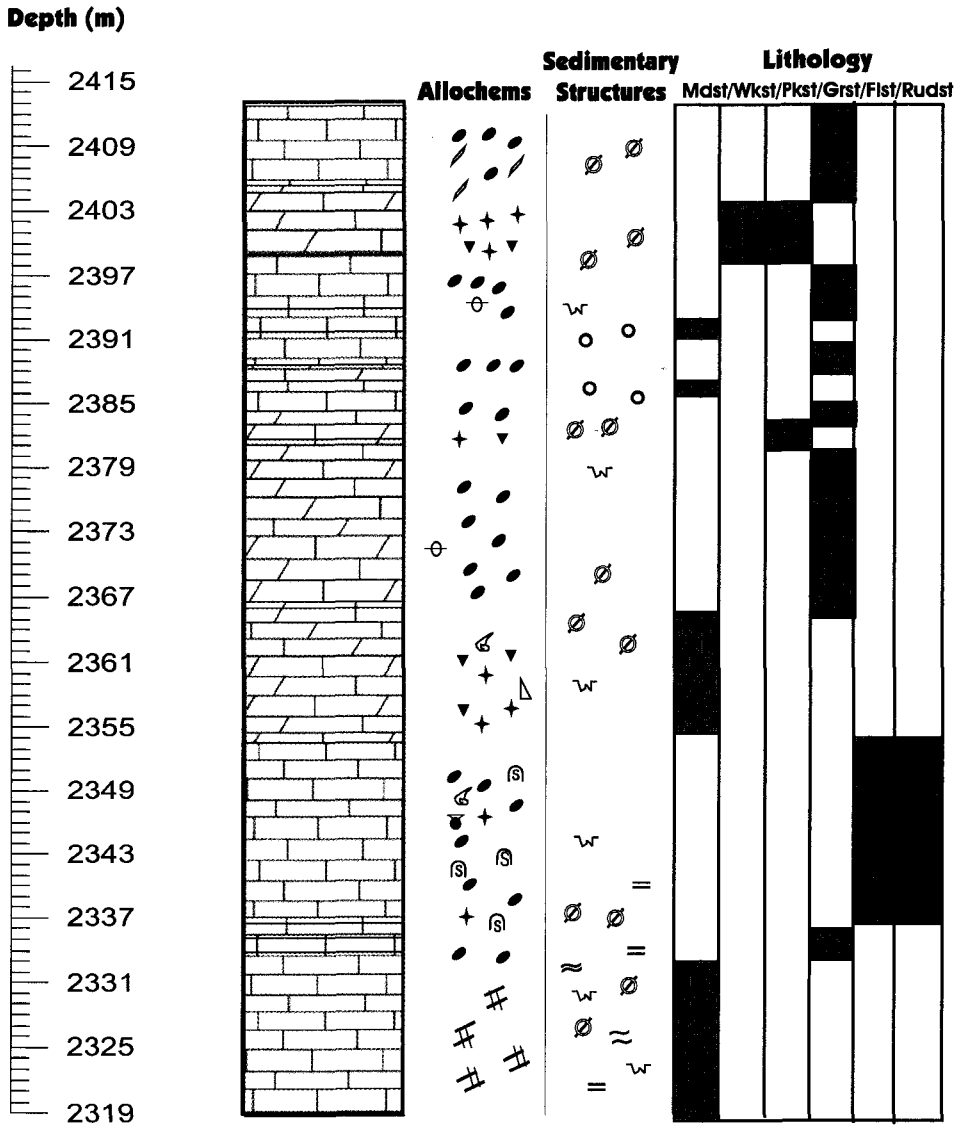
JEFF LAKE
WELL #2 : 11-23-25-29W4

Depth (m)

2649
2651
2653
2655
2657
2659
2661
2663
2665
2667
2669
2671
2673

Allochems

Sedimentary Structures

Lithology
Mdst/Wkst/Pkst/Grst/Flst/Rudst

136
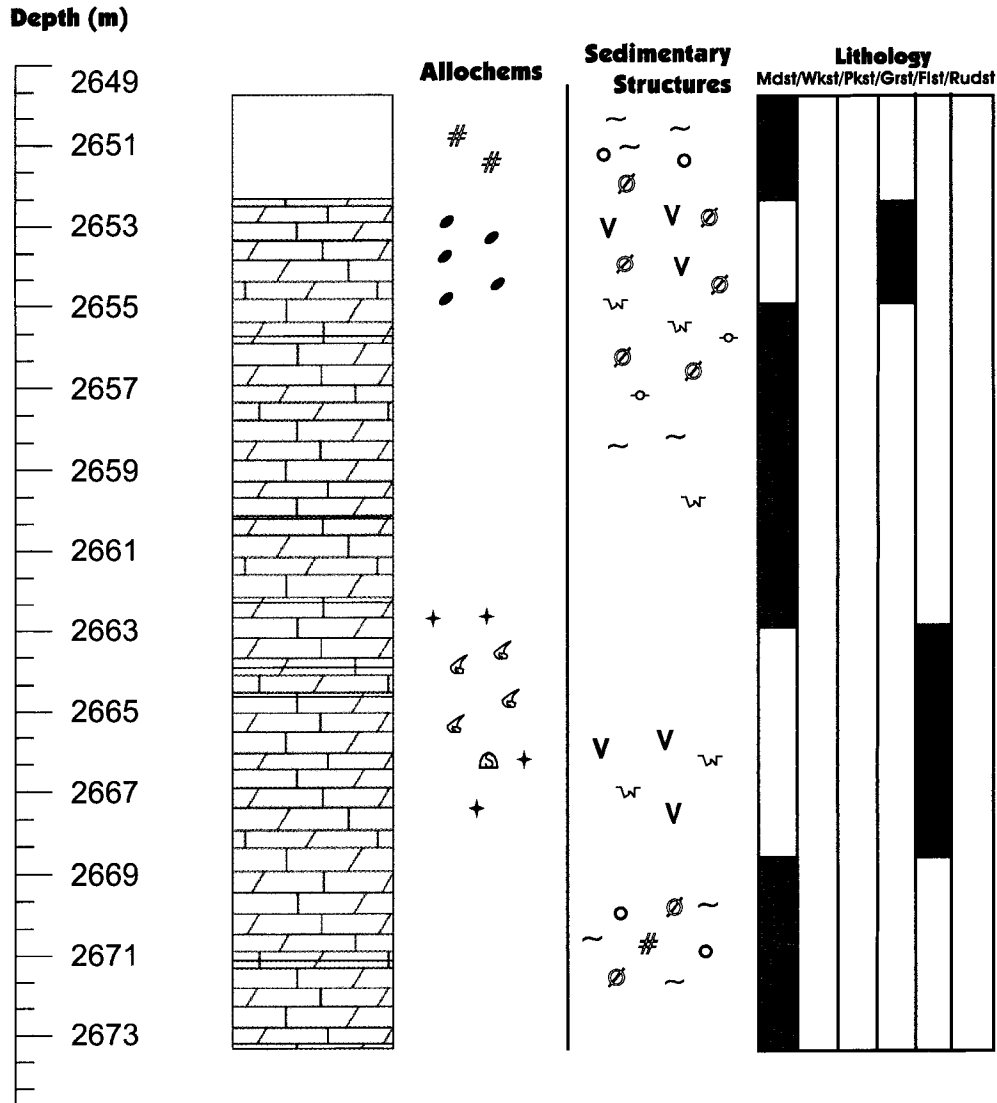
Inverness Acme
Well # 3: 13-12-29-27W4

Depth (m)

2245
2246
2247
2248
2249
2250
2251
2252
2253
2254
2255
2256
2257
2258
2259
2260
2261
2262
2263
2264

Allochems

Sedimentary Structures

Lithology
Mdst/Wkst/Pkst/Grst/Flst/Rudst

137
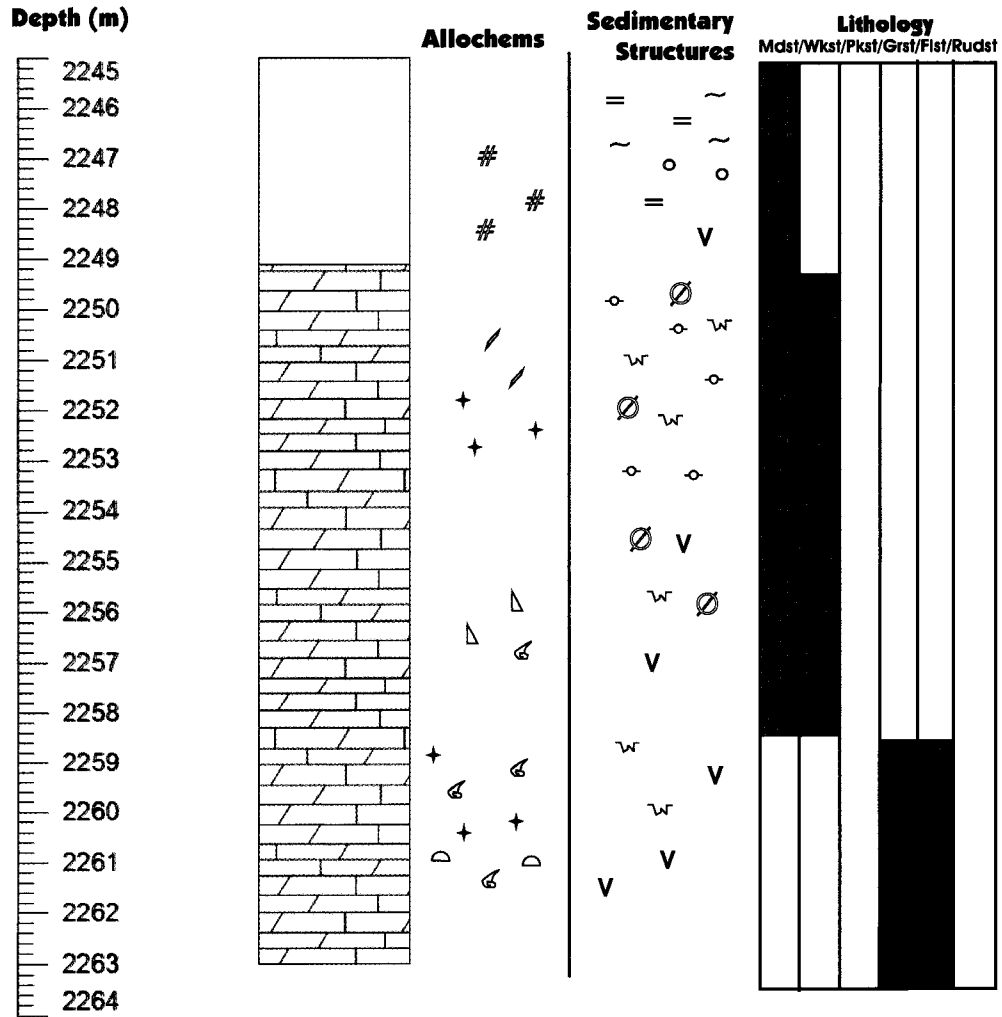
Canoxy Okotoks
Well # 4: 10-18-21-28W4

Depth (m)

Allochems | Sedimentary Structures | Lithology Mdst/Wkst/Pkst/Grst/Flst/Rudst

138

Amerada Olds
Well #5: 5-22-32-1W5

Depth (m)

Allochems

Sedimentary Structures

Lithology
Mdst/Wkst/Pkst/Grst/Flst/Rudst

139
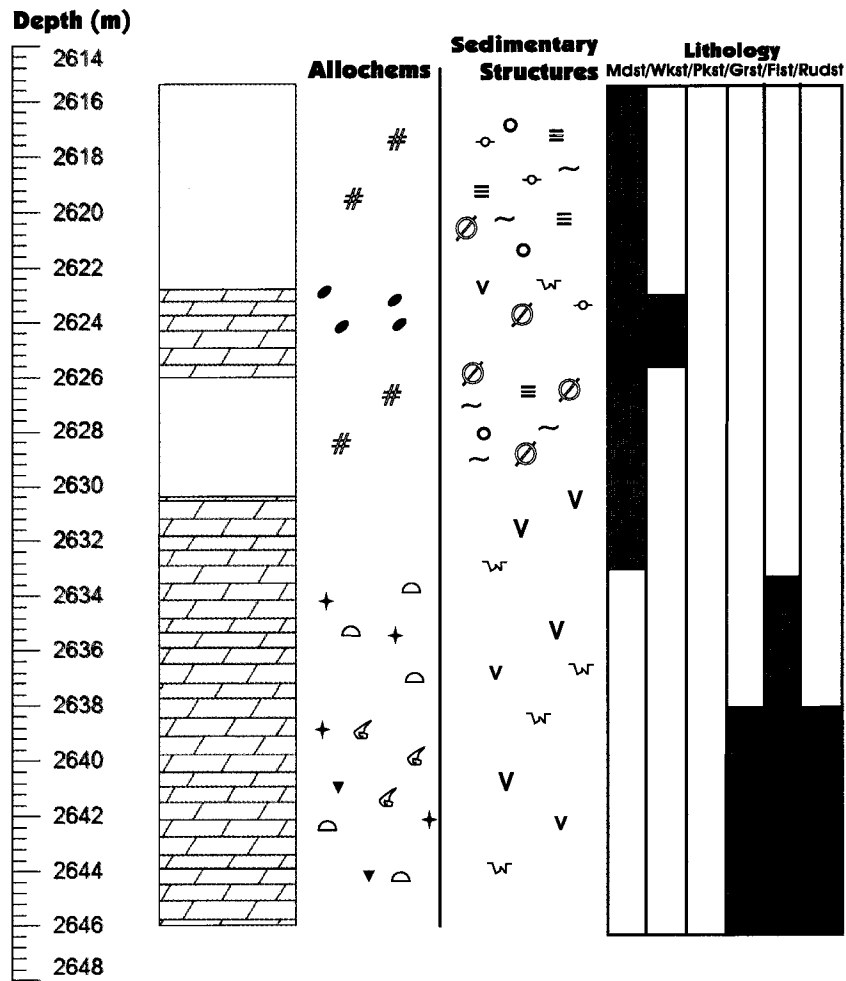
Primewest
Well #6: 10-23-30-28W4

Depth (m)

Allochems

Sedimentary Structures

Lithology
Mdst/Wkst/Pkst/Grst/Flst/Rudst

2384
2385
2386
2387
2388
2389
2390
2391
2392
2393
2394
2395
2396
2397
2398
2399
2400
2401
2402
2403

140
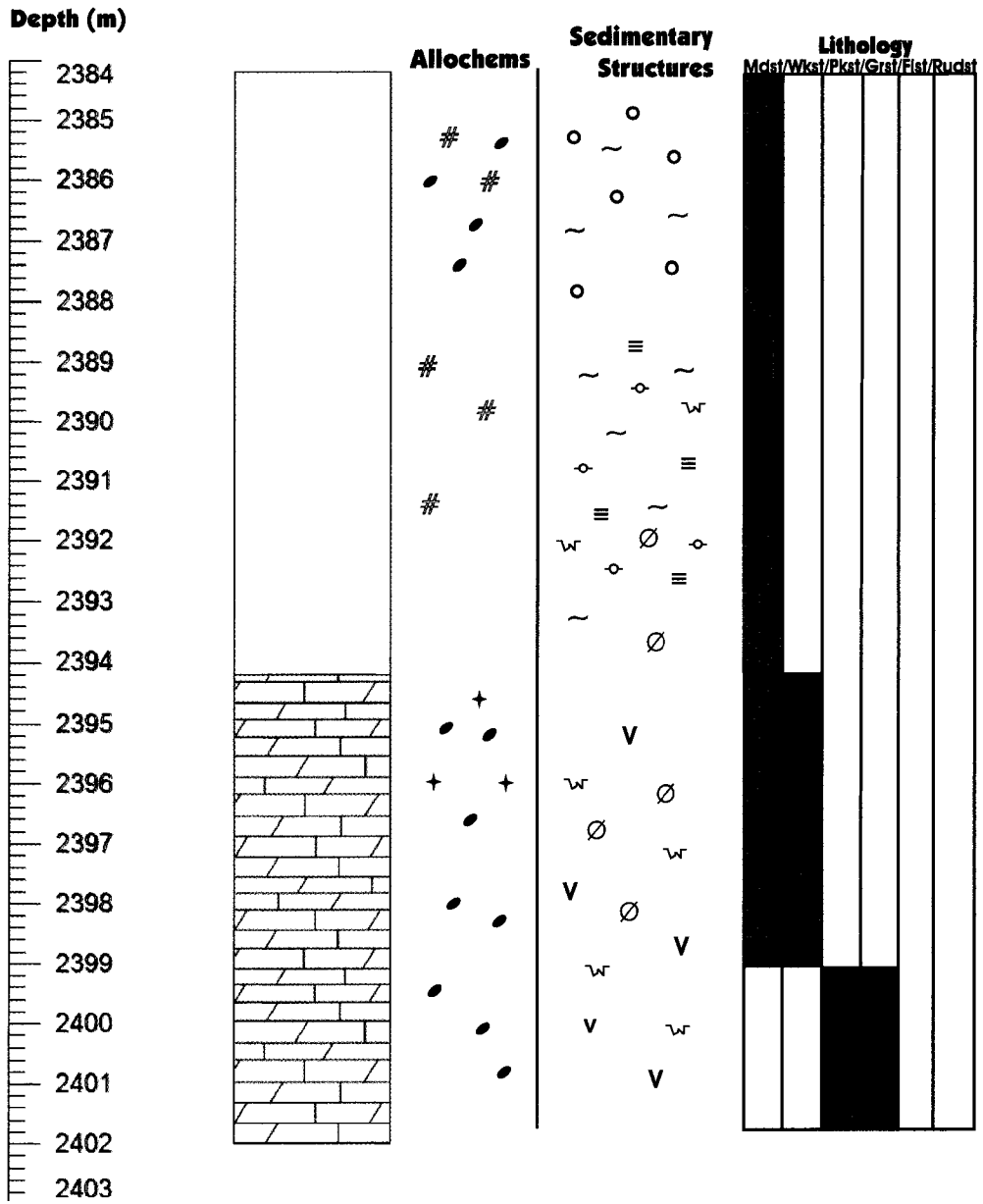
Northstar Garrington
Well # 7: 10-21-32-2W5

Depth (m)

Allochems

Sedimentary
Structures

Lithology
Mdst/Wkst/Pkst/Grst/Flst/Rudst
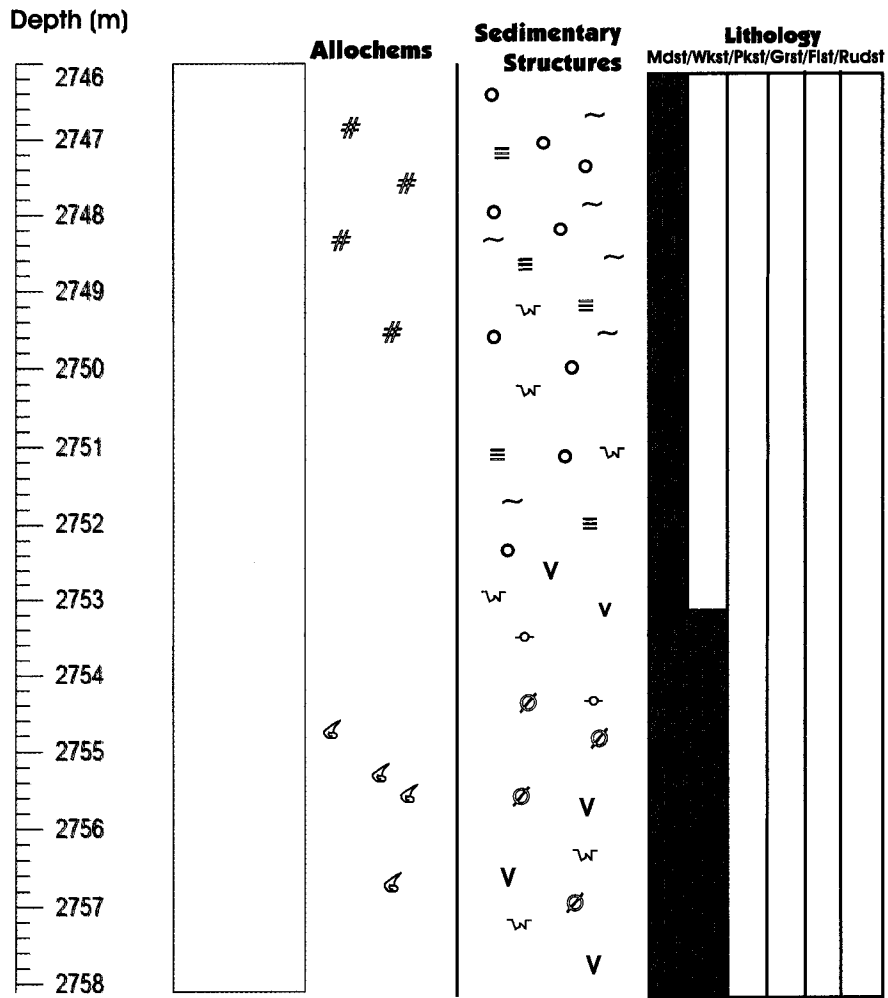
Burnt Timber
Well #8: 7-23-31-9W5

Depth (m)

Allochems
#

Sedimentary
Structures

Lithology
Mdst/Wkst/Pkst/Grst/Flst/Rudst

142
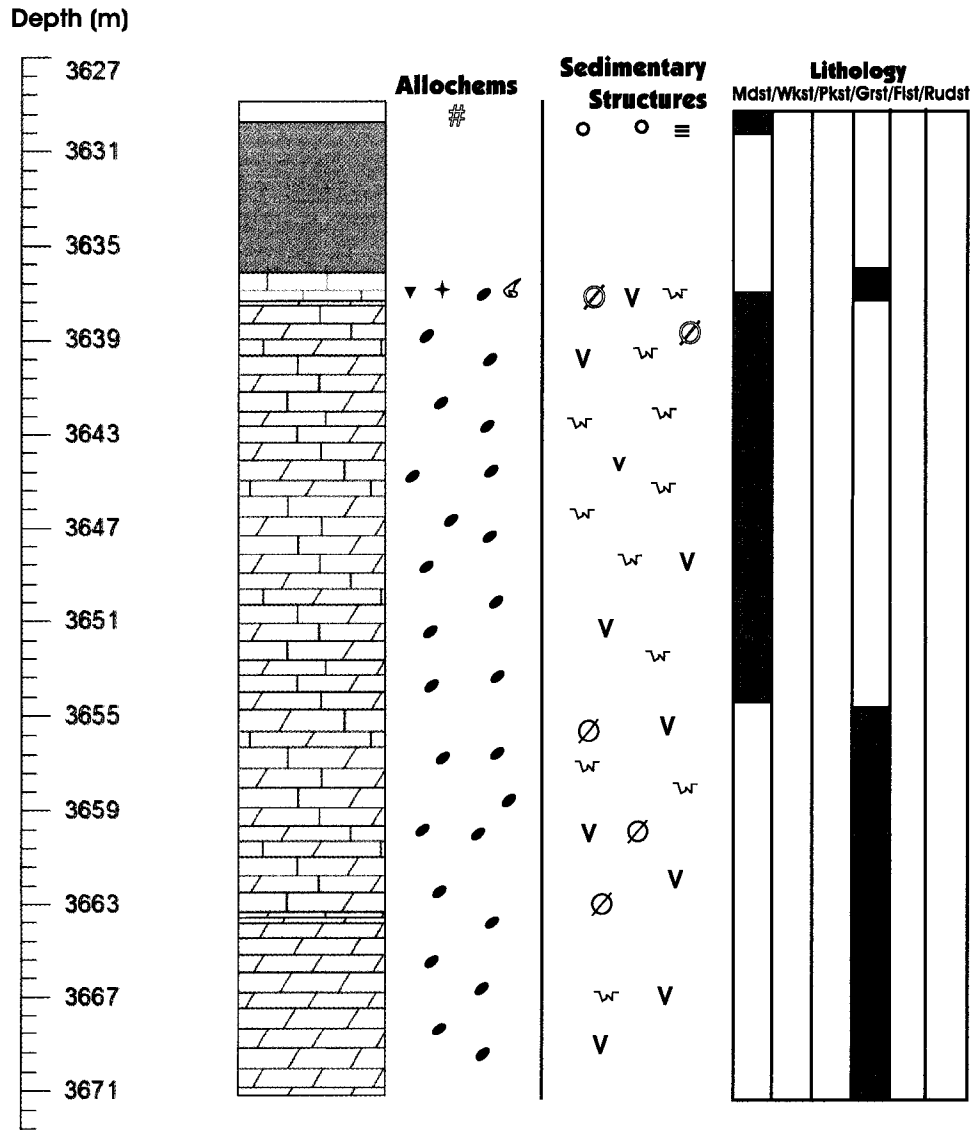
Panther River
Well # 9: 5-19-30-10W5

Depth (m)

Allochems

Sedimentary Structures

Lithology
Mdst/Wkst/Pkst/Grst/Flst/Rudst

143
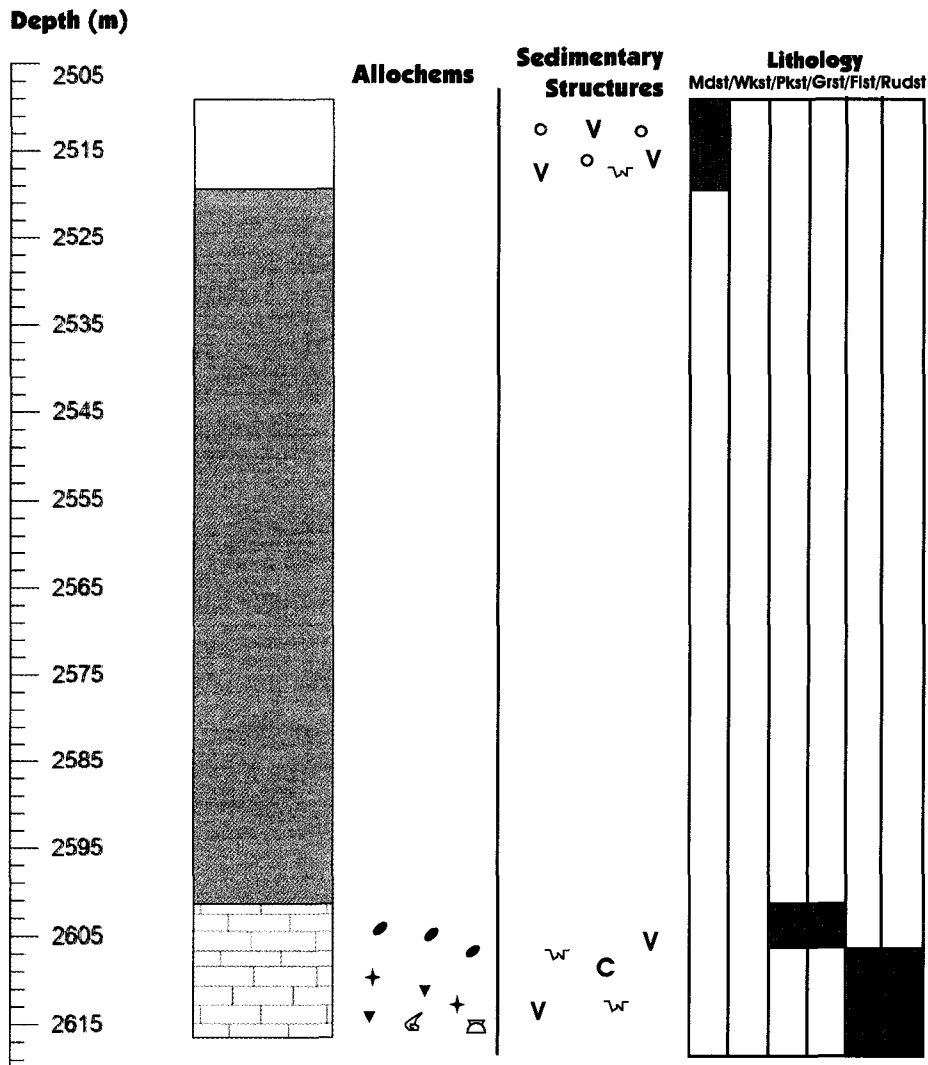
Moose Mountain
Well #10: 10-5-23-6W5

Depth (m)

	Allochems	Sedimentary Structures	Lithology Mdst/Wkst/Pkst/Grst/Flst/Rudst
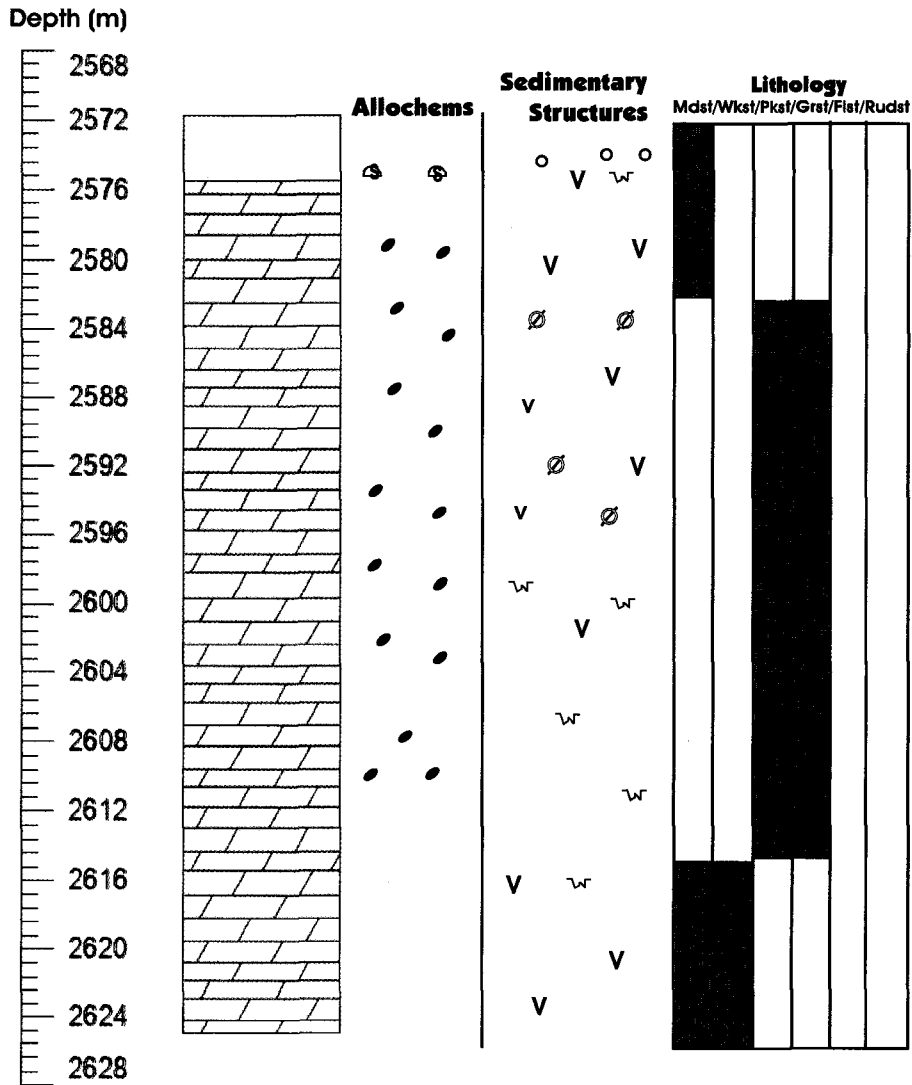
Benjamin Ghost
Well # 11: 10-13-26-8W5

Depth (m)

| 3573 |
| 3573 |
| 3574 |
| 3574 |
| 3575 |
| 3575 |
| 3576 |
| 3576 |
| 3577 |
| 3577 |
| 3578 |
| 3578 |
| 3579 |
| 3579 |
| 3580 |
| 3580 |
| 3581 |
| 3581 |
| 3582 |
| 3582 |

Allochems

No allochems
Preserved
destructive
Pervasive
Dolomitisation

Sedimentary Structures

Lithology
Mdst/Wkst/Pkst/Grst/Flst/Rudst

145
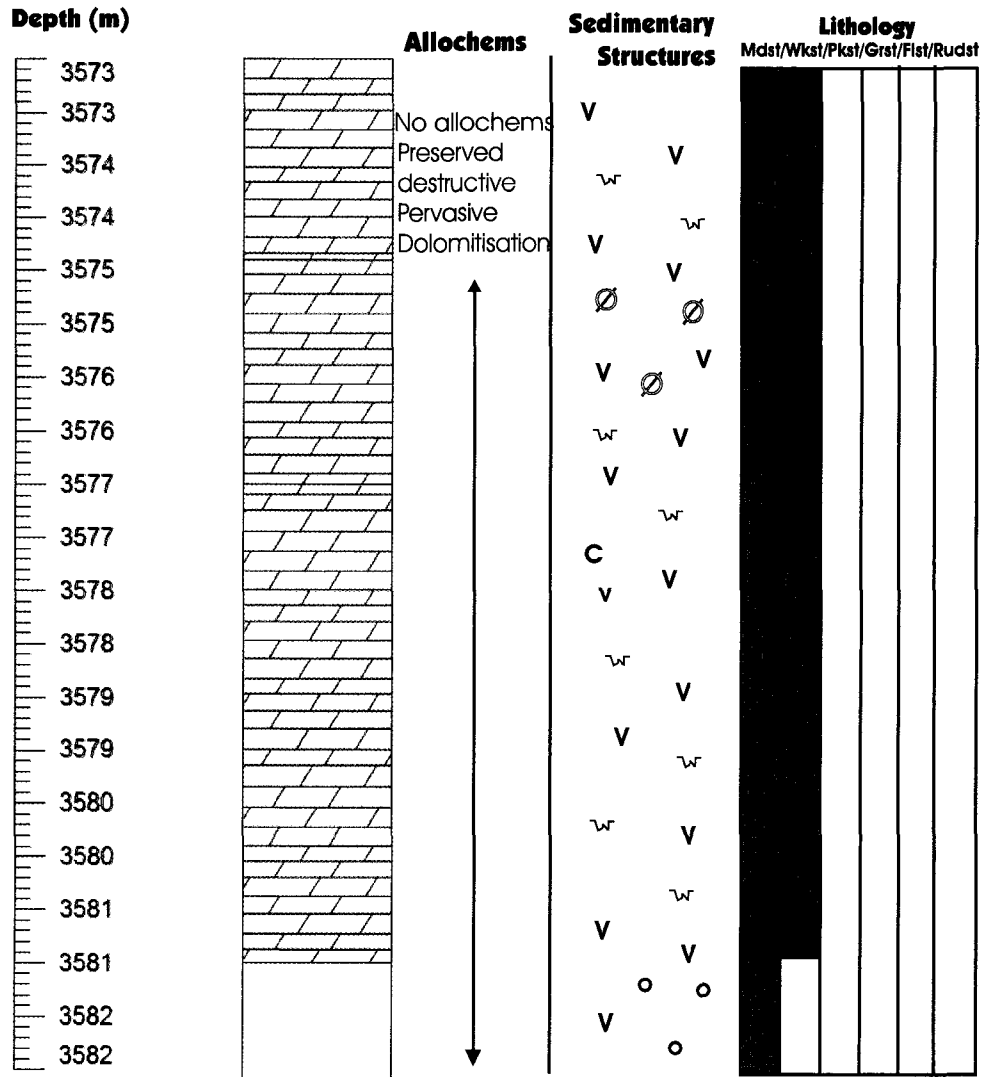
APPENDIX IV:

Oxygen and Carbon Results: $\delta^{18}O$ ‰ (VPDB) ‰ & $\delta^{13}C$ ‰(VPDB)

Sample	Well #	Phase	Depth (m)	Oxygen	Carbon
C-1-1-LM	Well # 1	Calcite	2400.54	-5.75	1.22
C-1-10-LM	Well # 1	Calcite	2412.19	-6.22	0.78
C-1-6-LM	Well # 1	Calcite	2406.85	-6.68	1.24
C-1-2-LM	Well # 1	Calcite	2402.92	-5.96	1.27
C-1-7-LM	Well # 1	Calcite	2408.10	-5.90	1.55
C-6-3-LM	Well # 6	Calcite	2385.87	-4.57	0.93
C-9-11-LM	Well # 9	Calcite	2614.27	-7.28	0.27
C-9-1-LM	Well # 9	Calcite	2511.73	-4.19	-0.09
M-10-1-CO	Well # 10	Calcite	2571.80	-3.96	-1.14
M-2-18-CR	Well # 2	SYN Calcite	2670.60	-4.38	0.44
C-1-6-SC	Well # 1	SYN Calcite	2406.85	-5.56	2.00
C-1-7-SC	Well # 1	SYN Calcite	2408.10	-6.05	1.47
C-10-13-BC	Well # 10	BLK Calcite	2623.41	-5.65	-9.66
C-2-14-BC	Well # 2	BLK Calcite	2663.28	-9.82	-5.95
C-2-15-BC	Well # 2	BLK Calcite	2664.13	-11.13	-12.54
C-1-4-BC	Well # 1	BLK Calcite	2404.14	-7.74	-1.11
C-4-23-BC	Well # 4	BLK Calcite	2635.83	-9.52	-22.60
C-4-29-BC	Well # 4	BLK Calcite	2640.18	-10.09	-18.02
C-6-12-BC	Well # 6	BLK Calcite	2397.30	-9.77	-15.83
C-8-3-BC	Well # 8	BLK Calcite	3637.48	-8.45	-19.42
C-4-22-BC	Well # 4	BLK Calcite	2634.99	-8.39	-15.42
C-4-28-BC	Well # 4	BLK Calcite	2639.47	-9.63	-17.58
C-10-6-BC	Well # 10	BLK Calcite	2575.97	-7.90	-5.50
C-2-6-BC	Well # 2	BLK Calcite	2650.51	-9.17	-15.16
C-8-8-BC	Well # 8	BLK Calcite	3659.18	-7.14	-10.90
C-10-5-BC	Well # 10	BLK Calcite	2575.79	-9.52	-21.64
C-11-3-VC	Well # 11	LV Calcite	3575.86	-9.32	-17.28
C-10-5-VC	Well # 10	LV Calcite	2575.79	-8.73	-16.66
C-11-3-LV	Well # 11	LV Calcite	3575.86	-8.24	-9.14
C-9-9-VC	Well # 9	LV Calcite	2607.39	-7.39	-0.39
D-10-5-DS	Well # 10	DS Dolomite	2575.79	-4.66	-1.09
D-9-11-DS	Well # 9	DS Dolomite	2614.27	-4.49	1.22
D-1-6-DS	Well # 1	DS Dolomite	2406.85	-6.02	2.14
D-1-10-DS	Well # 1	DS Dolomite	2412.19	-5.97	1.07
D-10-1-DS	Well # 10	DS Dolomite	2571.80	-6.51	-0.22
D-5-14-PD	Well # 5	Dolomicrite	2589.10	-5.64	0.86

146

Sample	Well #	Phase	Depth (m)	Oxygen	Carbon
D-2-19-PD	Well # 2	Dolomicrite	2671.85	-5.81	0.68
D-6-2-LAM	Well # 6	Dolomicrite	2385.09	-5.38	0.72
D-5-15-PD	Well # 5	Dolomicrite	2589.23	-5.69	1.11
D-2-11-PD	Well # 2	Dolomicrite	2656.30	-5.10	1.30
D-5-9-LAM	Well # 5	Dolomicrite	2584.22	-5.31	-0.91
D-4-15-PD	Well # 4	F-M Mat Dol	2626.00	-5.47	1.47
D-7-8-PD	Well # 7	F Mat Dol	2756.74	-5.72	0.51
D-9-3-PD	Well # 9	M Mat Dol	2515.62	-5.35	0.25
D-5-18-PD	Well # 5	F-M Mat Dol	2591.03	-5.58	1.08
D-6-10-PD	Well # 6	F-M Mat Dol	2394.92	-5.23	0.85
D-3-10-PD	Well # 3	F-M Mat Dol	2254.06	-5.58	0.73
D-3-5-PD	Well # 3	F Mat Dol	2248.21	-5.73	0.81
M-2-18-CR	Well # 2	F Mat Dol	2670.60	-5.34	0.46
D-4-32-PD	Well # 4	F-M Mat Dol	2644.65	-5.25	0.93
D-7-4-PD	Well # 7	F-M Mat Dol	2750.67	-2.82	0.22
D-3-17-PD	Well # 3	F-M Mat Dol	2263.00	-6.17	0.72
D-4-22-PD	Well #4	F-M Mat Dol	2634.99	-4.79	0.76
D-11-1-PD	Well # 11	C Mat Dol	3574.19	-5.47	0.64
D-10-5-PD	Well # 10	C Mat Dol	2575.79	-4.99	-0.14
D-10-6-PD	Well # 10	C Mat Dol	2575.79	-4.46	-1.14
D-2-6-PD	Well # 2	C Mat Dol	2650.51	-4.42	1.07
D-11-2-PD	Well # 11	C Mat Dol	3574.75	-5.75	0.83
D-8-7-PD	Well # 8	C Mat Dol	3657.30	-8.32	-0.82
D-6-15-PD	Well # 6	C Mat Dol	2401.77	-7.86	-1.09
D-8-8-PD	Well # 8	C Mat Dol	3659.18	-6.34	1.00
D-7-5-PD	Well # 7	C Mat Dol	2753.82	-5.10	0.55
M-10-1-CO	Well # 10	C Mat Dol	2571.80	-4.59	-1.12
D-9-1-PD	Well # 9	C Mat Dol	2511.73	-4.73	-0.04
D-4-20-PD	Well # 4	C Mat Dol	2633.02	-6.78	1.16
D-3-7-PD	Well # 3	C Mat Dol	2251.24	-6.09	0.67
D-10-9-PD	Well # 10	C Mat Dol	2583.69	-5.77	-0.16
D-2-7-PD	Well # 2	C Mat Dol	2651.12	-5.30	1.19
D-6-14-PD	Well # 6	C Mat Dol	2401.32	-6.54	0.80
D-8-10-PD	Well # 8	C Mat Dol	3670.40	-5.20	-0.58
D-11-4-PD	Well # 11	C Mat Dol	3577.26	-5.64	0.79
D-8-3-PD	Well # 8	C Mat Dol	3637.48	-5.41	-0.01
D-11-5-PD	Well # 11	C Mat Dol	3581.48	-4.91	-0.36
D-9-2-PD	Well # 9	C Mat Dol	2513.71	-4.91	0.02
D-11-3-PD	Well # 11	C Mat Dol	3575.86	-6.00	0.91
D-7-9-PD	Well # 7	C Mat Dol	2757.81	-5.75	0.74
D-2-7-PD	Well #2	C Mat Dol	2651.12	-5.30	0.85

147

Sample	Well #	Phase	Depth (m)	Oxygen	Carbon
D-10-8-PD	Well # 10	C Mat Dol	2582.27	-5.72	-1.08
D-11-3-SD	Well # 11	Sad Dol	3575.86	-6.59	-1.41
D-10-6-SD	Well # 10	Sad Dol	2575.97	-6.51	-3.43
D-10-8-SD	Well # 10	Sad Dol	2582.27	-6.99	-1.32
D-10-13-SD	Well # 10	Sad Dol	2623.41	-5.16	-3.39
D-5-18-D	Well # 5	PO Dol	2591.03	-6.23	0.93

148

VITA AUCTORIS

NAME:	**Samantha R. Raymus**
PLACE OF BIRTH:	**Fort Churchill, Manitoba, Canada**
YEAR OF BIRTH:	**1970**
EDUCATION:	**University of Winnipeg, Winnipeg, Manitoba** **1988-1992 BA (4YR) (History/International** **Relations)**
	University of Manitoba, Winnipeg, Manitoba **1995-2000 B.Sc. (Hons) (Geology)**
	University of Windsor, Windsor, Ontario **2004-2006 M.Sc. (Geology)**

149